Application of Membrane Separation Processes in the Pharmaceutical Industry – A Study of Process Development for Overcoming Membrane Limitations

By

Weiming Eugene Siew

Supervisors: Andrew G. Livingston

Alain Merschaert

Célal Ates

A Thesis Submitted As Part of the Requirement for the Degree of Doctor of Philosophy at Imperial College London

Department of Chemical Engineering

Imperial College London

United Kingdom

September 2013

Abstract

The prevalent business model in the pharmaceutical industry requires rapid and robust process development and flexible manufacturing processes. This work reports the attempts to develop structured procedures for membrane process development to meet these requirements.

The Donnan Steric Pore Model, in conjunction with a computational molecular dynamics programme, was evaluated as tool for membrane performance predictions to circumvent the need for tedious membrane screening experiments. However, the computational effort required was too onerous, making experimentation more efficient than computational method at this stage.

Process chemistry manipulation enabled the use of otherwise incompatible membranes for separation and reduced the time needed for membrane scoping. Firstly, through pH manipulation to selectively increase electrostatic sieving, the permeation selectivity of a membrane to 2 different solutes was changed. Secondly, a structured procedure for polyalkylation of an 'anchor' molecule to increase the steric hindrance of an organocatalyst was used to enable the total retention of the catalyst so that a single stage membrane recycling strategy for the catalyst could be enacted.

Published membrane processes were analysed and found to lack robustness and to be too sensitive to slight deviations in membrane performance. Hence new membrane processes were devised to address these challenges. Firstly, a membrane cascade process was used to enhance the rejection of an active pharmaceutical ingredient (API) over the single pass membrane rejection. This cascade process was then used for concurrent API concentration and solvent recovery. Secondly, a permeable stripping cascade configuration was used for the removal of an excess reagent from an API to enable the excess loading of the reagent to increase the yield of the API. The membrane cascades benefited from enhanced reliability, increased productivity and improved robustness.

Acknowledgements

I would like to express my gratitude and appreciation to my academic supervisor, Prof. Andrew G. Livingston, and my industry supervisors at UCB Pharma, Dr. Célal Ates and Dr. Alain Merschaert, for their guidance, support and most importantly their patience throughout my PhD.

I would also like to thank my colleagues at UCB Pharma , especially the team in Chemical Process Development, for their help in my research and showing me the ropes in process chemistry and synthesis. Much of my work would not have been possible without them. My time there has been most formative.

Finally I am grateful to my family for their continued support and understanding throughout my PhD studies.

I would like to acknowledge funding from the 7th Framework Programme of the European Commission's Marie Curie Initiative (grant no. PITN-GA-2008-214226-Nemopur).

Publications

Part of this thesis has been accepted for publication in peer-reviewed journals. The first publication was written with material in Section 5.2. The second publication was written with material in Section 5.1 while the final article was written with material in Section 3.2.

1. Siew, W. E., Livingston, A. G., Ates, C., Merschaert, A. (2013). Continuous solute fractionation with membrane cascades – A high productivity alternative to diafiltration. *Separation and Purification Technology, 102*, 1–14.
2. Siew, W. E., Livingston, A. G., Ates, C., Merschaert, A. (2012). Molecular Separation with an Organic Solvent Nanofiltration Cascade – Augmenting Membrane Selectivity with Process Engineering. *Chemical Engineering Science.* [Online]. Available from: http://dx.doi.org/10.1016/j.ces.2012.10.028 [Accessed 14th January 2013].
3. Siew, W. E., Ates, C., Merschaert, A., Livingston, A. G. (2013). Efficient and productive asymmetric Michael addition: development of a highly enantioselective quinidine-based organocatalyst for homogeneous recycling via nanofiltration. *Green Chemistry.* [Online]. Available from: http://dx.doi.org/10.1039/C2GC36407G. [Accessed 14th January 2013]

Table of Contents

List of Figures

List of Schemes

List of Tables

Acronyms & Abbreviations

API	Active pharmaceutical ingredient
AMS	N-acetylated amino acid
CMO	Contract manufacturing organisation
DM	DuraMem®
DMG	Dimethylglycine
DSPM	Donna Steric Pore Model
EtOAc	Ethyl acetate
EWG	Electron withdrawing group
f	Function placeholder, f
h	Function placeholder, h
MeOH	Methanol
MS	Amino acid
NF	Nanofiltration
OSN	Organic solvent nanofiltration
PEG	Poly (ethylene glycol)
pI	Isoelectric point
SMX	Sulfamethoxazole
THF	Tetrahydrofuran
THSH	2,3,4,5-tetrahydroxy-6-sulfooxy hexanoic acid

Nomenclature

Symbol	Description	Unit
A	Membrane area	m^2
A_j	Coefficient for description of concentration profile in retentate of stage *j*	g L^{-1} min^{-1}
B_j	Initial concentration of retentate in stage *j*	g L^{-1}
c_i	Concentration of solute *i* in the membrane pore or membrane interface	mol m^{-3}
C_i	Concentration of solute *i* in the bulk solution	mol m^{-3}
$C_{i,p}$	Bulk concentration of solute *i* in the permeate	mol m^{-3}
$C_{i,r}$	Bulk concentration of solute *i* in the retentate	mol m^{-3}
$D_{i,m}$	Species *i* diffusivity in across membrane	m^2 s^{-1}
$D_{i,o}$	Species *i* diffusivity in bulk solution	m^2 s^{-1}
$D_{i,p}$	Species *i* diffusivity across membrane pore	m^2 s^{-1}
f_j	Permeate flux of stage *j*	L m^{-2} h^{-1}
F	Feed flow	L min^{-1}
$\bar{F}$	Faraday's constant 96 485.3365 C mol^{-1}	C mol^{-1}
j_i	Solute *i* flux across membrane	mol m^{-2} s^{-1}
J_p	Solvent flux across membrane	m s^{-1}
k	Boltzmann constant 1.38065 x 10^{-23} J K^{-1}	J K^{-1}
k_i	Mass transfer coefficient of solute *i*	m s^{-1}
K_i	Partition coefficient of species *i* across between bulk solution and membrane	-
$K_{i,c}$	Solute *i* hindrance factor for convection	-
$K_{i,d}$	Solute *i* hindrance factor for diffusion	-
l	Position across pore length	M
M_i	Molecular weight of solute *i*	kg mol^{-1}
Pe_i'	Modified Peclet number	-
p_{ei}	Pressure at location *i* along the x-axis	bar
p_j	Effective transmembrane pressure in stage *j*	bar
P_j	Permeate flow leaving stage *j*	ml min^{-1}
r	Distance away from membrane wall	m
r_p	Membrane pore radius	m
R	Recycle ratio, $\frac{W_p}{P_p}$	-
$\bar{R}$	Universal gas constant 8.314 4621 J mol^{-1} K^{-1}	J mol^{-1} K^{-1}
$R_{i,j}$	Rejection of solute i in stage j, where $R_{i,j} = 1 - \frac{y_{i,j}}{x_{i,j}}$	-
$R_{i,o}$	Rejection of solute *i* over the whole cascade, where $R_{i,o} = 1 - \frac{y_{i,p}}{x_{i,1}}$	-
t	Filtration time	min
T	Temperature	K
T_j	Pump flow feeding into stage *j*	L min^{-1}
u	Solvent velocity in membrane pore	m s^{-1}
v_i	Partial molar volume of species *i*	m^3 mol^{-1}
V	Solute velocity in membrane pore	m s^{-1}
$V_j\|_t$	Volume of retentate in stage *j* at filtration time *t*	L
$V_{Pj}\|_t$	Volume of permeate from stage *j* at filtration time *t*	L

W_j	Retentate flow leaving stage *j*	ml min^{-1}
x	Position in x-axis of membrane pore or membrane	m
$x_{i,j}$	Concentration of species *i* in retentate leaving stage *j*	g L^{-1}
$x_{i,j}\|_t$	Concentration of species *i* in retentate leaving stage *j* at time *t*	g L^{-1}
$x_{i,product}$	Concentration of species *i* in retentate stream leaving cascade	g L^{-1}
$X_{i,d}\|_t$	Purity of solute *i* in the retentate at time *t*	-
X_{23}	Friction coefficient between solute and membrane	N s m^{-1} mol^{-1}
χ_{im}	Proportionality constant between solvent *i* and membrane	J s m^{-2} g^{-1} mol^{-1}
χ_{jm}	Proportionality constant between solute *j* and membrane	J s m^{-2} g^{-1} mol^{-1}
y	Position in y-axis of membrane pore	M
$y_{i,j}$	Concentration of species *i* in permeate leaving stage *j*	g L^{-1}
$Y_{i,d}\|_t$	Purity of solute *i* in the permeate at time *t*	-
$\overline{y_{i,j}}\|_t$	Concentration of species *i* in permeate collected from stage *j* at filtration time *t*	g L^{-1}
$y_{i,product}$	Concentration of species *i* in permeate stream leaving cascade	g L^{-1}
z_i	Charge on solute *i*	-
$z_{i,F}$	Concentration of species *i* in the feed	g L^{-1}
ε	Membrane porosity	-
η	Solution viscosity	Pa s
Δl	Membrane thickness	m
Δp_e	Effective transmembrane pressure difference	bar
ΔW_i	Born solvation energy of solute *i*	J
$\Delta \Psi_D$	Donnan potential	V
μ_i	Chemical potential of solute *i*	J mol^{-1}
v_p	Superficial velocity of solvent across membrane	m s^{-1}
ϕ_i	Steric partitioning coefficient factor of solute *i*	-
λ_i	Ratio of solute *i* radius to membrane pore radius	-
φ_i	Force exerted by solute *i* molecule on pore wall	J g^{-1} mol^{-1}
γ_i	Activity coefficient of solute *i* in the membrane pore	-
γ_i^0	Activity coefficient of solute *i* in the bulk solution	-
τ	Shear stress	N m^{-2}
θ_j	Stage cut of membrane stage *j*	-

1. Introduction

The international pharmaceutical market is huge, with a worldwide turnover of $800 billion in 2009 (am Ende, 2011). However, the industry now faces increasing cost pressures due to decreasing profit margins and shrinking product pipelines. Improving the efficiency of manufacturing is imperative in maintaining the competitiveness of the industry since production accounts for an estimated 30% of the overall cost of a drug (Filtration+Separation, 2006). Furthermore, the increasing complexities of syntheses for the active pharmaceutical ingredients (API's) of upcoming drugs will disproportionately contribute to increases in production costs. Therefore there is an industry trend to minimise the cost of API manufacturing, while doing so in a safe and environmentally benign way (Federsel, 2006). Meanwhile, separation processes account for somewhere between 40-70% of the capital and operating costs of the chemical industry (Spear, 2006), hence optimisation of separation processes in API manufacturing will likely play an important part in driving efficiency gains in the pharmaceutical industry.

Nanofiltration (NF) has gained attention in recent years for its potential to streamline separation processes. NF involves the separation of solutes, based on their size and charge, through the use of a pressure difference across a membrane. NF membranes tend to retain solutes that are larger than the nanometre range, while smaller solutes and solvents can permeate easily through them. NF and organic solvent nanofiltration (OSN), which sprung up with the development of NF membranes stable in organic solvents in the last 2 decades (See Toh et al., 2007a; See Toh et al., 2007b; See Toh, 2008; Vandezande et al., 2008; White & Nitsch, 2000), have the potential to be used in a myriad of industrial processes and lab scale syntheses in the pharmaceutical industry. Thermal degradation and side reactions can be minimized due to their lower operational temperatures relative to distillation, while their energy consumptions are lower than distillation and crystallization. Solvent exchange from a high-boiling point to a low-boiling point solvent can also be performed more easily than distillation. Moreover the modular nature of the membrane setup makes continuous processing simple (Vandezande et al., 2008).

UCB Pharma SA (henceforth called UCB Pharma in the rest of this thesis), like many other companies dealing with chemical synthesis of API's, faces a significant challenge in applying OSN to its processes. While OSN membranes typically show molecular weight cutoffs (MWCO) of 200-1000Da (Vandezande et al, 2008), the typical compounds dealt with at UCB Pharma have molecular weights

in the low hundreds of Daltons. In many cases, the solutes are similar in sizes, posing a greater purification challenge.

1.1 Process Development in Pharma

Patents applied after 1995 are typically valid for 20 years from the earliest application date, giving pharmaceutical companies limited market exclusivity for any of their drugs. While further innovations such as improved indications or formulations can extend the exclusivity for 3-5 years (FDA, 2011), this is short compared to the 10-15 years of research required to bring a new compound to market. Hence securing the availability of a drug as quickly as possible remains one of the highest priorities of pharmaceutical companies and process development has to cater to this need (am Ende, 2011). Furthermore, the productivity and cost pressures faced by the pharmaceutical industry make identification of optimum production processes as early as clinical studies in phase II a necessity (Federsel, 2006). Due to this time constraint in developing processes that have to be robust and quantifiably 'optimum', tools and methods for process development in the pharmaceutical industry have to be predictable and quick to scale up.

Process development is also driven by the demands of API manufacturers. Plants used in API production are primarily batch-operated multipurpose plants which allow flexibility in response to product demand (am Ende, 2011), with the trend of pharmaceutical companies outsourcing their manufacturing to contract manufacturing organisations (CMO) (Morvan, 2012) likely to cement the prevalence of such plants. Therefore compatibility with the multipurpose batch plant model is necessary for any process to gain widespread adoption in API production. On the other hand, new processes should also be forward compatible with continuous operations as the industry gradually switches to continuous processing (LaPorte et al., 2011). This switch will likely occur as ICH (2000) has cleared the regulatory hurdle to batch tracking in continuous processing by allowing a batch to correspond to a defined fraction in a continuous process.

OSN can potentially meet the process development needs of the pharmaceutical industry. The modular design of OSN equipment makes OSN flexible and easily scalable between batch and continuous operation, while the dominance of membrane processes in the desalination/water treatment industry (Zarkadas & Sirkar, 2011) should be a testament of the predictability of OSN performance.

1.2 Overview of OSN Applications

The proliferation of publications which purport to apply OSN technology on API production masks the low adoption rate of OSN in the pharmaceutical industry. Most works published are largely academic with few examples of industrial use. This is despite the seemingly good fit of OSN with the requirements of the pharmaceutical industry. In this section, notable OSN applications are summarised in an attempt to identify the resistance to adopting this technology in the industry. In general, these applications can be grouped into solvent exchange, solvent recovery and solute fractionation. The retention/rejection of a solute is often used to quantify membrane performance and is expressed according to Equation 1.1 (See Toh et al., 2007b). Do note this differs from the definition by Mulder (1996) as the common apparatus used for the characterisation of membrane performance in OSN (See Toh et al., 2007a; See Toh et al., 2007b; Sereewatthanawut et al., 2008) measures the concentration in the retentate and not the feed. The terms for the equation are illustrated in Figure 1.1.

$$R_{i,j} = 1 - \frac{y_{i,j}}{x_{i,j}} \qquad \textbf{Equation 1.1}$$

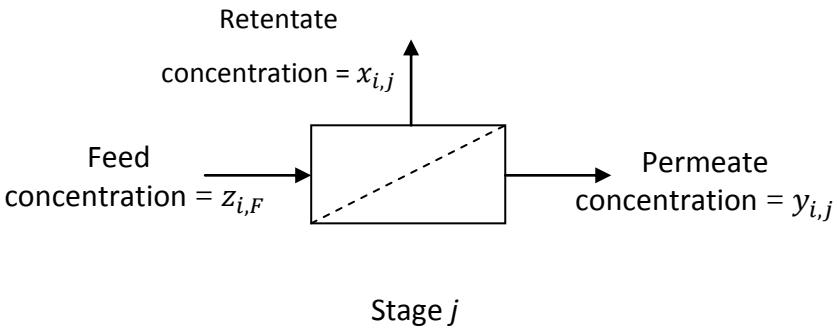

Figure 1.1: Schematic for NF membrane stage *j* and the terms for concentrations for the streams into and out of the NF unit.

1.2.1 Solvent recovery

The success and increasing prevalence of membrane filtration in water treatment (Fritzmann et al., 2007) have raised interest in the use of OSN for solvent recovery. The efficiency of organic solvent usage in the pharmaceutical industry is abysmal though solvents are widely used in the industry

(Hellweg et al., 2004). In fact, while solvent use accounts for an estimated 80-90% of the mass utilization in a typical pharmaceutical batch chemical operation, recovery rates of organic solvents are low with GlaxoSmithKline (GSK) quoting solvent recycle rate of less than 50% (Constable et al., 2006). Improving organic solvent recycling rates can be part of the strategy to reduce solvent wastage and OSN might help realise it. However, the success in water treatment might not be directly translational in many cases because the solute in solution is often a desirable product and needs to be recovered. Water treatment on the other hand tends to employ destructive processes for solute removal in pre-membrane water treatment.

It has been aptly pointed out that significant energy savings can be realised if a single-stage OSN process is used as an alternative to distillation for every solvent recovery step (Darvishmanesh et al., 2011; Geens et al., 2007; Rundquist et al., 2012a; Rundquist et al., 2012b). The success of OSN in solvent recovery relied on the use of a membrane with a high retention of the solute, with only membranes having rejections of >0.95 considered. However, such high rejections are not always possible even with the extensive membrane screening (Darvishmanesh et al., 2011; Geens et al., 2007; Rundquist et al., 2012a ; Rundquist et al., 2012b).

The use of multiple membrane passes in batch diafiltration has been demonstrated in response to inadequate membrane performance (Katraro et al., 1997; Rundquist et al., 2012b), with concurrent progress also being made in the development of continuously operated membrane cascade for solvent recovery (Abejon et al., 2012; Caus et al., 2009).

1.2.2 Solvent exchange

Solvent exchange is a common unit process in the pharmaceutical industry, usually performed using batch distillation with intensive use of energy and solvent (Zarkadas & Sirkar, 2011). Sheth et al. (2003) demonstrated how OSN can enable an easy solvent switch at ambient temperature, even switching to a solvent that has a lower boiling point. An ethyl acetate solution of erythromycin was switched to methanol using a batch diafiltration process, employing hydrophobic SelRO® membranes that gave high single pass rejection of erythromycin of 0.8-0.95. Yields of 84-96% of erythromycin were achieved. Rundquist et al. (2012a) also managed a solvent exchange with low API losses of 2.3%, using Starmem™ 240 membrane which had >0.99 retention of the API.

A solvent exchange can also be performed continuously using OSN. Lin & Livingston (2007) demonstrated the use of a membrane cascade in switching a toluene solution of tetraoctylammonium bromide to a more volatile methanol solution by employing STARMEM^{TM} 122 membranes which had retentions of between 0.74 and 0.99 for the ammonium salt. Salt losses were minimised when the rejection of the salt approached unity for every stage.

1.2.3 Solute fractionation

Emulating the success in aqueous ultrafiltration (Cheang & Zydney, 2003; Zydney, 1998), OSN membranes have already been used in a number of solute fractionating processes, such as homogeneous catalyst recycling (Anyanwu & Venkataraman, 2005; Ferreira et al., 2007; Dijkstra et al., 2002; Nair et al., 2002; Tsoukala et al., 2012), intermediate purification (Ghazali, 2006; So et al., 2010) and API purification (Pink et al., 2008; Sereewatthanawut et al., 2010, Székely et al., 2011; Székely et al., 2012). These examples mostly employed diafiltration, with a partiality towards constant volume diafiltration. The authors for these works relied on membrane screening for the highest possible retention for the most retained solute to develop a successful separation procedure.

Continuous operation of OSN units for solute fractionation is absent in literature, though the concept has been demonstrated for protein fractionation in water (Mayani et al., 2010) using ultrafiltration membranes.

1.3 Scope of Study and Objectives

The relatively low volumes and short life-times of most products in the pharmaceutical industry (Roberge et al., 2005) necessitate rapid process development and the use of flexible processes. A review of the OSN examples listed in Section 1.2 showed that speedy development of OSN process for use in the industry is not easy. A high membrane rejection of the target solute was critical for the success of these processes, with complete rejection of the target compound the optimum condition sought after. Membranes were screened laboriously, searching for the membrane with the highest rejection and not all screenings culminated in a suitable membrane. While membranes can be custom-made for a particular solute-solvent system to achieve complete rejection, membrane development is often tedious and not in the scope of API producers. Furthermore the membranes were often dedicated to a particular process and rarely interchangeable due to the sensitivity of the

process to membrane rejection, making membrane screening necessary for each and every application.

Process development can be sped up, with the use of appropriate tools for membrane performance predictions, by reducing the effort required for membrane screening. Modifying the process parameters such as process solvent to suit the capabilities of the membrane available can also eliminate the need for extensive membrane screening. Despite single stage diafiltration being the state-of-the-art for the application of OSN, forays into developing staged membrane cascade systems have attempted to achieve superior separation performance over the single stage process. Therefore, it is evident that manipulation of process configuration is another tool available to API producers to circumvent membrane limitations and avoid membrane screenings.

The first objective of this work is to determine tools for the prediction of membrane performance to hasten membrane process development. The next objective is to showcase how both process modifications and manipulation of process configuration can be used to make OSN applications work in spite of the performance limitations of commercially available membranes. Hopefully, this work can help minimise the need for membrane screening, which is so ubiquitous in published OSN works.

In order to meet the objectives stated above, the following deliverables are planned as part of this thesis:

1. Review of various membrane transport models (Chapter 2).
2. Case study on the use of process modifications on solutes to improve OSN separation, including their relevance in improving solute rejection and their use for membrane performance predictions (Chapter 3).
3. Review of common OSN processes and their inherent limitations (Chapter 4).
4. Case study for the use of process engineering to address the limitation of the state of the art OSN processes (Chapter 5).
5. Conclusion for this thesis, recommendation for future work and review of what was achieved against the stated objectives of this thesis (Chapter 6).

2. Membrane Transport Modelling

Henceforth, a distinction is made between a membrane process model, which describes variables in a membrane process, and a membrane transport model, which describes transport across the membrane itself.

An accurate membrane transport model, especially one that can provide an *a priori* prediction of membrane performance, can contribute to a better adoption rate of OSN technology in the pharmaceutical industry by enabling the selection of suitable membranes with greater certainty.

A number of transport models have been proposed to explain the transport of solvent and solutes across membranes. While all of them are semi-empirical at best, they do offer users a tool to understand membrane transport. Broadly speaking, these models can be classified as either a solution-diffusion model or a pore flow model.

2.1 Solution-diffusion Model

In the mathematical description of solution-diffusion models (Wijmans & Baker, 1995), the fluxes of solvents and solutes through the membrane are scaled by the membrane permeability constants of the solvents and solutes respectively. Firstly, the transport of solvent *i* through a membrane can be described by

$$J_p = \frac{D_{i,m} K_i C_{i,r} v_i}{\Delta l \bar{R} T} (\Delta p_e) \qquad \textbf{Equation 2.1}$$

Where the partitioning between the bulk solution and membrane, due to the difference in activity coefficients in both phases, is accounted for with the partitioning coefficient, shown in the equation below.

$$K_i = \frac{\gamma_i^0}{\gamma_i} \qquad \textbf{Equation 2.2}$$

Secondly, the flux of solute *j* can be expressed as

$$j_j = \frac{D_{j,m} K_j}{\Delta l}\left(C_{j,r} - C_{j,p}\right) \qquad \textbf{Equation 2.3}$$

Hence one can see that the permeabilities of solvents and solutes are proportional to both the diffusivity of the species through the membrane, and the sorption of the species onto the membrane. Solute-solvent separation, as described by this mechanism, occurs when the solute diffuses and/or sorbs into the membrane at a different rate than the solvent.

The species diffusivities ($D_{i,m}$) and sorption coefficients (K_i), which the permeability constants are dependent upon, are often concentration dependent (Wijman & Baker, 1995) and are hard to determine independently without direct testing on the specific solvent-solute-membrane system. This makes experimentation necessary whenever a new solvent-solute-membrane system is employed. Without a correlation of the solute diffusivity and solute sorption on the membrane with measureable membrane variables, an *a priori* prediction tool using the solution-diffusion model is impossible.

2.2 Pore-flow Model

The pore-flow models on the other hand tend to relate membrane transport to the pressure gradient through the membrane. Solvent flow is often described in continuum with a hydrodynamic equation such as the Hagen-Poiseuille equation or a modification of it. Solute transport on the other hand is described in two parts. Firstly the "partitioning" equation gives a measure of the affinity of the solute to the membrane, mathematically relating the concentration of solute in the bulk solution to the concentration of solute in the pore. Secondly, the transport equation relates the rate of solute transport through the membrane pore. Solute-solvent separation occurs due to the difference in the rate of transport of solute and solvent through the membrane pore and also due to the higher or lower affinity for solute sorption into the membrane pore than solvent sorption.

The surface force pore flow (SFPF) model proposed by Matsuura & Sourirajan (1981) implies that "partitioning" of solutes occurs due to a potential resulting from the interaction between the pore on the membrane surface and the solute *j* in bulk solution according to

$$c_j = C_j \exp\left(\frac{-\varphi_j}{\bar{R}T}\right) \qquad \textbf{Equation 2.4}$$

A result of the partitioning is a reduction or increase of solute concentration in the pore compared to the immediate bulk solution when the potential is repulsive or attractive respectively. The solutes are then co-transported with the solvent, hindered by friction forces, between the solute and solvent and between the solute and pore wall. The flux of solute *j* through a pore can be mathematically expressed as

$$j_j = \frac{-\bar{R}T}{\chi_{ij} + \chi_{jm}}\left(\frac{dc_j}{dl}\right) + \chi_{jm}\frac{c_j u}{\chi_{ij} + \chi_{jm}} \qquad \textbf{Equation 2.5}$$

Where the proportionality constant between solute and membrane is

$$\chi_{jm} = \frac{-F_{jm}c_j}{j_j} \qquad \textbf{Equation 2.6}$$

And the proportionality constant between solute and membrane is

$$\chi_{jm} = \frac{-F_{ij}}{V - u} \qquad \textbf{Equation 2.7}$$

Solvent transport is not described in this model as the model relies on fitting with experimental flux data. While the friction force in this model can be determined easily from the diffusivity of the solute in solvent, the potential has to be obtained empirically through fitting with experimental data. Therefore this model is not designed for the *a priori* prediction of membrane transport.

The finely porous model developed by Jonsson & Boeson (1975) and explored by Niemi & Palosaari (1993) describes partitioning as a result of an equilibrium distribution between the pore fluid and bulk solution. For the finely porous model, assuming a porosity of unity, the permeate flux of a solution containing solute *i* can be expressed as

$$J_p = \frac{\varepsilon r_p^2}{8\eta}\left(\frac{\Delta p_e}{\Delta l} - X_{23}\frac{j_i}{M_i}\right) \qquad \textbf{Equation 2.8}$$

While the solute *i* flux can be expressed with

$$j_i = -\frac{\bar{\bar{R}}T}{X_{21} + X_{23}}\frac{dc_i}{dx} + \frac{X_{21}c_i u}{X_{21} + X_{23}}$$ **Equation 2.9**

Hence one can see that solvent transport follows a modified Hagen-Poiseuille equation, with the velocity slowed down by friction between solute and membrane, while solute transport is described as a combination of diffusive and viscous flows (co-transport with solvent). Therefore solvent and solute transports are dependent on the friction forces between solute-membrane, solute-solvent and solvent-solute. While the friction coefficient between solute and solvent can be determined from the diffusivity of solute in solvent, the determination of friction coefficient between solute and membrane using the diffusivity of solute in membrane is harder and will require fitting with experimental data. Hence this model is not suited for the *a priori* prediction of membrane transport either.

The Donnan Steric Pore Model (DSPM), employed by Bowen & co-workers (Bowen et al., 1997; Bowen & Mohammad, 1998; Bowen & Welfoot, 2002) and Déon et al. (2007), stands out amongst the pore flow models. Partitioning of uncharged solutes in this model is solely dependent on a size factor that can potentially be determined through independent measurements of the solute and the membrane, without the need to fit with experimental data. As such, *a priori* predictions of membrane performance are possible with this model. Similar to the finely porous model, solute transport occurs as a result of pressure driven solvent flow and diffusive flow of solute in solution in the pore. Solvent transport in this model follows the Hagen-Poiseuille equation.

It should be noted that for solvent volume to be conserved on both sides of a membrane, solvent velocity through the pores has to be higher than the actual permeate flux, if the porosity of the membrane is less than unity. This mathematical condition runs contrary to the solution diffusion models. However, this was not been taken into account by a number of pore flow modellers (Matsuura & Sourirajan, 1981; Bowen & Welfoot, 2002; Deon et al., 2007), hence they might have underestimated the significance of viscous transport of solute in their analysis.

2.2.1 Donnan-steric pore model

The DSPM, proposed by Bowen et al. (1997), where ion transport is described by the extended Nernst-Planck equation and equations added to account for hindered transport of ions and solutes due to steric and electrostatic hindrance, was successfully used in the prediction of aqueous NF

performance in dye-salt diafiltration (Bowen & Mohammad, 1998) and the prediction of various solutes and inorganic salts rejection in continuous NF (Bowen and Welfoot, 2002; Déon et al., 2007).

This model assumes the following:

1. A porous membrane structure with uniform pore sizes and pores with tortuosity of unity
2. Negligible concentration polarisation
3. Pores that can be charged, depending on pH and ionic strength of the solution the membrane is in
4. Pores have hard walls while the solutes in the model are represented by hard spheres that obey the Stokes-Einstein equation
5. Solvent behaves as a continuum

The DSPM uses 3 main equations to describe solute rejection. Unhindered solvent transport is modelled using a Hagen-Poiseuille type equation. Both the sieving effect of the membrane, which is accounted for by the partitioning equation, and the solute transport in the membrane pore, described using a hydrodynamic model, are used to describe hindered solute transport across a membrane.

2.2.1.1 Solvent transport equation

Solvent transport in the DSPM is expressed in the form of Equation 2.10, with the assumption that the membrane contains only straight pores of identical sizes.

$$J_p = \frac{-r_p^2 \Delta p_e}{8\eta\left(\frac{\Delta l}{\varepsilon}\right)} = \upsilon_p \varepsilon \qquad \textbf{Equation 2.10}$$

Do note that this equation differs slightly from the equation used by Bowen & Welfoot (2002) and Déon et al. (2007) because they neglected to consider the direction of pressure drop despite expressing the pressure drop from the retentate to the permeate side. The porosity of the membrane, which these two groups neglected, is also represented in this equation. Implicitly, their membranes were modelled as having a porosity of unity, contradicting observations of a dense separation layer on the membrane under microscopy (Tung et al., 2009). A more detailed derivation of this equation is presented in Appendix 8.1.

The magnitude of water flux has been shown to fit well with this Hagen-Poiseuille equation variant (Bowen & Mohammad, 1998; Bowen & Welfoot, 2002), hence the equation should be a good model of solvent flow behaviour through the membrane pore. However there are questions on the quantification of solution viscosity increase, relative to the viscosity in the bulk solution, due to the confinement of solvent molecules in the membrane pore (Bowen & Welfoot, 2002; Silva et al, 2005).

2.2.1.2 Partitioning equation

The partitioning equation describes the probability of finding a solute particle in a pore, which is in contact with the bulk solution of a certain solute concentration. The most commonly used partitioning coefficient is (Bowen & Welfoot, 2002)

$$\frac{\gamma_i c_i}{\gamma_i^0 C_i} = \phi_i exp\left(\frac{-z_i \bar{F}}{\bar{R}T}\Delta\Psi_D\right) \qquad \textbf{Equation 2.11}$$

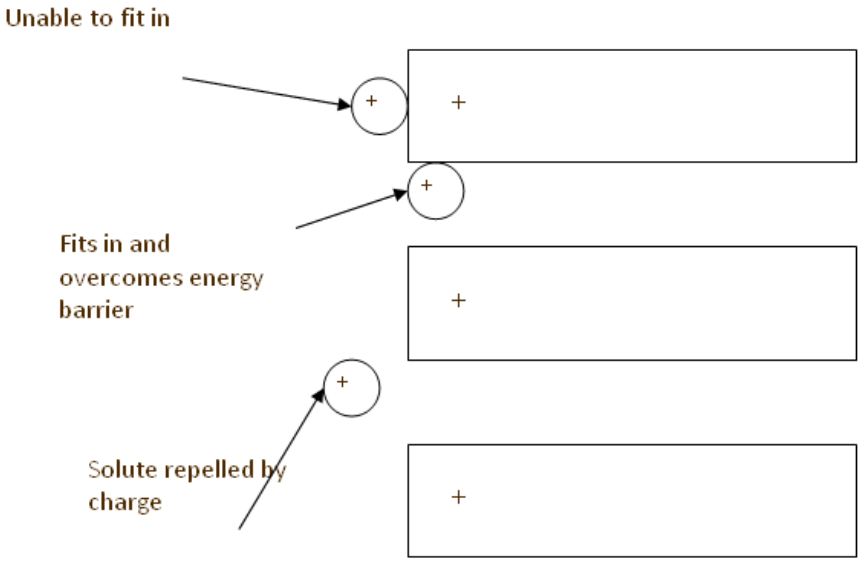

Figure 2.1. Schematic illustrating solute partitioning between the bulk solution and the membrane pore. The solute must overcome steric hindrance, through chance, and charge hindrance, by having sufficient energy, before it can enter a membrane pore for transport across the membrane.

The equation implies that for a solute to enter a pore, it has to both be able to orientate itself into the pore and overcome the energy barrier due to electrostatic interactions between it and the

membrane. A schematic representation is shown in Figure 2.1. The ϕ_i ($\phi_i = (1-\lambda_i)^2, \lambda_i \leq 1$) term represents the steric hindrance to a solute *i* entering a pore. The larger the solute size is relative to the pore size, the lower the concentration of the solute in the pore compared with the bulk solution concentration. When the solute is larger than the pore it will not be possible for solute to enter the pore and the concentration of solute in the pore will always be zero. The exponential term represents the electrostatic energy barrier to the solute entering the pore and accounts for the increasing ease at which a solute can enter a pore if it has attractive interactions with the membrane and the difficulty when there are repulsive interactions.

On the other hand Bowen & Welfoot (2002) proposed the addition of an extra exponential term to account for the theoretical increase in difficulty for the solvation of ions in the pore, modifying Equation 2.11 to

$$\frac{\gamma_i c_i}{\gamma_i^0 C_i} = \phi_i exp\left(\frac{-z_i F}{\bar{R}T}\Delta\Psi_D\right) exp\left(\frac{-\Delta W_i}{kT}\right) \qquad \textbf{Equation 2.12}$$

This additional term will always be smaller than unity if the orientation of solvent molecules at the pore wall leads to a reduction of dielectric constant, and therefore increases the energy barrier to ion salvation in the pore (Bowen & Welfoot, 2002). This additional term calculated from the Born model becomes more significant when an ion is larger, representing the relative difficulty for a larger ion to be solvated into the pore. This is similar to the steric hindrance factor, but is only in effect when the solute is charged. The equation suggests that the hindrance to an ion will be larger than an uncharged solute of equivalent size.

An important feature of the DSPM is that the ions of an electrolyte are partitioned individually hence the constituent ions of a salt can be split. While the studies on application of the DSPM by Bowen & co-workers (Bowen & Mohammad, 1998; Bowen & Welfoot, 2002) and Déon et al. (2007) have been limited to strong neutral inorganic salts that can be considered fully ionized in solution, Antonucci et al. (2002) demonstrated the displacement of benzenesulfonate ions with chloride ions through the diafiltration of the benzenesulfonate salt of an API with a LiCl solution, giving strong evidence that the ions in an organic salt can be split. Furthermore, the work of Antonucci et al. (2012) showed that even if one of the ions is non-permeating, the permeating counterion can still be transported through the membrane, possibly with the counter or co-transport of a more mobile and permeable H^+ ion (Nghiem et al., 2005) across the membrane to maintain charge neutrality.

2.2.1.3 Solute transport equation

The equation used to describe solute transport across the pore is the hydrodynamic model, modified to include hindered convection and diffusion within the pores as shown below. Equation 2.13, derived and proposed by Anderson and Quinn (1974) and Deen (1987), assumes that the solute molecules are hard spheres in dilute solution. The equation was derived from the balance of the chemical potential of a solute, as it moved along the pore, and the drag force on the solute.

$$j_i = \frac{-c_i D_{i,p}}{\bar{R}T}\frac{d\mu_i}{dl} + K_{i,c} c_i \upsilon_p \qquad \textbf{Equation 2.13}$$

The solute diffuses at a slower rate through the membrane pore than through the bulk solvent. The bulk diffusivity of the solute is modified by the hindrance factor for diffusion to obtain this lowered pore diffusivity (Equation 2.14).

$$D_{i,p} = K_{i,d} D_{i,o} \qquad \textbf{Equation 2.14}$$

The hindrance factor for diffusion, for a range of solute radius to pore radius ratios, has been determined using finite element techniques with a centre-line approach for a spherical solute moving inside a cylindrical pore of infinite length and fitted to an empirical model (Bowen & Mohammad, 1998) as shown below.

$$K_{i,d} = \left(1.0 - 2.30\lambda_i + 1.154\lambda_i^2 + 0.224\lambda_i^3\right) \qquad \textbf{Equation 2.15}$$

Solute transport via viscous flow with the solvent is also hindered. The hindrance factor for convection of solute *i* in the pore, determined using the same method as the hindrance factor for diffusion, is shown in Equation 2.16.

$$K_{i,c} = (2 - \phi_i) \times \left(1.0 + 0.054\lambda_i - 0.988\lambda_i^2 + 0.441\lambda_i^3\right) \qquad \textbf{Equation 2.16}$$

The change in potential across the pore is a result of the change in activity (due to the concentration gradient across the pore), pressure (due to the application of a higher pressure on the retentate side) and electrical potential (due to the interaction of charged particles, if any, with the membrane) across it. Hence Equation 2.13 can be expanded to Equation 2.17.

$$j_i = \frac{-c_i D_{i,p}}{\gamma_i}\frac{d\gamma_i}{dl} - D_{i,p}\frac{dc_i}{dl} - \frac{c_i D_{i,p}}{\bar{R}T} v_i \frac{dp}{dl} - \frac{c_i D_{i,p}}{\bar{R}T} z_i \bar{F}\frac{d\Psi}{dl} + K_{i,c} c_i v_p \quad \textbf{Equation 2.17}$$

It can be deduced from the model that a lower potential gradient across the pore will result in slower transport across the membrane. Also, according to the Wilke-Chang correlation, diffusivity is inversely proportional to the power of 0.6 of the partial molar volume of the solute and proportional to the square root of the product of the molecular weight of the solvent and the association factor between the solvent and the solute (See Toh et al., 2007b). Hence through the use of a larger solute or the use of a solvent which has low affinity for the solute, diffusivity can be decreased to lower the potential gradient across the pore.

Additionally, if the solute concentration in the pore was low to begin with, solute transport across the pore would be low due to the unfavourable convective transport (denoted by the last term in Equation 2.17) and slow diffusion caused by a low chemical potential gradient across the pore (denoted by the other terms in the equations). This can be achieved through increasing the sieving of the solute by increasing its size or its repulsive interaction with the membrane pore.

Analytically Equation 2.17 can be solved when there is no change in the activity coefficient and if the solute in question was uncharged. Rejection of solute *i* in this single stage can be expressed as

$$R_{i,s} = 1 - \frac{C_{i,p}}{C_{i,r}} = 1 - \frac{\left(\frac{K_{i,c} + Y_i}{\varepsilon}\right)\phi_i}{1 - \left[1 - \left(\frac{K_{i,c} + Y_i}{\varepsilon}\right)\phi_i\right] exp\left(-Pe_i'\right)} \quad \textbf{Equation 2.18}$$

Where

$$Y_i = \frac{D_{i,p}}{\bar{R}T} v_i \frac{8\eta}{r_p^2} \quad \textbf{Equation 2.19}$$

And

$$Pe_i' = \frac{J_p}{D_{i,p}} \Delta l \frac{K_{i,c} + Y_i}{\varepsilon} \quad \textbf{Equation 2.20}$$

This conclusion differs from that of Bowen & Welfoot (2002) because of the difference in sign convention for the solvent transport equation used. In most cases encountered, where the partial

molar volume of solutes are low, the difference in both equations would not make too much of a difference.

Comparison between the use of different variants of DSPM

As an example, glycerol transport through a membrane of thickness of 1000nm, with a uniform pore size of 0.5nm, was determined using both the model proposed by Bowen & Welfoot (2002) and the DSPM proposed in this work. The transmembrane pressure was arbitrarily set at 10bar and a dilute aqueous solution of glycerol was assumed. The hydrodynamic radius of glycerol were obtained from the work of Bowen & Welfoot (2002).

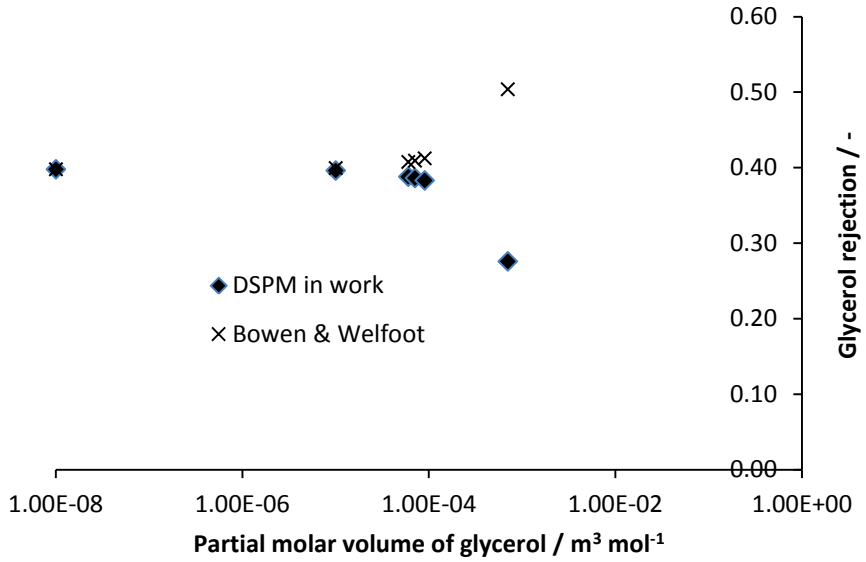

Figure 2.2. Comparison between the glycerol rejections determined by the DSPM model in this work and the DSPM model proposed by Bowen & Welfoot (2002). Note that the predictions by these 2 models converged when the partial molar volume of the solute was low and diverged when it was high.

The rejections of glycerol determined by both models were very similar when the partial molar volume of glycerol (7.08E-5 m^3 mol^{-1}) was used. In fact, the rejection determined using these 2 models converged as the partial molar volume decreased. Only in cases where the partial molar volume was high will the rejection values predicted by both models diverge (see Figure 2.2).

2.2.1.4 DSPM use for OSN

While the DSPM has only been utilised in the aqueous systems (Bowen & Mohammad, 1998; Bowen & Welfoot, 2002; Déon et al., 2007), it is equally capable of correlating experimental data in organic systems. As an example, the model was fitted with experimental data from the work of Peeva et al. (2004) in the filtration of a high concentration docosane-toluene solution across polyimide STARMEM® 122 membranes (See Figure 2.3). Concentration polarisation is known to increase solute concentration on the membrane surface (Peeva et al., 2004) according to

$$c_i = (C_{i,r} - C_{i,p})exp\left(\frac{u}{k_i}\right) + C_{i,p} \qquad \textbf{Equation 2.21}$$

This in turn leads to an observation of a rejection that is lower than the true rejection. Hence for high solute concentrations, concentration polarisation should be accounted for.

Using Microsoft Excel on a laptop computer, Equation 2.18 to Equation 2.20 were simultaneously solved with an iterative method from the initial values of membrane pore radius, membrane thickness and membrane porosity typical in an OSN membrane (Stawikowska & Livingston, 2012). The solute rejections obtained from the equations were compared with the experimental solute rejection and the sum of squares computed. The 3 parameters were modified one by one to obtain the least sum of squares, at which point the iteration was stopped.

The model was largely in agreement with the experimental data though numerous parameters had to be fitted. Due to the number of parameters being fitted, there is also uncertainty in the relative values of each parameter. Accounting for concentration polarisation in the model worsened the fit of the model with experimental data, hence it was not included in the fit. This was probably because the Van't Hoff equation was unable to accurately account for osmotic pressure and the corresponding reduction in pressure driving force through the membrane, as exemplified by the presence of solvent despite the Van't Hoff equation predicting otherwise. In any case, the parameters for the best fit model was

1. Membrane pore radius (0.48nm);
2. Membrane thickness (640nm);
3. Membrane porosity (1.00).

The straight pores assumption and membrane porosity of unity are contradictory to observed membrane structures. Independent determination of the 3 mentioned membrane structural properties, which is beginning to be possible at high resolution (Stawikowska & Livingston, 2012), and using them in the DSPM would be needed to verify the validity of this model.

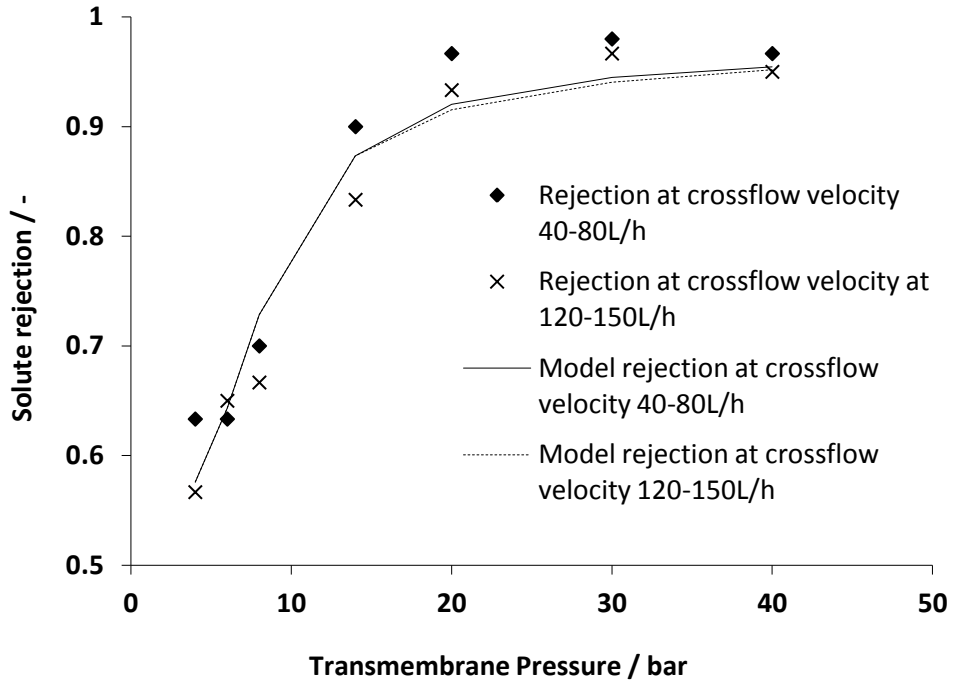

Figure 2.3: Fitting of the DSPM model to experimental rejection of docosane in toluene across STARMEM® 122 membranes. The crossflow velocity seemed to have little influence on the rejection of the solute. Concentration polarisation was not accounted for in this example because accounting for it decreased the convergence between the model and experimental data.

The DSPM predicts that the most straightforward method of increasing rejection is to increase the size of the solute. An increment of solute radius from 0.43nm (the Stoke-Einstein radius of docosane in toluene) to 0.48nm gradually increases the rejection of the solute at all pressures towards unity (See Figure 2.4). On the other hand, total rejection through charge exclusion, while not obtainable mathematically, may be approached if charge exclusion effects are high enough. Strategies to increase solute retention based on these hypotheses were tested and are presented in Chapter 3.

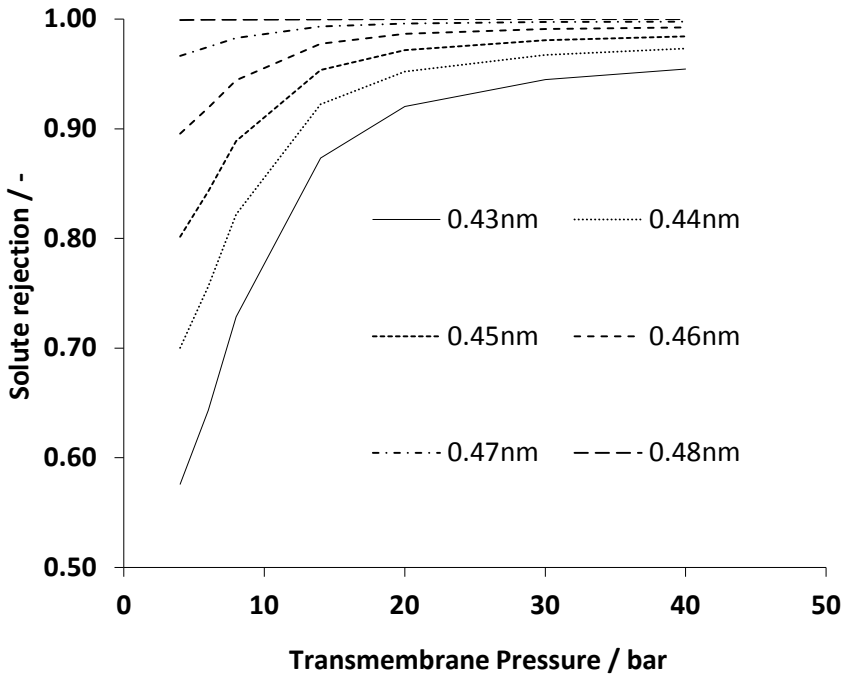

Figure 2.4 Calculated increase in solute rejection in a toluene solution as the solute radius increases from 0.42nm to 0.48nm, for a membrane containing cylindrical pores of 0.48nm radius. When the size of the solute is the same as the pore, total rejection of the solute occurs.

2.2.2 Application of molecular dynamics to DSPM

Solvent flux has often been the main variable used in DSPM model fitting (Bowen & Welfoot, 2002; Déon et al., 2007). An *a priori* determination of solvent flux through a membrane can be used in conjunction with the DSPM as a predictive tool for membrane performance, provided that the structural properties of the membrane (pore size, membrane thickness, tortuosity, porosity) can be defined accurately. The simple Hagen-Poiseuille equation (Equation 2.10) has been used to model water fluxes through aqueous membranes (Bowen et al., 1997; Bowen & Mohammad, 1998; Bowen & Welfoot, 2002; Déon et al., 2007) and may be used for membrane flux prediction. The applicability of this equation to OSN was investigated by plotting the fluxes of various solvents through a polyimide Starmem® 122 membrane at 30bar and 30˚C (Rundquist, 2011) against the inverse of the dynamic viscosities of these solvents. While the equation predicted that the flux of a solvent through a membrane was inversely proportion to the solvent's viscosity, this was not always the case in the study (See Figure 2.5). For example, methanol permeated almost 4 times as much as toluene despite

having a slightly higher viscosity. Bowen & Welfoot (2002) hypothesised that the solvents constrained in a membrane pore have much higher viscosities than the bulk solvent. They proposed an arbitrary method to quantify this increase which leads to solvents with larger sizes having higher increases in viscosity. However, the use of this method was unable to account for the higher pore viscosity of toluene compared to methanol to justify the decreased toluene flux.

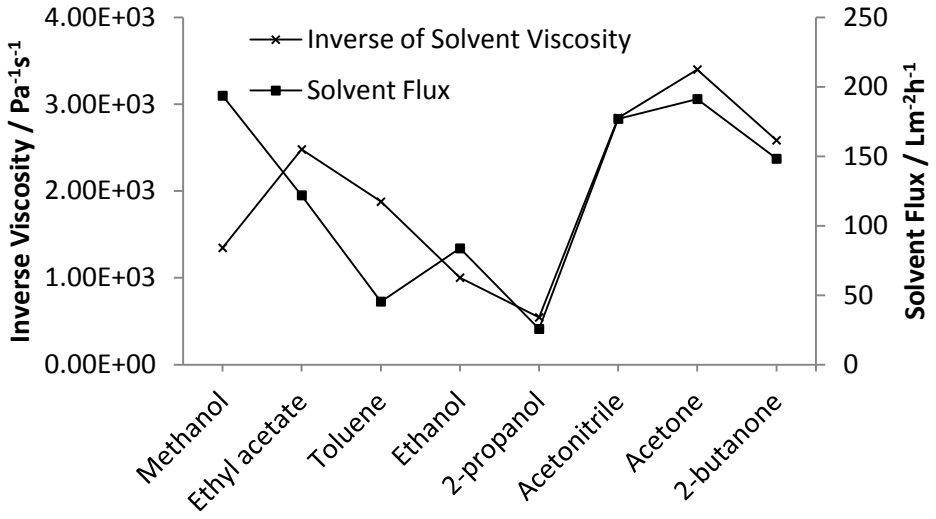

Figure 2.5: Fluxes of various solvents through Starmem® 122 at 30bar, with solvent temperature maintained at 30˚C. The inverse of the solvent viscosities at 30˚C are plotted for comparison with the fluxes. If the Hagen-Poiseuille equation is valid, the values for inverse of viscosity and corresponding fluxes should correlate perfectly. (Data source: Peeva et al., 2004)

A more accurate method for the determination of solvent flux, at least its order of magnitude, using easily available solvent physical properties was sought. Molecular dynamic has been used to model gas permeation through porous coal beds (Salih, 2010) and has the potential to be used in place of the Hagen-Poiseuille for solvent flux prediction through porous OSN membranes.

2.2.2.1 Simulation method

Simulations were performed using a Fortran programme written by Avendano Jimenez & Frentrup (2010). The membrane was envisioned to be made up of straight slit pores, with each wall of the pore being a hexagonally packed closed lattice formed with benzene molecules. The programme was used to form the structured walls of the pore and the solvent molecules were inserted into the

remaining space of the wall using a Monte Carlo type sequence until the specified solvent density was fulfilled. Following which, a force in the x-direction was exerted in a region at the end of the pore on the molecules there. As periodic boundary conditions were used, molecules leaving one end of the pore return from the other end. The number of molecules traversing the reference line in the middle of the pore in the x-direction was counted to determine the solvent flux in the simulations. Interactions between the solvent molecules and between the pore wall and solvent molecules were determined with the Lennard-Jones potentials, truncated and shifted at 2.5σ to reduce the computational effort required for the simulations. The potential well and σ of the Lennard-Jones potential were estimated using the critical temperature and critical volume of the molecules simulated, respectively. Simulations were performed for up to 3 000 000 time steps until the system approached steady state. The simulations took up to 2-14 days each on a laptop computer.

The permeation of methanol, toluene and acetone through Starmem® 122 were simulated and compared with experimental data to determine the relative accuracy of the simulations.

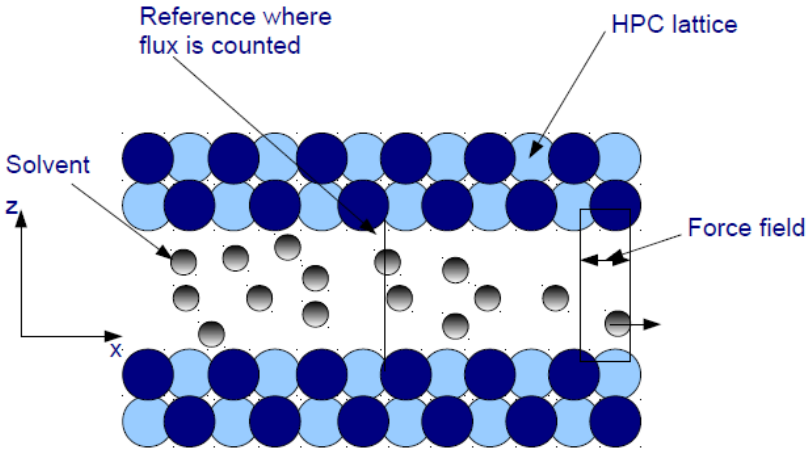

Figure 2.6: Schematic of slit pore and solvent molecules in the pore. A force was applied in the simulation in the force field to push the solvent molecules in the x-direction. The number of solvent molecules traversing the reference point, in the x-direction, in the middle of the pore was counted at each frame to determine the solvent flux through the pore at each discrete time step.

2.2.2.2 Simulation results

The solvents' permeations were first simulated at 30bar and 30˚C. The absolute values of the flux were 10^{16} order lower than experimental data. The order of flow was also not in the correct order for toluene relative to acetone and methanol (Compare Figure 2.5 with Figure 2.7). Simulations were done for an increased pressure of 60bar and membrane permeability was determined via an interpolation between solvent fluxes at these 2 pressures. Methanol had a much higher permeability than toluene, in agreement with experimental data. However, acetone had little flux at both pressures, resulting in almost zero permeability and not in agreement with experimental data.

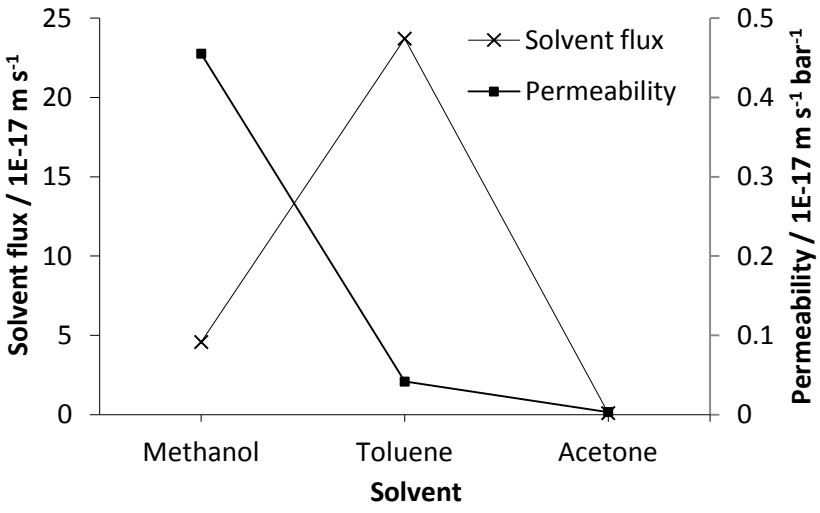

Figure 2.7: Solvent flux simulated at 30bar and membrane permeability for the solvents for pressures between 30-60bar. Solvents simulated were methanol, toluene and acetone. (Data source: Rundquist, 2010)

2.2.2.3 Use in process development

The programme was unable to give an accurate prediction of solvent flux at the specified pressure. While it has been shown to provide a decent estimate for the order of permeability of methanol and toluene through a membrane, the amount of time required for simulation was high. Comparatively, experimentation for solvent flux determination was faster, with each experiment requiring only a few hours, and inspired more confidence since the results were tangible. The use of molecular dynamics will likely be attractive, compared to direct experimentation, only when simulation times

can be significantly reduced to the order of minutes. As such, further development of this tool was not pursued.

2.3 Conclusion of transport model

Various transport models have been presented with emphasis on the DSPM as it related membrane transport to structural properties of the membrane. The DSPM predicts that increased membrane retention can be achieved through increased steric hindrance by increasing the size of the solute, or through increased electrostatic sieving by increasing the charge on the solute. These strategies have been pursued and are presented in Chapter 3.

The use of the DSPM and molecular dynamics to produce a predictive tool for membrane transport has been presented. The DSPM would require more work with independently determined membrane structural characteristics to validate the model. The molecular dynamics approach to solvent transport prediction was time consuming compared to conventional experimental determination of solvent flux. Furthermore its accuracy was not satisfactory. Unless the computational time and accuracy can both be improved, it will unlikely be an option in research development in the pharmaceutical industry.

3. Process Modification with Process Chemistry

The DSPM suggest that an increase in solute rejection can be achieved with an increase in solute exclusion from the membrane pore. Such an increase would require either a change of solute charge or an increase in the size of the solute. Through the use of process chemistry, either of these changes is possible. In the first part of this chapter, pH manipulation as a technique to increase solute rejection is reviewed. A demonstration of how this technique was used to improve NF of 2 similarly-sized solutes is also presented. Later in the chapter, methods used to enlarge solutes are reviewed and presented. Following which, a variant of such a method, termed polyalkylation, is presented to showcase how it can be used to increase the membrane retention of an organocatalyst, hence improving its separation from the reaction mixture.

3.1 Manipulation of Solute Rejection with pH

It has been observed that NF membranes allow easy permeation of monovalent ions while rejecting most multivalent ions through charge exclusion (Bowen & Welfoot, 2002; Déon et al., 2007). This phenomenon has been used in the demineralization of whey (Cuartas-Uribe et al., 2007), dyes (Bowen & Mohammad, 1998) and water (Van der Bruggen et al., 1999).

In the case when the solute is not charged, pH manipulation can be used to induce a charge. This has been used to improve the retention of an alkaline API, sulfamethoxazole (SMX), in water through a relatively loose polyamide NF-270 membrane (Nghiem et al., 2005). The polyamide membrane contained both ionisable carboxylic and amine functional groups, and as a function of pH became more positively charged as pH decreased and negatively charged as pH increased (Childress & Elimelech, 1996; Childress & Elimelech, 2000). The retention of SMX remained almost constant at 0.20-0.30 in pH range 3.5-5.0 before rising rapidly to above 0.90 at pH8.0. This coincided with the increased anionic speciation of SMX from pH4.0-8.0 (See Figure 3.1) and the increase in negative charge character of the membrane at pH above its isoelectric point of about pH3.5 (Nghiem et al., 2005). The observation was in agreement with the increased “sieving” effect of SMX at pH>5.0 predicted by the partitioning equation.

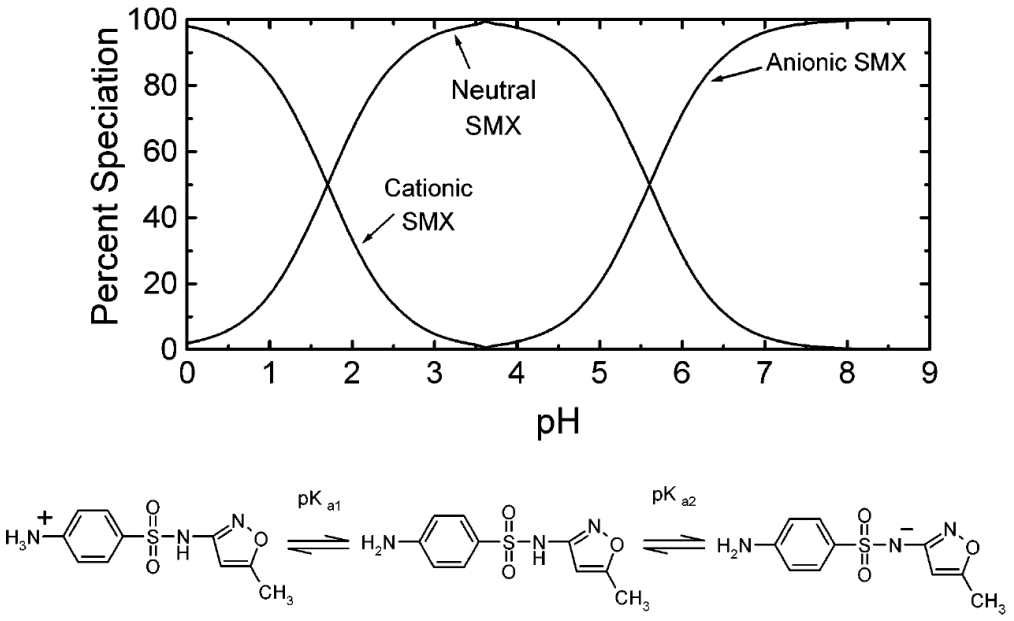

Figure 3.1 Speciation of the amino acid SMX. Source: Nghiem et al., 2005

A similar process which was used to improve NF performance in the purification of an acidic API, 2,3,4,5-tetrahydroxy-6-sulfooxy hexanoic acid (THSH), from a crude product mixture containing an amino acid impurity, dimethylglycine (DMG), has been patented (Da Silva et al., 2008). In this process, calcium hydroxide was added to the crude product to form the calcium salt of THSH, and to increase the pH of the mixture to a range of pH4.5-9.0. The mixture was then diafiltered using a polyamide Desal-5 membrane to flush out DMG while retaining the THSH salt. Examples in the patent application showed that after about 180 diafiltration volumes, all of the dimethylglycine was removed while THSH was enriched. A study of the speciation showed that in the pH range dictated by the patent application, DMG exists predominantly in the uncharged zwitterionic form, whereas the bivalent anionic form of THSH dominates (Figure 3.2). The Desal-5 membrane used has an isoelectric point of pH4.0, hence the membrane was negatively charged in the operating pH range (Hagmeyer & Gimbel, 1998). Therefore, while the “sieving” effect of the uncharged DMG was neither augmented nor suppressed due to the lack of electrostatic interactions with the membrane pores, the negatively charged bivalent THSH anions encountered repulsive electrostatic interactions with a negatively charged membrane surface which increased the “sieving” and rejection of THSH.

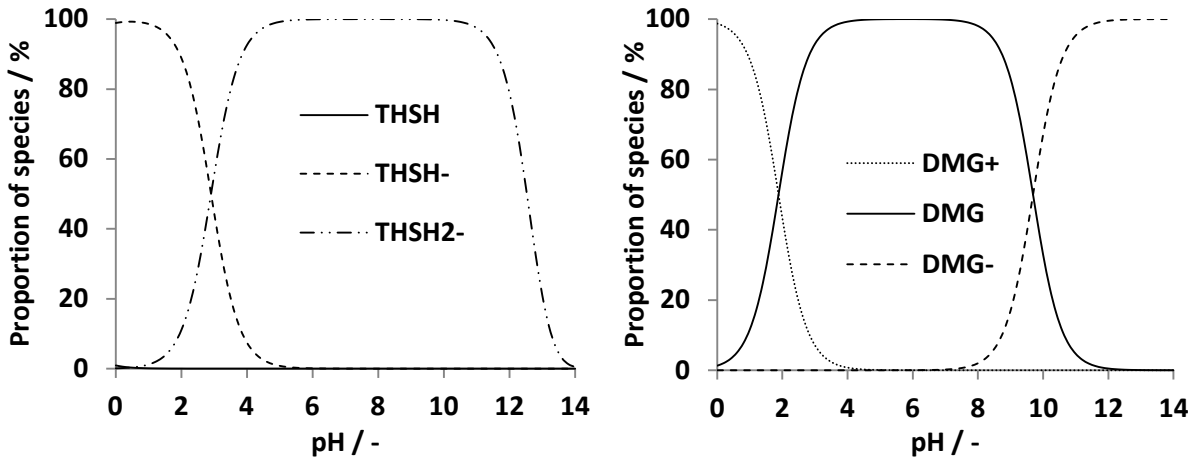

$$THSH \overset{K_{a1}}{\longleftrightarrow} THSH^{-} \overset{K_{a2}}{\longleftrightarrow} THSH^{2-}$$

$$DMG^{+} \overset{K_{a1}}{\longleftrightarrow} DMG \overset{K_{a2}}{\longleftrightarrow} DMG^{-}$$

Figure 3.2: Speciation of 2,3,4,5-tetrahydroxy-6-sulfooxy hexanoic acid (THSH) on left and dimethylglycine (DMG) on the right as a function of pH in aqueous solution. Note that THSH is highly ionised at all pHs and only low levels of unionised THSH exists.

While this approach might seem a proven method to improve solute separation in NF, the paucity of examples for it raises questions on its limits and applicability. Hence to investigate its effectiveness, this concept was applied to the NF separation of 2 ionisable and similarly-sized solutes.

3.1.1 Case study and process development

The synthesis of an API at UCB Pharma was possible starting from a racemic N-acetylated amino acid (AMS(DL)). The L-isomer of this compound was selectively deacetylated to the L-isomer of the amino acid, MS(L). Following which, the D-isomer of the compound, AMS(D), and MS(L) were separated before further reactions on AMS(D) could be performed to form the API. Recycling of MS(L) was desired for reduction of waste and cost, therefore a full separation of AMS(D) and MS(L) to high purities was required. This scheme is illustrated in Scheme 3.1. The high water solubilities for both compounds and their similar polarities meant traditional liquid-liquid extraction and crystallisation were not effective for their purification. Hence NF was an attractive technique to evaluate for their separation.

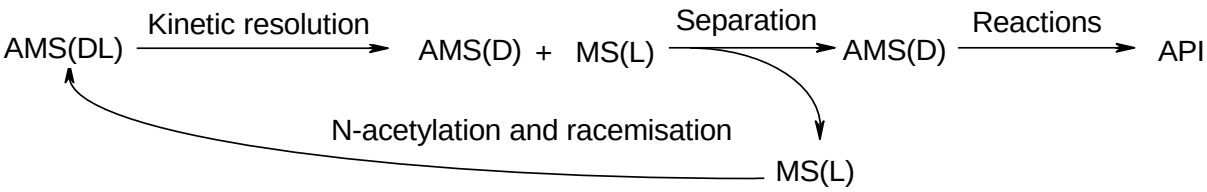

Scheme 3.1: Scheme illustrating production of an API from the racemic mixture of AMS. The racemate was asymmetrically hydrolysed to form the L-isomer of MS. The D-isomer of AMS was then separated out before it could be used in reactions to form the API. The purified L-isomer of MS was reformed back to a racemic mixture of AMS to recycle the MS.

AMS, a strong acid, was known to deprotonate progressively with increasing pH. On the other hand, MS, a zwitterionic amino acid, becomes positively charged at pH's below its isoelectric point (pI) and negatively charged at pH's above its pI. The degrees of ionisation of the 2 compounds are illustrated in Figure 3.3.

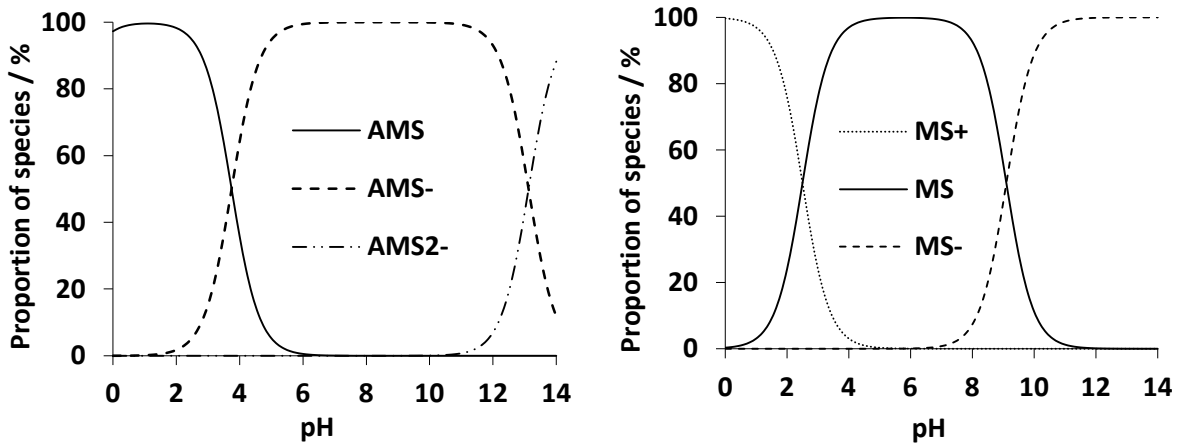

$$AMS \overset{K_{a1}}{\longleftrightarrow} AMS^{-} \overset{K_{a2}}{\longleftrightarrow} AMS^{2-}$$

$$MS^{+} \overset{K_{a1}}{\longleftrightarrow} MS \overset{K_{a2}}{\longleftrightarrow} MS^{-}$$

Figure 3.3: Speciation of AMS, on the left, and MS, on the right, in aqueous solution. In the region pH6.0-7.5, AMS^{-} dominates while MS, in its uncharged form, dominates.

Following the example presented by Da Silva et al. (2008), an operating pH where one solute was uncharged and the other charged had to be chosen. From the speciation diagram (See Figure 3.3),

one can deduce the possible operating pHs were pH0 and in the range pH6.0-7.5. Given the instability of the membrane at extreme pHs, a conscious decision was made to designate the operating pH at about 7.

3.1.2 Results and discussions

3.1.2.1 Effects of charge manipulation on solute retention

An initial investigation on how salt formation between AMS and different bases will affect AMS retention was performed. A relatively loose DuraMem® 300 membrane was used in the NF comparison to elucidate the effect of electrostatic "sieving". Solutions containing AMS and MS at concentrations of 0.025M each were filtered. Bases calcium hydroxide, magnesium hydroxide and quinine were later added to the solutions to investigate the effect of different bases. Bases were used to adjust the pH of the solution from the initial value of 2.8 to 6.8. This pH was chosen as attempts to go above this pH were hard due to the proximity of this pH to the equivalence point.

A large and consistent increase (0.13-0.32) in AMS rejection was observed when any base was added to the solution (Figure 3.4). This was in agreement with the DSPM which predicted that an increase in charge character of AMS increased the hindrance to the "partitioning" of AMS into the pore (Bowen & Welfoot, 2002). The use of different bases, while shown to influence AMS rejection, did not affect the rejection as much as pH effects, with the change in base causing increases of 0.03-0.11 in rejection. Hence the effect of pH was the overriding factor in determining AMS retention. The addition of base was also noted to increase MS rejection (0.06-0.19), but at a smaller extent than for AMS (See Figure 3.5). A consequence of this was a change in membrane selectivity for AMS retention over MS at pH6.8, as opposed to MS retention at pH2.8. This was akin to chromatography, with the membrane acting as a stationary phase that retained solutes at different rates when different diafiltering fluid (mobile phase) conditions were used.

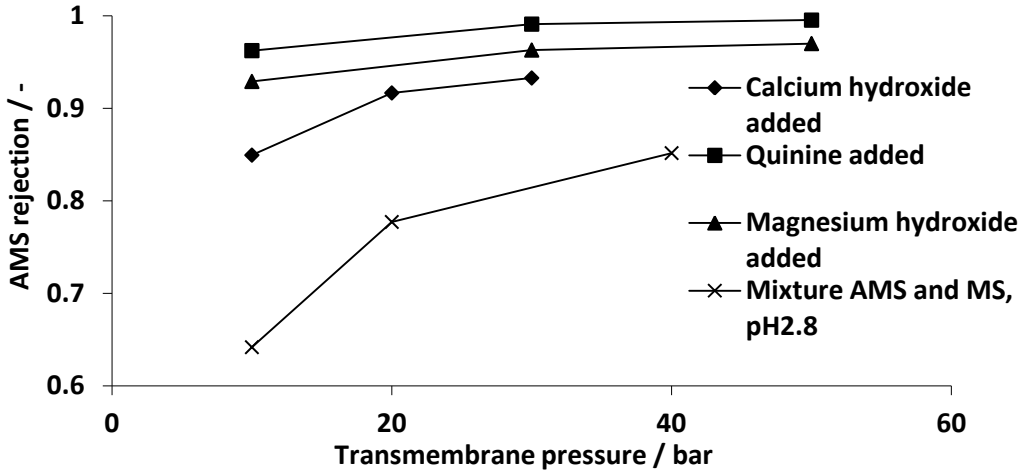

Figure 3.4: Dependence of the rejection of AMS during filtration of an equimolar solution, containing 0.025M AMS and 0.025M MS, on the added bases at various pressures. The bases (calcium hydroxide, quinine and magnesium hydroxide) were added to change the pH of each solution to 6.8. The equimolar solution of AMS and MS, put in the graph for comparison, had a pH of 2.8.

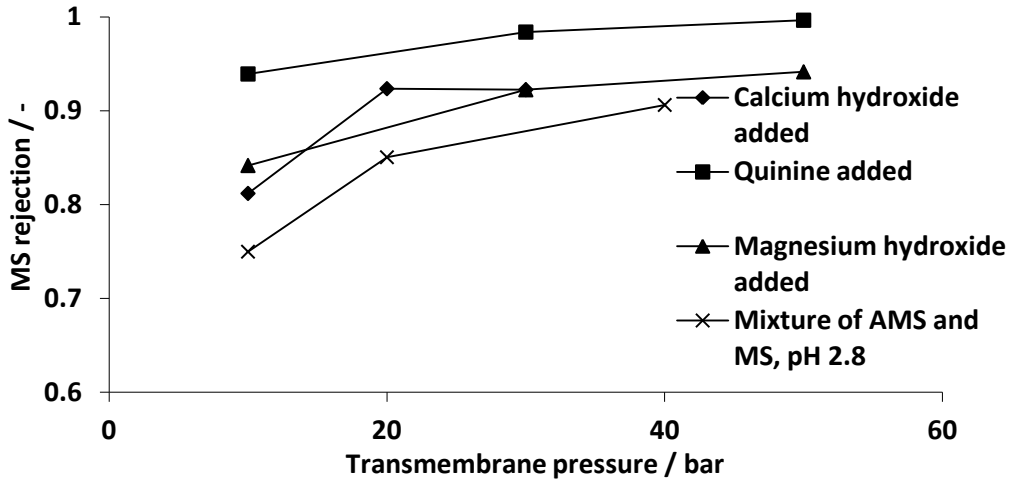

Figure 3.5: Dependence of the rejection of MS during filtration of an equimolar solution, containing 0.025M AMS and 0.025M MS, on the added bases at various pressures. The bases (calcium hydroxide, quinine and magnesium hydroxide) were added to change the pH of each solution to 6.8. The equimolar solution of AMS and MS, put in the graph for comparison, had a pH of 2.8.

While the addition of a base improved AMS retention, it also decreased membrane flux due to an increase in osmotic potential in the retentate which reduced the effective pressure driving permeation through the membrane (See Figure 3.6). A weaker base like quinine resulted in a larger decrease in flux than the stronger mineral bases due to the larger amount of base that had to be added to increase the pH to the same value. About twice the number of moles of quinine had to be added to increase the pH compared to the mineral bases. From this observation, it would seem advantageous to use a strong base in such a rejection augmentation strategy to minimise the amount of base added.

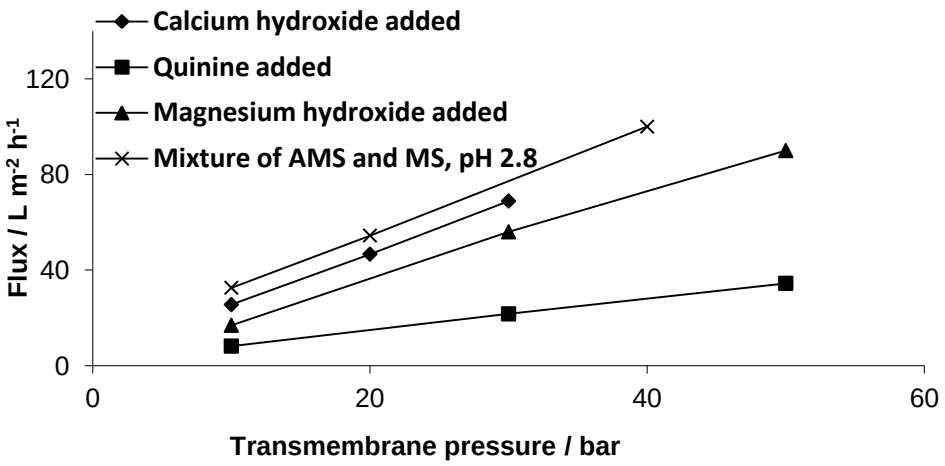

Figure 3.6: Dependence of the solvent flux during filtration of an equimolar solution, containing 0.025M AMS and 0.025M MS, on the added bases at various pressures. The bases (calcium hydroxide, quinine and magnesium hydroxide) were added to change the pH of each solution to 6.8. The equimolar solution of AMS and MS, added to the graph for comparison, had a pH of 2.8.

3.1.3 Application to constant volume diafiltration

A demonstration of how such changes in retention through pH manipulation can be used to improve the diafiltration separation of AMS and MS was carried out. Magnesium hydroxide was used as the base as it increased the rejection of AMS significantly while not diminishing membrane flux excessively. The aim for the separation was to achieve a full separation of AMS and MS using diafiltration because both solutes were desired. The parameters represented by equations 3.1 – 3.4 were used to characterise the performance of the diafiltration process after filtration time, *t*.

The purity of solute *h* enriched in the retentate was expressed by Equation 3.1

$$X_{h,d}|_t = \frac{x_{h,d}|_t}{x_{h,d}|_t + x_{i,d}|_t} \quad \textbf{Equation 3.1}$$

The purity of the enriched solute *i* in the permeate was represented by

$$Y_{i,d}|_t = \frac{\overline{y_{i,d}}|_t}{\overline{y_{h,d}}|_t + \overline{y_{i,d}}|_t} \quad \textbf{Equation 3.2}$$

The yield of the solute *h* enriched in the retentate was expressed as

$$Yield_{h,d}|_t = \frac{x_{h,d}|_t}{x_{h,d}|_0} \quad \textbf{Equation 3.3}$$

The yield of the solute *i* enriched in the permeate was expressed as

$$Yield_{i,d}|_t = 1 - \frac{x_{i,d}|_t}{x_{i,d}|_0} \quad \textbf{Equation 3.4}$$

An acidic retentate caused an enrichment of MS in the retentate while the addition of base to pH6.8 effected an enrichment of AMS in the retentate by increasing the rejection of AMS. One such example is shown in Figure 3.7, where diafiltration over a Desal 5 membrane was performed first without a base and later with a base. In the first case, AMS concentration in the retentate decayed at a faster rate than for MS, while the reverse was true for the 2nd case. The rejections of AMS and MS (See Table 3.1) were obtained by fitting the decrease in concentrations of the individual solutes in the retentate over 15h to Equation 3.5 (Mulder, 1996; Sereewatthanawut et al., 2010), assuming constant rejection throughout the whole diafiltration.

$$x_{i,j}|_t = x_{i,j}|_0 e^{-N|_t(1-R_{i,j})} \quad \textbf{Equation 3.5}$$

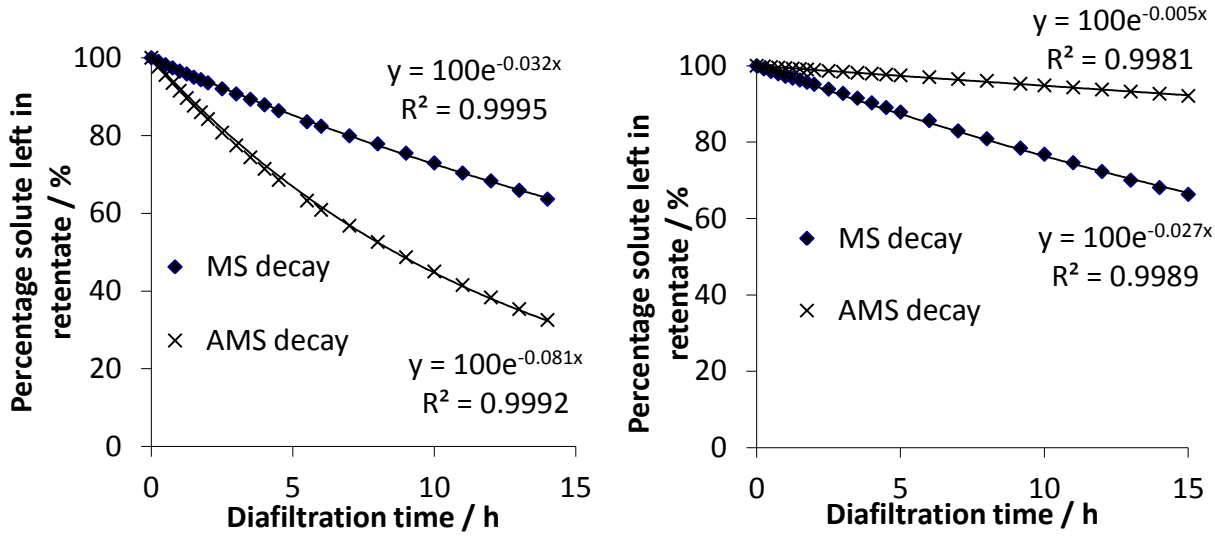

Figure 3.7: Concentration profile in the retentate for AMS and MS during constant volume diafiltration performed for 15h using the Desal 5 membrane; about 15 diafiltration volumes of fresh solvent were used over 15h. The figure on the left shows the solute profile for the diafiltration of an equimolar solution of AMS and MS at pH2.8, with an enrichment of MS in the retentate. The figure on the right represents the diafiltration of an equimolar solution of AMS and MS when $Mg(OH)_2$ was added to increase the pH to 6.8, resulting in an enrichment of AMS

The slow decay in solute concentration meant long separation cycle times and high diafiltration volumes for complete separation (Refer to Table 3.1). Hence simulations were made with the rejection data of the solutes to predict if full separation of the solutes could be accomplished with a single stage constant volume diafiltration. The diafiltrations were designed to enrich the better retained solute in the retentate to a purity of 0.95 from an equimolar solution of AMS and MS. While simulations show that the purity was achievable, the yields of enriched solutes were low for all entries, at between 0.04-0.46. The addition of a base improved the yield of the more retained solute by increasing the retention of the better retained solute by up to 31 percentage points. However, a complete separation was not possible, with even the best separation in Entry 4 producing a permeate stream of 0.65 purity for the more permeable solute (MS in this case). While the yield was high, the purity was too low for use. A full retention of one of the solutes is required to guarantee complete separation. While the addition of more base to increase the pH to 14 so that the bivalent anionic species of AMS dominates might bring the rejection of AMS to unity, this would pose a challenge to equipment design with the DuraMem® series membranes and Desal® series membranes tested to be unstable and dissolving at high pH.

The similar sizes of both solutes, with the MW of AMS being about 40 higher than MS due to the additional acetyl group, resulted in low rejection differences between these solutes which led to large diafiltration solvent requirements (28-130 diafiltration volumes) in all entries. A change in the membrane process used is needed to improve the separation performance and productivity of this process.

Table 3.1: Attempts to separate an equimolar solution of AMS and MS by diafiltration to obtain a retentate stream enriched (purity of 0.95) in the better retained solute. The rejection values of the individual solutes were obtained through model fitting of the decay curves of the solutes. In entries 1-2 where no base was added, MS was enriched in the retentate. For entries 3-5 where $Mg(OH)_2$ was added to adjust the initial solution pH to 6.8, AMS was enriched in the retentate.

No.	Membrane	Base added	Rejection of AMS / -	Rejection of MS / -	Diafiltration volumes / -	Yield of enriched solute in retentate / -	$Y_{i,d}$ / -	Yield of enriched solute in permeate / -
1	DM200	-	0.888	0.955	44	0.14	0.54	0.99
2	Desal 5	-	0.926	0.971	65	0.15	0.54	0.99
3	DM200	$Mg(OH)_2$	0.988	0.962	110	0.26	0.57	0.99
4	Desal 5	$Mg(OH)_2$	0.994	0.971	130	0.46	0.65	0.98
5	DM300	$Mg(OH)_2$	0.886	0.780	28	0.04	0.51	1.00

3.1.4 Summary of results

The targeted formation of solute charge through pH changes was able to increase the rejection of the targeted solute. Such a change caused the selectivity of membrane retention for 2 similarly sized solutes to be reversed. However, it proved insufficient for the complete separation of these solutes when constant volume diafiltration was used.

3.2 Covalent Bonding with an Anchor Molecule

The technique of anchoring a solute to a bulky anchor molecule, to enlarge the solute and increase its membrane retention, has been widely used to improve homogeneous catalyst recycling with NF (Dijkstra et al., 2001). A common approach to this technique involved the use of a polymer chain to anchor a single or multiple catalysts to improve membrane retention of the catalyst (Giffels et al.,

1998; Wöltinger et al., 2001). Monodispersed polymer supported catalysts, however, were tedious to synthesise, in stark contrast with simple one-step procedures which usually produced uncontrollable and polydispersed polymer supported catalysts (Dickerson et al., 2002; Schlenk et al., 2000; Toy & Janda, 2000).

Another approach involved the attachment of catalysts to dendrimers. Dendrimers are tree-like molecules with very well-defined macrostructures whose dimensions are easily altered to allow optimisation of retention of such catalysts while allowing precise catalysts loading to be defined as compared to catalysts attached to polymers (Dijkstra, 2001). Dendritic catalysts have been highly retained by SelRO-MPF-50 NF membranes (Kleij et al., 2000). However, the synthesis of dendrimers that are monodispersed and well-defined also involved expensive and tedious procedures (Schlenk et al., 2000).

In response to the flexibility of dendrimers which prevents the total retention of the attached catalysts, rigid aromatic backbones, synthesised using tedious procedures, were used as anchors instead by Dijkstra and co-workers (Dijkstra et al., 1999; 2001; 2003). They found that an increase in size of a metallic catalyst by anchoring to a rigid backbone led to a proportional increase in membrane retention of the catalyst.

A concern that has not been addressed in all these approaches is the recovery of the original solute from the anchor moiety. Experience in synthesis suggests the addition of reaction steps to anchor a solute and eventually recover the solute would decrease total process yield and make the process inefficient. As such, this anchoring technique might be more relevant to improving catalyst recycle. There is an exception to this statement as the use of PEG as an anchor to a growing peptide chain in lieu of a solid phase support has been demonstrated to improve the process efficiency of peptide synthesis (So et al., 2010).

The relative complexity in synthesising viable anchors makes the development of a simple anchoring strategy an attractive proposition. The strategy for anchoring has largely been fixated on enlarging the anchor as much as possible, with molecular weights often in excess of thousands of Daltons. Enlargement of the anchors have been achieved by adding “spacer” molecules to the anchor, which bear no functional purpose other than to add bulk to the anchor. The work presented below surmises that a more efficient approach to anchoring the target solute exists.

3.2.1 Case study and process development

Despite remarkable advances in the field of asymmetric organocatalysis in the last decade, its industrial application is limited (Berkessel & Groger, 2005; Groger, 2008). O-desmethylquinidine is an organocatalyst used in the asymmetric synthesis of an advanced intermediate (**2**) at UCB Pharma S.A. for the production of a developmental API (See Scheme 3.2). While the catalyst enabled a relatively fast reaction and high enantiomeric selectivity, the catalyst loading required was high (2.5mol% of nitrostyrene loading) and no catalyst recycling scheme was in place. Therefore there was a need to develop a viable catalyst recycling strategy for the scheme.

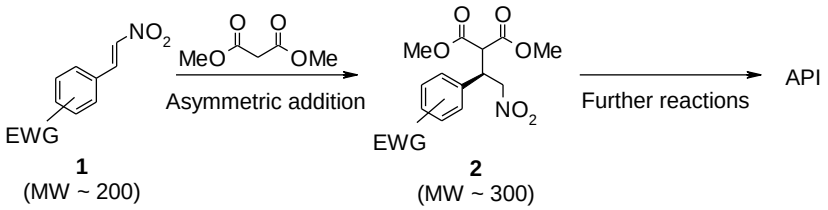

Scheme 3.2: Reaction scheme for the Michael addition of dimethyl malonate to a nitrostyrene, 1, for the asymmetric synthesis of an advanced intermediate, 2, at UCB Pharma S.A.

If heterogeneously supported, the organocatalyst can be easily recycled via solid-liquid separation (Han & Janda, 1997b). However, heterogeneous catalysts tend to have reduced catalytic activities and selectivities, while costing more than non-supported catalysts.

O-desmethylquinidine, derived from cinchona alkaloids, has multiple loci where modifications can take place (See Figure 3.8). These loci make the catalyst versatile as multiple anchoring strategies can be explored. The versatility of this class of organocatalyst extends to its utility. Depending on the modifications made, the resulting catalyst can be used for either Michael addition (Chen et al., 2007; Dixon & Hynes, 2005; Li et al., 2004; Li et al., 2005), phase transfer catalysis (Park & Jew, 2009; Lee et al., 2007; Park et al., 2001; Park et al., 2009) and asymmetric dihydroxylation (Hajamis et al., 1999; Han & Janda, 1997a; Han & Janda, 1997b; Zhang et al., 1999).

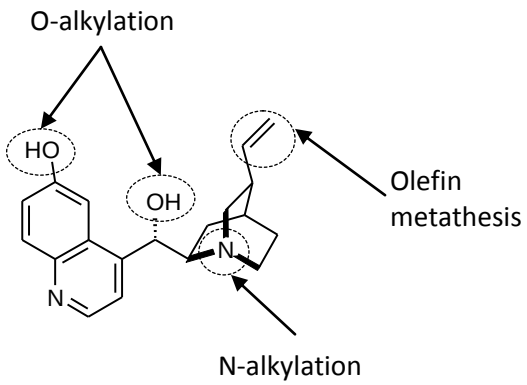

Figure 3.8: Structure of O-desmethylquinidine and potential modification site indicated by dotted circles.

The core business of UCB Pharma SA is not in catalyst development, hence the commercial availability and the simplicity of the anchor molecule were key considerations in developing an enlargement strategy for O-desmethylquinidine. To this end, 4 commercially available anchor candidates were chosen for, in 3 different approaches to enlarge the organocatalyst. These approaches were

1. Olefin metathesis, using either quinidine or 1-dodecene as the anchor;
2. PEGylation, using polyethylene glycol (PEG) as the anchor;
3. Polyalkylation, using 1,3,5-tris(bromomethyl)benzene as the anchor.

3.2.1.1 Olefin metathesis

Cross metathesis of the double bond (Pariya et al., 1998), first attempted with only quinidine (See Scheme 3.3), to ascertain if a coupling of quinidine would result from the catalytic effect of the Grubb's catalyst was unsuccessful with no reaction observed.

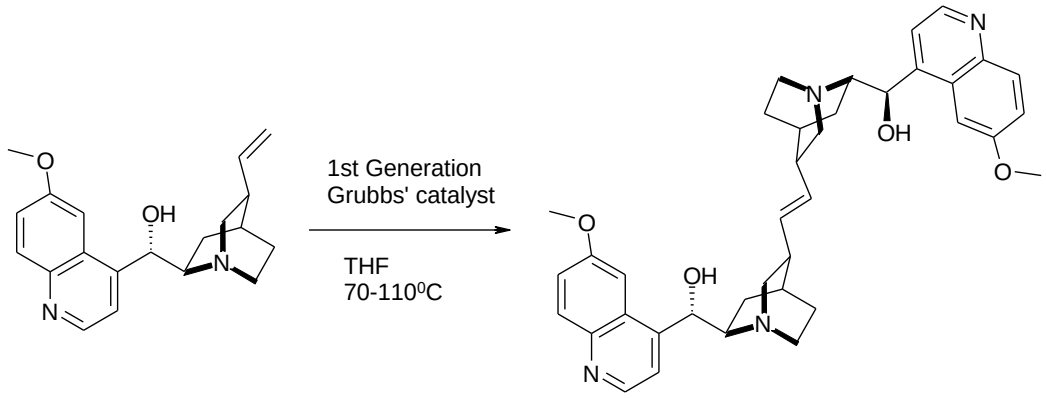

Scheme 3.3: Attempted metathesis of quinidine. The yield for this reaction was very low.

Further cross metathesis was attempted between 1-dodecene and quinidine (See Scheme 3.4). However, the yield was low, with only 3% of the original quinidine converted. Therefore this approach was aborted.

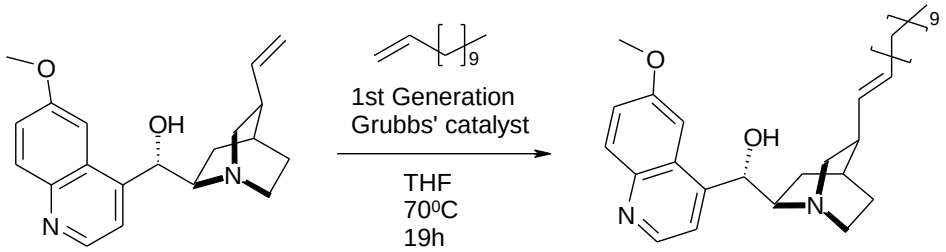

Scheme 3.4: Attempted metathesis of quinidine with 1-dodecene. No discernible reaction occurred.

3.2.1.2 PEGylation

PEGylation of quinidine (Danelli et al., 2003; Ghoshal et al., 1998) was attempted via a commercially available alkylating PEGylating agent with an average molecular weight of 2000 (See Scheme 3.5). The yield was low, with 24% of the quinidine converted, due to competing side reactions of the PEGylating agent with sodium hydride (NaH) to form polyethylene glycol (PEG) and sodium bromide. On the other hand, the PEGylating agent was not monodispersed which made control of the size of the enlarged catalyst impossible. For these reasons, this approach was not developed further.

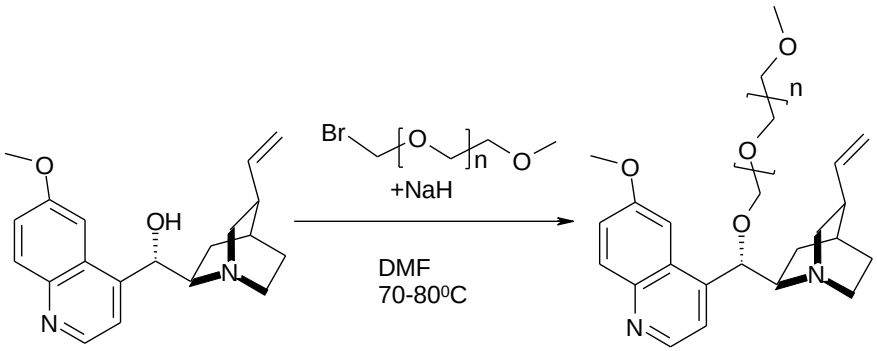

Scheme 3.5: PEGylation of quinidine with a brominated PEGylating agent. The yield for this reaction was very low.

3.2.1.3 Polyalkylation

Polyalkylation, which was a modification of the other 'anchoring' strategies (Chen et al., 2008; Chen et al., 2010; Yan et al., 2009), was attempted to increase the amount of catalyst loaded in each enlarged catalyst moiety and reduce the amount of non-functional 'spacers' in the enlarged molecule. This was achieved by attaching multiple organocatalyst to every 'anchor' molecule. The commercial availability of the alkylating 1,3,5-tris(bromomethyl)benzene influenced the choice of it as an anchor. Additionally, the stiffness of the short bond between the catalyst and the benzene backbone would decrease the flexibility of the resulting molecule, maintaining the increased size of the catalyst at all orientations.

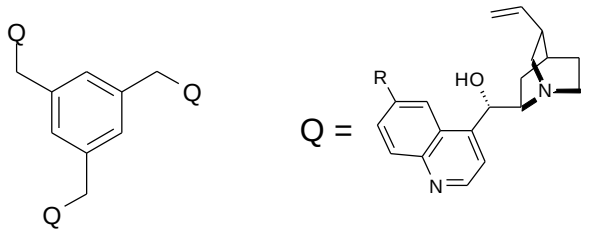

Figure 3.9: Concept of polyalkylation. Multiple molecules of the organocatalyst are attached to a 1,3,5-tris(methyl)benzene anchor by alkylation. In effect the molecular weight of the resulting catalyst is a multiple of the number of catalysts attached.

The versatility of this approach is aptly illustrated in Scheme 3.6, which shows the various enlarged catalysts synthesized. Quinidine, a low cost and commercially available cinchona alkaloid, was easily transformed to 4 different enlarged catalysts in 1-2 steps.

The synthesis of the advanced intermediate (Scheme 3.2) had to be performed in THF. Hence the new catalyst had to be soluble in THF for membrane recycling. Only **5** – **7** fulfilled this requirement and were tested further for membrane retention and catalytic performance, along with quinidine (**3**) and O-desmethylquinidine (**4**). The results from these tests are described in sub-Sections 3.2.2 to 3.2.4.

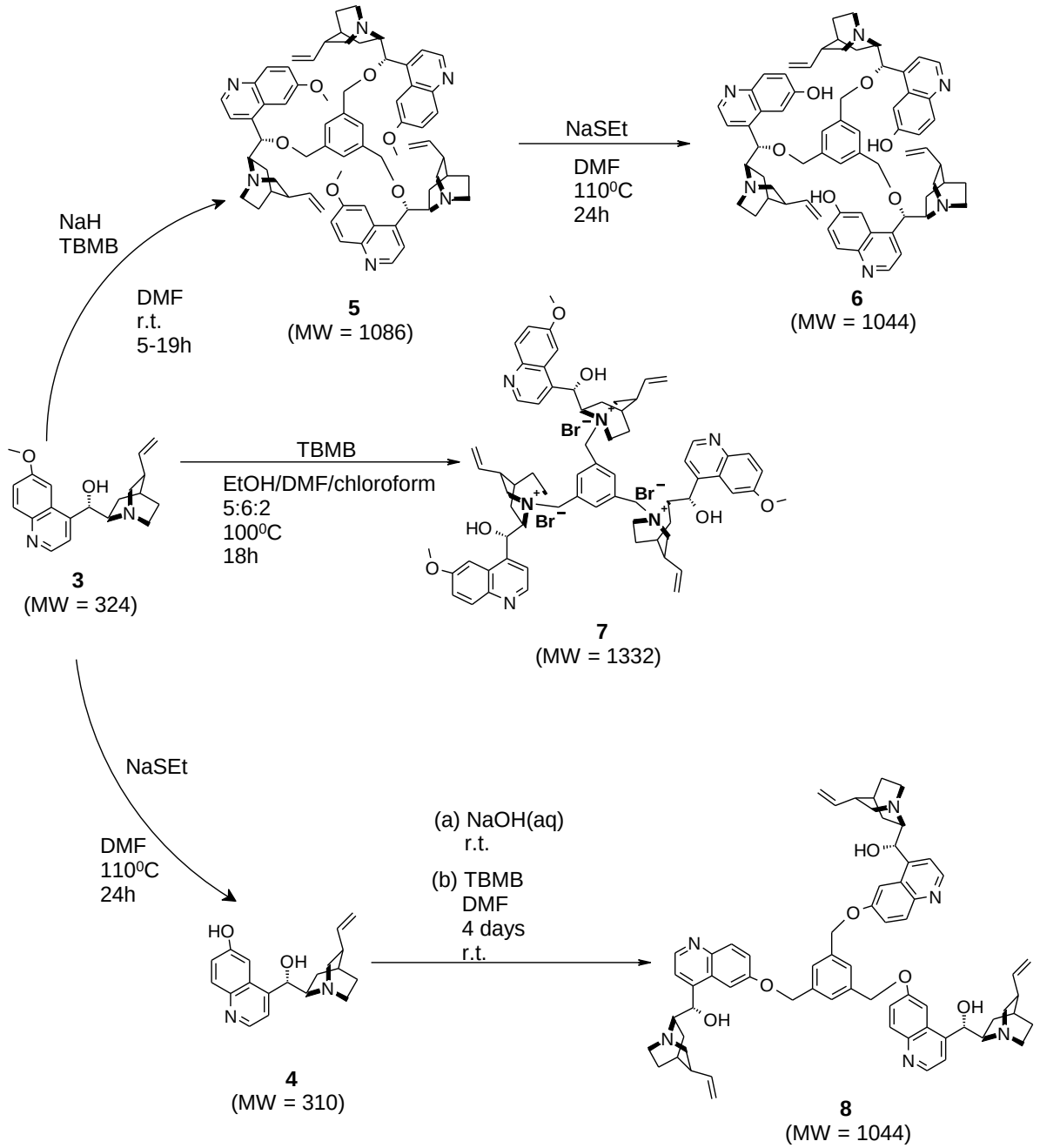

Scheme 3.6: Synthesis routes for the various catalysts from commercially available quinidine. NaH = sodium hydride, NaSEt = sodium ethanethiolate. TBMB = 1,3,5-tris(bromomethyl)benzene.

3.2.2 Membrane retention of catalyst

All the compounds listed in Scheme 3.6, less **8**, were tested on the loosest membranes available in the inventory at the time of catalyst synthesis, DuraMem® 500 and DuraMem® 300. The use of a single membrane stage for catalyst recycle necessitated a catalyst rejection approaching unity, with high solvent flux through the membrane a secondary quality sought after.

The newly polyalkylated catalysts (**5** – **7**) had almost consistently higher rejections than the non-polyalkylated catalysts (quinidine and O-desmethylquinidine). This proved that polyalkylation was a feasible strategy for rejection enhancement. However, polyalkylation alone was not necessarily sufficient in enhancing rejection to the required level; only **6** and **7** had membrane rejections approaching unity on both membranes.

O-desmethylquinidine, formed from the demethylation of quinidine, was better retained than quinidine by DuraMem® 500 and DuraMem® 300. The effect of demethylation was also apparent in the polyalkylated catalyst. **6** was rejected at a substantially higher level than **5** on both DuraMem® 500 and DuraMem® 300 membranes. This might be due to the ability of the phenolic hydroxyl group in forming hydrogen bonds with THF, giving the catalysts with the phenolic hydroxyl group a larger hydrodynamic radius compared to catalysts with the methoxy group.

Charge formation, which was previously shown in Section 3.1 to increase solute retention, unsurprisingly increased catalyst rejection. While the electrically neutral **5** had a lacklustre rejection value, the presence of the trivalent charge in **7** caused an elevation of rejection which approached unity.

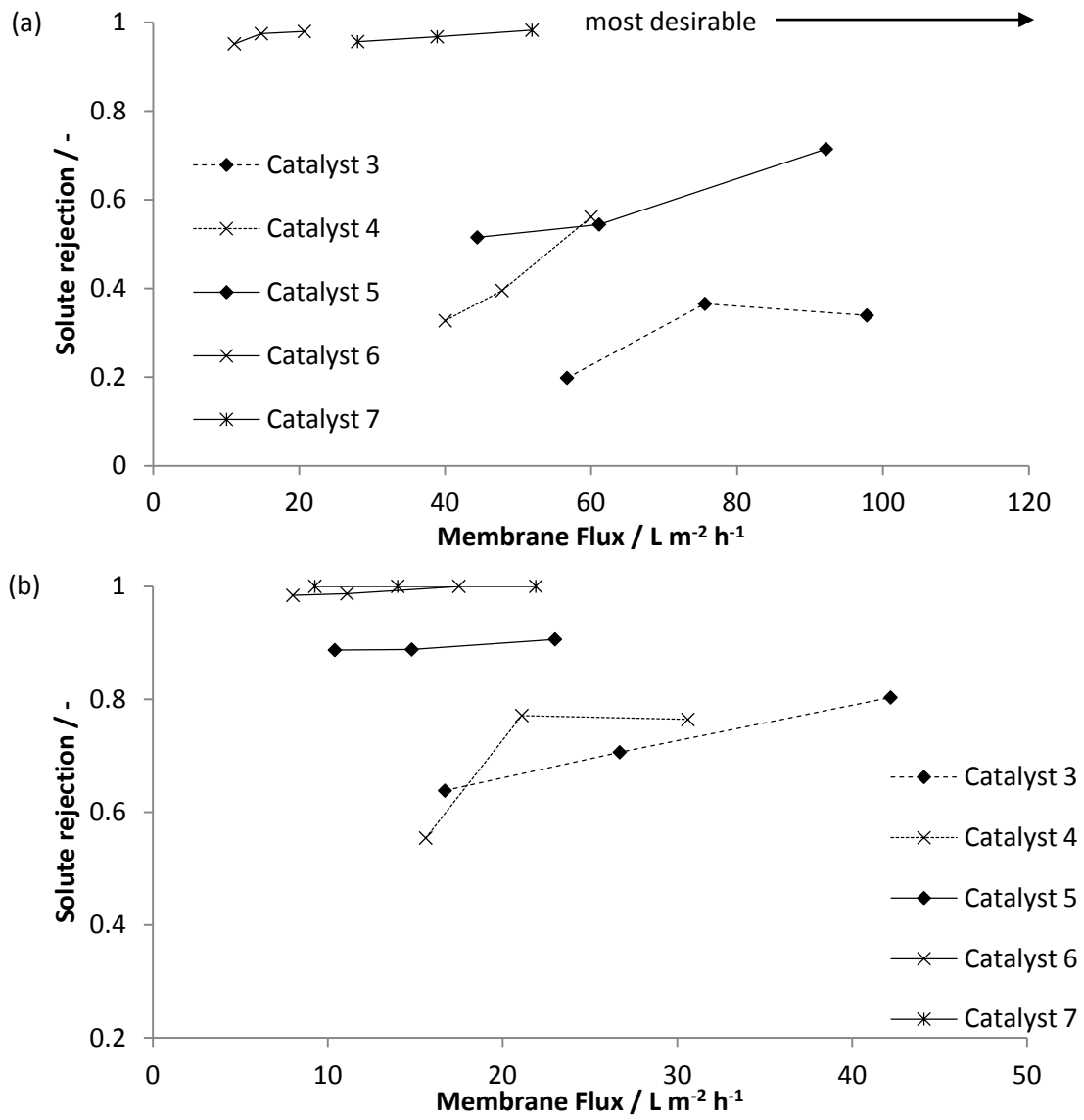

Figure 3.10: (a) Rejection and flux data of the various catalysts from recirculation experiments of individual catalyst solutions in THF across DuraMem® 500 flatsheet membranes. (b) Rejection and flux data of the various catalysts from recirculation experiments of individual catalyst solutions in THF across DuraMem® 300 flatsheet membranes. The most desirable membrane-solute combination possesses both a high membrane flux and solute rejection that is at unity.

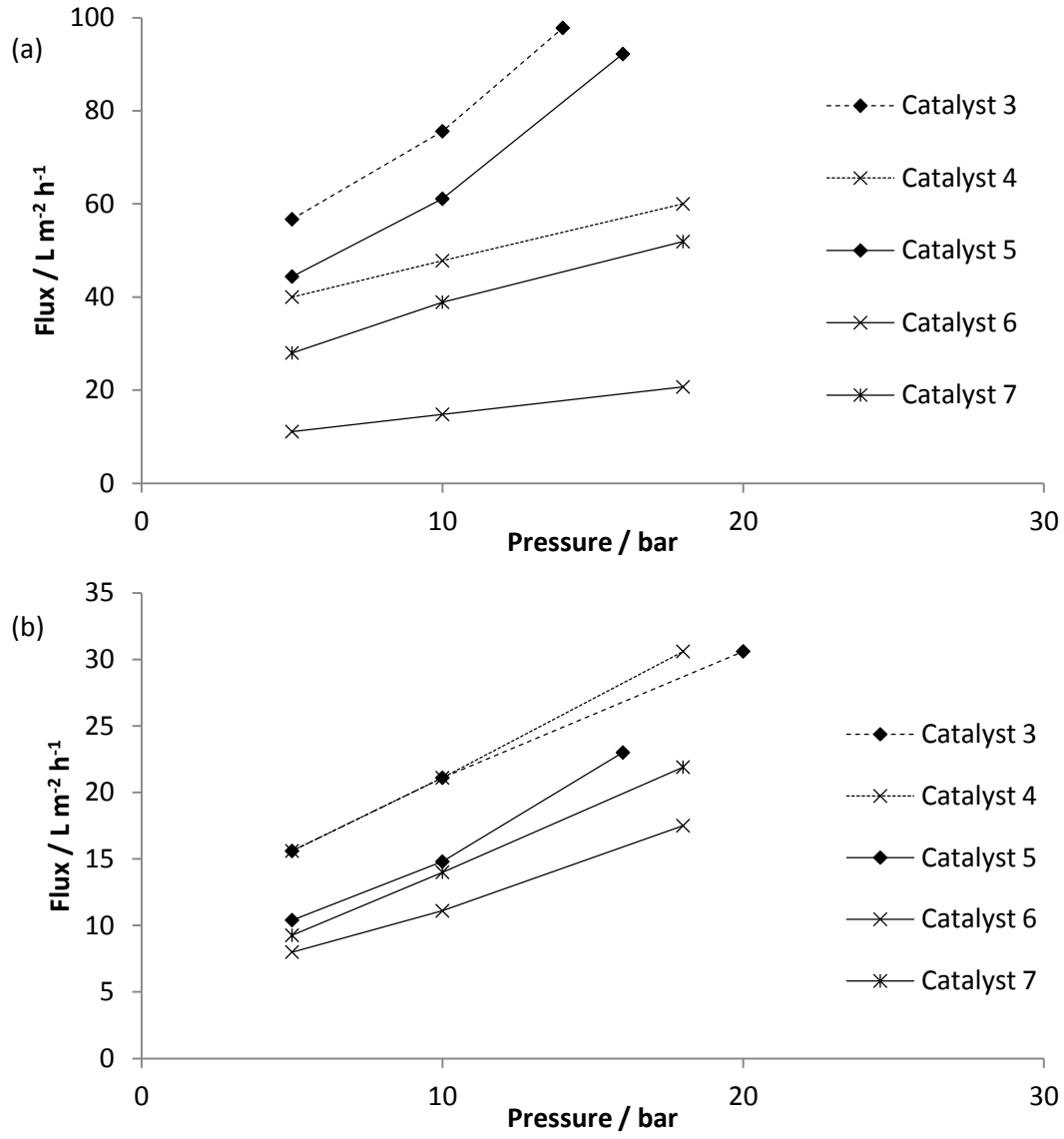

Figure 3.11: (a) Resulting membrane flux, obtained from recirculation experiments utilising DuraMem® 500 flatsheet membranes, at various applied transmembrane pressures. (b) Resulting membrane flux, obtained from recirculation experiments utilising DuraMem® 300 flatsheet membranes, at various applied transmembrane pressures.

3.2.3 Catalytic performance of catalyst

3.2.3.1 Comparison of polyalkylated catalysts

While the catalyst had to be rejected highly by the membranes used in the process, it was also critical for the catalyst to fulfil its catalytic function in the asymmetrical Michael addition used to

form the advanced intermediate (See Scheme 3.2). Therefore the catalyst candidates in Scheme 3.6 were tested and compared, in particular with the original catalyst, **4**. The original catalyst has been patented (Deng et al., 2009) and reaction performance data exists for the addition of dimethyl malonate to trans-β-nitrostyrene, **9**, (See Scheme 3.7). This reaction has been frequently used as a benchmark for the performance of new Michael addition catalysts (Chen et al., 2007; Deng et al., 2009; Li et al., 2004; Ye et al., 2005), therefore it was used to benchmark the performance of the polyalkylated catalysts.

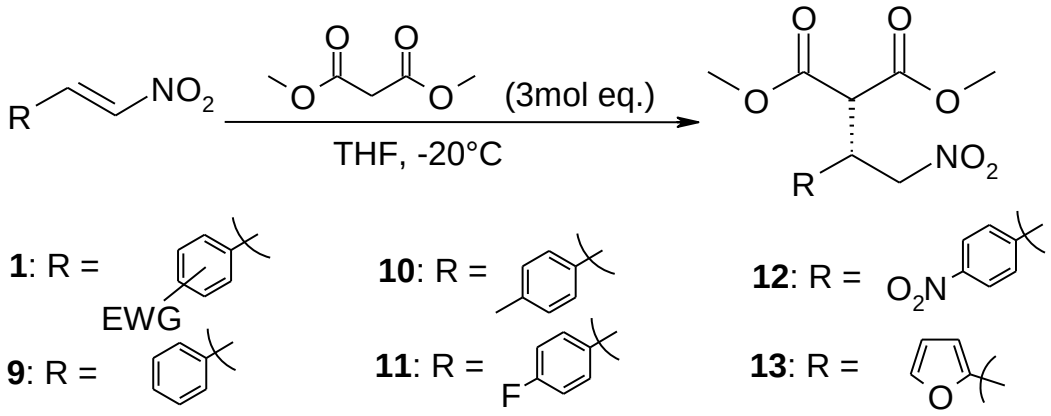

Scheme 3.7: Scheme for the Michael addition of dimethyl malonate (in excess) to various nitrostyrenes

To maintain the consistency in comparison, the polyalkylated catalysts loadings were at 3.3mol%, with respect to the amount of nitrostyrene **9** used, compared to 10.0mol% for the non-polyalkylated catalysts. This ensured that the same number of catalytic sites were used in each reaction. The performances of the catalysts were quantified by the extent of conversion of the **9** after 24h and the enantiomeric excess (ee) of the R isomer over the S isomer after full conversion of **9**.

It has been suggested that cinchona-derived organocatalysts serve as bifunctional catalysts and the Michael addition requires the hydroxyl and quinuclidine functionalities for the stabilisation and organisation of the transition state (Li et al., 2004). The performances of the catalysts were in agreement with this hypothesis. Without an electron-rich quinuclidine group, **7** was unable to catalyse the Michael addition (Entry 5, Table 3.2). On the other hand, the lack of a phenolic hydroxyl group in quinidine (**3**) resulted in a slower catalysed reaction compared to O-desmethylquinidine (**4**) (Compare Entries 1 and 2, Table 3.2). Polyalkylation of quinidine lowered the catalysis rate even further as no hydroxyl group was available (Entry 3, Table 3.2). The importance of the phenolic

hydroxyl group over the aliphatic hydroxyl should not be understated; the catalysis with **6** was much faster than both **3** and **5** despite the absence of the aliphatic hydroxyl group in **6** (See Entries 3-5, Table 3.2).

Table 3.2: Summary of Michael addition of dimethyl malonate to trans-β-nitrostyrene (9) with the various catalysts.

Entry	Catalyst (loading mol%)	Conversion 24h[a] / %	Time[b] / day	Yield[c] / %	ee[d] / %
1	**3** (10.0mol%)	45	12	52	19
2	**4** (10.0mol%)	99	1	82	86
3	**5** (3.3mol%)	41	18	44	7
4	**6** (3.3mol%)	90	3	62	94
5	**7** (3.3mol%)	No reaction	N.A.	N.A.	N.A.

[a] Determined by HPLC analysis under comparison with a naphthalene internal standard after 24h.
[b] Total time taken for the reactions, which were run with 0.4mmol of **9** and 3mol eq. of dimethyl malonate at -20°C until all of **9** was consumed as determined by HPLC analysis at λ = 230nm.
[c] Isolated yield of product using preparative chromatography
[d] Determined by chiral HPLC analysis.

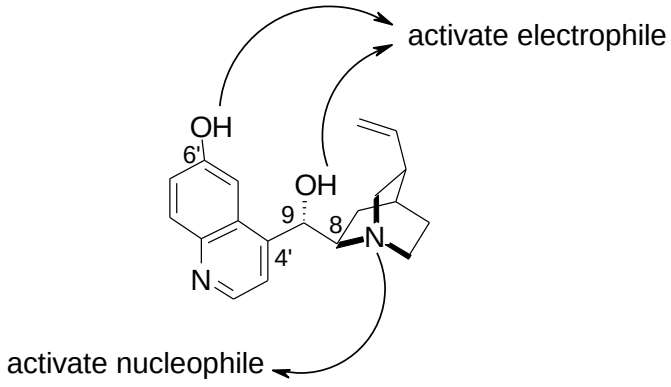

Figure 3.12: Mechanistic action of O-desmethylquinidine

The short methyl chain between the anchor and the catalytic site in **6** prevents easy rotation of the catalytic site around the benzene backbone, making **6** conformationally rigid. This is a common feature of many efficient chiral catalysts (Li et al., 2004) and was in agreement with the increased enantioselectivity of catalyst **6** over catalyst **4** (See Entries 2 and 4, Table 3.2). However, this

increased enantioselectivity was achieved at the expense of the slower rate of reaction, possibly because the same rigidity prevented easy access of the substrate into the catalytic site.

3.2.3.2 Increased catalytic loading

The decreased catalytic activity can be remedied with a higher catalyst loading since the catalyst can be easily recovered using OSN. By tripling the catalytic loading, the amount of time required for the completion of the Michael addition was cut from 3 days to 1 day (Compare Entries 1 and 2 in Table 3.3). The potential for increased catalytic loading also opened up new process design possibilities. A tripling of catalytic loading enabled the reaction to take place with the use of only 1mol eq. of dimethyl malonate, as opposed to the 3mol eq. originally used. Enantiomeric selectivity was largely unchanged at ee of 93% compared to 94% when 3mol eq. of dimethyl malonate was used (See Entries 1 and 3 in Table 3.3), albeit with a slight increase in time required for completion of the reaction to 4 days from the original 3 days. The use of equimolar amounts of reagent can eliminate a separation step downstream for the purification of the Michael addition adduct from the excess dimethyl malonate. This would simplify the synthesis process and reduce waste incurred from the excess dimethyl malonate loading.

Table 3.3: Comparison of Michael addition reaction at different catalytic loadings and dimethyl malonate loading.

Entry	Nitrostyrene (catalyst loading mol%)	Conversion 24h[a] / %	Time[b] / day	Yield[c] / %	ee[d] / %
1	**9** (3.3%)	90	3	62	94
2	**9** (10%)	100	1	89	94
3	**9** (10%)[e]	87	4	89	93

[a] Determined by HPLC analysis under comparison with a naphthalene internal standard after 24h.
[b] Total time taken for the reactions using **6**, which were run with 0.4mmol of **9** and 3mol eq. of dimethyl malonate at -20°C until all of **9** was consumed as determined by HPLC analysis at λ = 230nm.
[c] Isolated yield of product using preparative chromatography.
[d] Determined by chiral HPLC analysis.
[e] 1mol eq. of dimethyl malonate

3.2.3.3 Catalyst applicability to advanced intermediate synthesis

Since **6** had the best enantioselectivity amongst the polyalkylated catalysts, it was further tested with the nitrostyrene used in the advanced intermediate synthesis (Scheme 3.2). In a bid to elucidate the effects of the nitrostyrene substituent on the Michael addition, the reaction of various nitrostyrenes were also examined (Scheme 3.7).

6 was a versatile catalyst, catalysing the addition reactions asymmetrically with enantiomeric excesses above 90% for all nitrostyrenes (See Table 3.4).

Table 3.4: Michael addition of various nitrostyrenes to dimethyl malonate using 6.

Entry	Nitrostyrene	Conversion 24h[a] / %	Time[b] / day	Yield[c] / %	ee[d] / %
1	**9**	90	3	62	94
2	**10**	76	5	62	93
3	**11**	93	3	81	94
4	**12**	100	1	88	95
5	**13**	94	3	92	96
6	**1**	98	2	67	92

[a] Determined by HPLC analysis under comparison with a naphthalene internal standard after 24h.
[b] Total time taken for the reactions using **6**, which were run with 0.4mmol of nitrostyrene and 3mol eq. of dimethyl malonate at -20°C until all nitrostyrene was consumed as determined by HPLC analysis at λ = 230nm.
[c] Isolated yield of product using preparative chromatography.
[d] Determined by chiral HPLC analysis.

The rate of reaction varied with the degree of activation by the substituent. The more electron-donating substituents (Entries 1 and 2 in Table 3.4) retarded the reaction while the electron-withdrawing substituents accelerated the rate of reaction (Entries 3 – 6 in Table 3.4). Note that the nitrostyrene used in the advanced intermediate synthesis was known to be electron-withdrawing.

In any case, the suitability of **6** for the desired Michael addition was established. Hence effort was put in to develop a membrane process for the recycling of this catalyst.

3.2.4 Catalyst recycling with OSN

Fortuitously **6**, which gave the best catalytic performance amongst the polyalkylated catalysts, was also highly retained by the membranes tested. A process was developed to separate the catalyst from the product (**2**), using the membranes tested. In the test case for catalyst recovery it was assumed that the reaction was performed, with equimolar quantities of nitrostyrene **1** and dimethyl malonate, batch wise until all the nitrostyrene was consumed. This can be done with no loss in enantioselectivity as long as a huge excess of catalyst was used, as shown in Table 3.3.

3.2.4.1 Membrane process development

Recirculation experiments were performed by filtering a solution containing both **6** and the product (**2**) across DuraMem® 300 and DuraMem® 500 flatsheet membranes. While both membranes retained the catalyst at rejection values close to unity, DuraMem® 500 allowed much better permeation of the product (See Figure 3.13). Do note that while there seemed to be a slight decrease in catalyst rejection over DuraMem 500 at 10bar, this probably due to the HPLC method uncertainty in the determination of concentration of the catalyst, as illustrated by the error bars in the Figure. In any case this was not important in this work as the aim was to screen for an operating pressure where catalyst rejection is close to unity.

In order to determine the best conditions, out of the pressures tested, to perform constant volume diafiltration, the constant volume diafiltration equation (Equation 3.5) was used with the assumption of constant solute rejection at all concentrations to determine the change of Michael addition product and **6** concentration in the retentate at each tested operating pressure over the diafiltration period. While both membranes were capable of selectively retaining the catalyst for recycling, DuraMem® 500 was more productive in the separation, requiring significantly lower number of diafiltration volumes and filtration times for the separation. The number of diafiltration volumes and filtration times, if the same amount of membrane area was used, were 2 orders of magnitude higher for DuraMem® 300 than for DuraMem® 500 (See Figure 3.14). Therefore the choice of DuraMem® 500 for the diafiltration was obvious. The highest operating pressure of 18bar was used for the diafiltration as catalyst retention in the retentate at this pressure was predicted to be quantitative, while 38% and 52% of the catalyst losses were predicted for operating pressures of 5bar and 10bar.

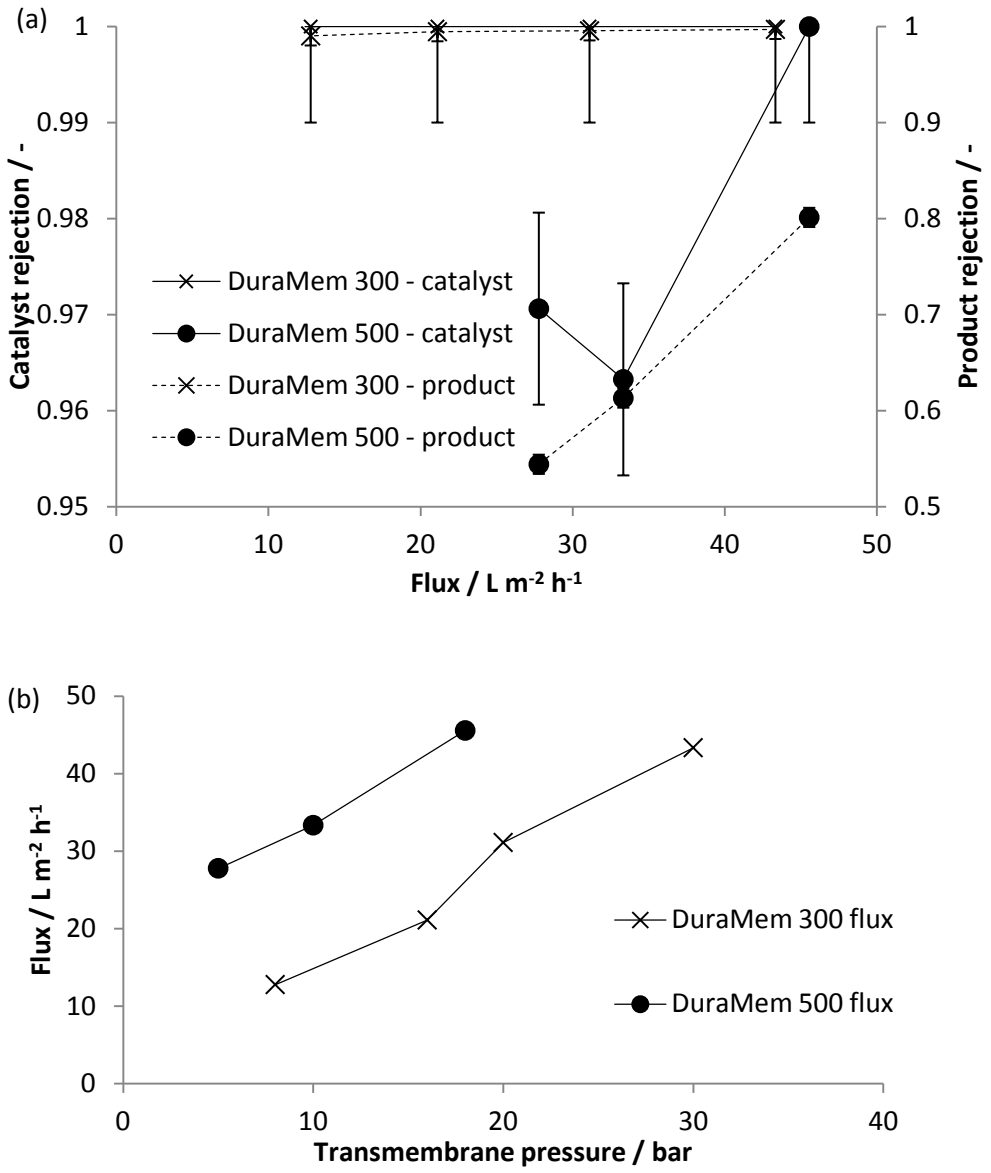

Figure 3.13: (a) Rejection and flux data for organocatalyst 6 (solid lines) and the Michael addition product 2 (dotted lines) in THF solution from recirculation experiments using DuraMem® 300 and DuraMem® 500. (b) Flux dependence on applied transmembrane pressure obtained from the same recirculation experiments.

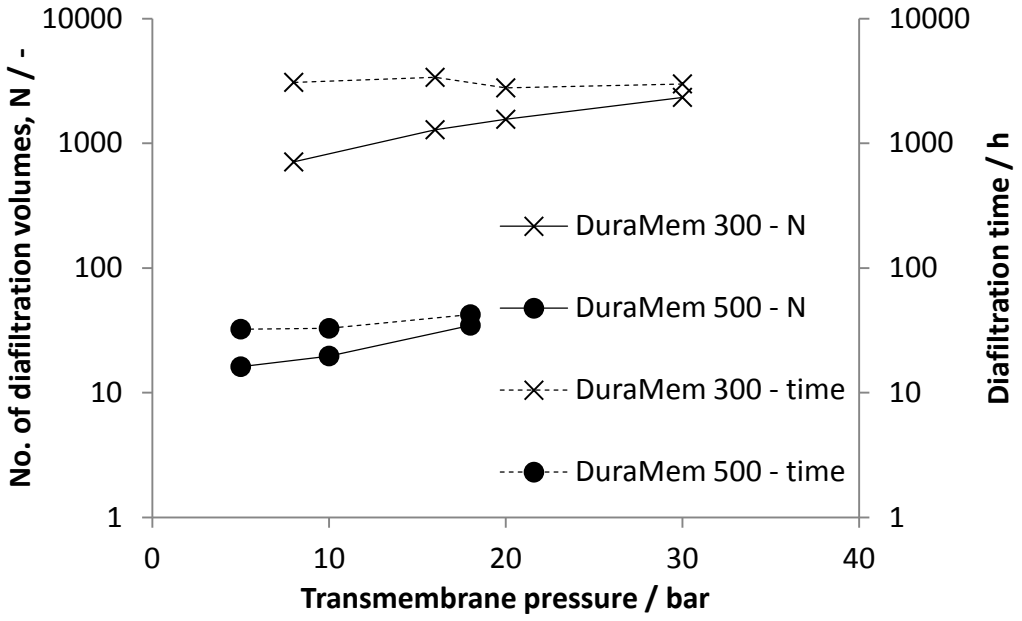

Figure 3.14: Productivity of diafiltration, expressed in terms of the number of diafiltration volumes and total diafiltration time, in the removal of the Michael addition product from catalyst *2.* A 300ml solution containing 10g of the product (2) and 1g of the catalyst (6) was diafiltered in this simulation until the retentate contained pure catalyst, at 99% weight purity of the total solute mass.

To make the process more productive, and since DuraMem® 300 was able to retain the product effectively (rejection above 0.99) at all the pressures tested, a second membrane stage was incorporated in series with the catalyst recycle stage. This stage was used to recycle the solvent from the permeate of the first stage so that the solvent can be reused in the diafiltration for the separation of the catalyst from the product. At the same time, a concentrate product stream was produced which facilitated recovery of the product via evaporation of the solvent. The schematic of the membrane separation process is presented in Figure 3.15.

3.2.4.2 Membrane separation process setup

The process consisted of two membrane stages connected in series. The first membrane stage, termed the catalyst retention stage, employed a looser DuraMem® 500 membrane coupon which retained **6** in the retentate tank (RT1). It was necessary to use a crossflow Evonik-MET cell to implement this stage. The forced circulation of fluid through a small aperture in the crossflow membrane unit (M1) from RT1, driven by a recirculating gear pump (RCP), provided sufficient

turbulence to mitigate fouling of the membrane by “oiling” out of the product and the catalyst. An attempt to use a magnetic stirrer in a deadend membrane cell and another attempt to force circulation through a wider ¼” aperture both resulted in membrane fouling which elevated losses of the catalyst through the permeate. The reaction mixture, on total consumption of the nitrostyrene, was charged into RT1 which had a capacity of 500ml. M1 held a flatsheet membrane coupon with an active filtration area of 54cm^2. Membrane filtration in the first stage was pressure-driven, with pressure provided by a stream of nitrogen gas, from a gas cylinder, charged into RT1. The pressure was controlled with a proportional relief valve, through which nitrogen gas was able to flow out slowly. A resistance temperature probe inserted into RT1 provided temperature reading for the retentate in RT1. This probe also provided feedback to the hotplate on which RT1 was placed so that the retentate temperature could be regulated. A stream of THF from T1 was fed into RT1 using Pump 2, a HPLC pump, to flush out the product in the permeate from M1. This stream was regulated by controlling Pump 2 using a PI controller code implemented on LabView, with feedback from the weighing scale on which RT1 and the hotplate were placed. This regulation kept the level in RT1 constant for an automated implementation of constant volume diafiltration in the catalyst retention stage.

The permeate stream was fed into a buffer tank, T2, which fed into the second membrane unit, M2, of the solvent recovery stage via Pump 3. The level in T2 was maintained with a PI controller, also implemented with LabView, that regulated Pump 3 based on feedback from the weighing scale on which T2 was placed. M2 was a modified deadend membrane filtration unit with a holdup volume of 500ml. It held a flatsheet DuraMem® 300 membrane coupon with an effective membrane filtration area of 54cm^2. M2 was placed on a hotplate which regulated the temperature of the retentate in it based on feedback from the resistance temperature probe inserted into the retentate. The hotplate was also a magnetic stirrer that spun the magnetic flea suspended a short distance above the membrane coupon. This provided convection to mitigate concentration polarisation on the membrane. M2 was pressurised with fluid fed in with Pump 3, and the pressure was controlled with a back pressure regulator, PCV2, which allowed a concentrated solution of the product to flow out while maintaining the pressure in M2. This resulting pressure drove permeation of a pure recovered THF stream from M2. This permeate stream was recycled back into T1 for reuse in the diafiltration in the catalyst retention stage.

The loss of fluid via the retentate stream in the solvent recovery stage necessitated the input of fresh THF into T1 from T0. This input was regulated by controlling Pump 1 with a PI controller, based on feedback from the weighing scale T1 was placed on, so that the level in T1 was constant.

3.2.4.3 Performance of catalyst recycling process

In an example, the process shown in Figure 3.15 was used to diafilter a 250ml solution containing 1g of **2** and 1g of **6** continuously over 72h. The rejection of product **2** was 0.95 during the diafiltration while the rejection of the catalyst **6** was 1.00; the catalyst was undetectable in the permeate. These rejection values were significantly higher than those obtained from recirculation experiments (see Section 3.2.4.1) and were probably due to the inconsistency in the membrane flatsheet performance on different parts of the flatsheet where the coupons were cut.

After diafiltration for 3 days, the retentate streams from RT1 and M2 and the solutions in T1, T2 and T3 were collected. These fractions were evaporated to dryness separately and weighed to determine the total mass of product and catalyst in each fraction. The dried residues were analysed using HPLC to determine the composition of the residues. The mass balance of the analysis is presented in Table 3.5.

Table 3.5: Summary of mass balance at the start and the end of the 3-day diafiltration of a 250ml THF solution containing 1g of the product 2 and 1g of the catalyst 6 using the equipment shown in Figure 3.15

	0h		72h	
	Product mass / g	Catalyst mass / g	Product mass / g	Catalyst mass / g
T1	0.00	0.00	0.00	0.00
RT1	1.00	1.00	0.30	0.52
T2	0.00	0.00	0.00	0.00
M2	0.00	0.00	0.35	0.00
T3	0.00	0.00	0.43	0.00
Total	1.00	1.00	1.08	0.52

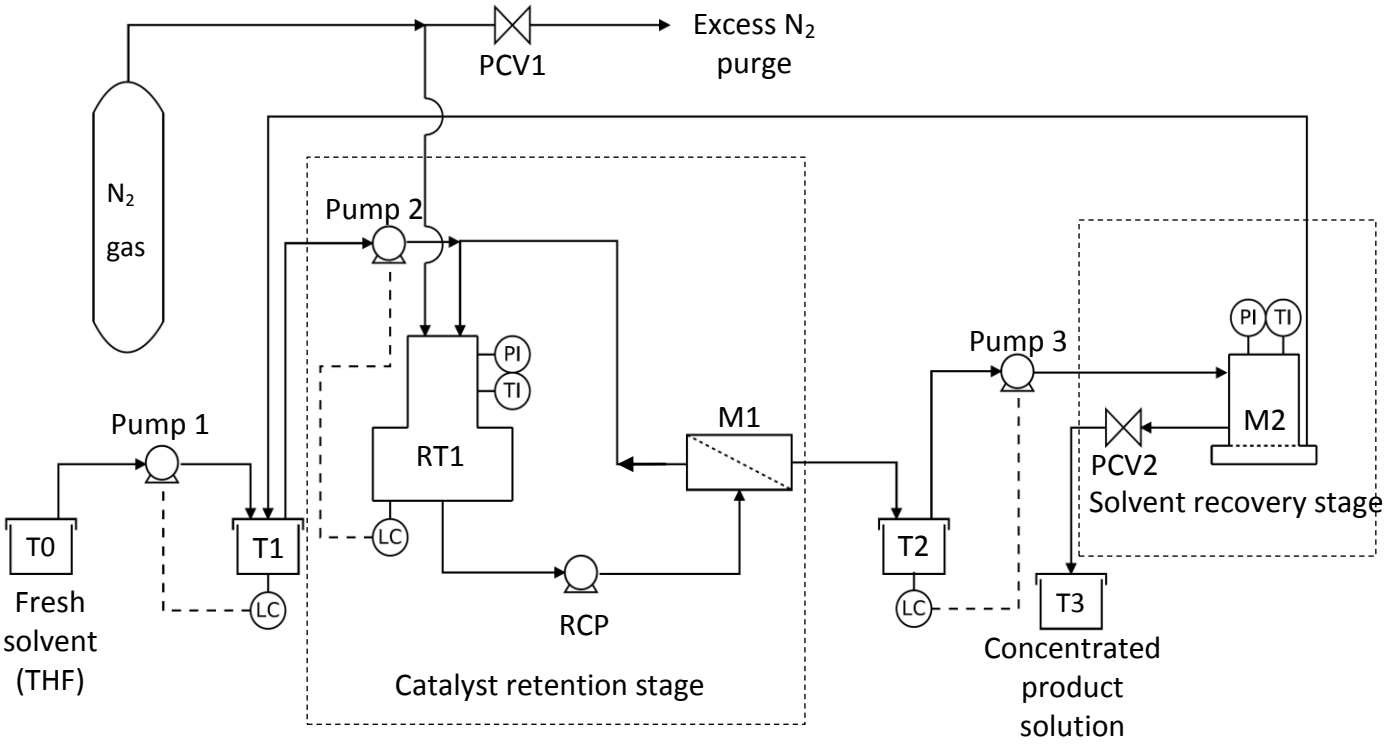

Figure 3.15: Schematic of membrane cascade setup used for organocatalyst recycling. T1 and T2 were buffer tanks, M1 and M2 were membrane units holding flatsheet membrane coupons (DuraMem® 500 in M1 and DuraMem® 300 in M2) and RT1 was the retentate holding tank for M1. M1 was used to retain the catalyst while letting the Michael addition product permeate through. M2, holding a tighter membrane, was used to retain and concentrate the product, while producing a pure recovered solvent stream for reuse in M1. The dotted lines denote control loops which controlled the pumps to maintain the levels in T1, T2 and RT1. LC = level controller; PCV = pressure control valve; PI = pressure indicator; RCP = recirculating pump; TI = temperature indicator.

The product permeated selectively through the membrane in M1, resulting in a loss of 0.78g of product from RT1 which was collected downstream in M2 and T3. This was confirmed by the collection of 0.30g of **2** in RT1. The mass balance of **2** was largely conserved with a small 8% increase in mass of **2** collected at the end of the diafiltration over the original mass put into the system. The small increase in mass could be attributed to sheared O-ring and seal material that were visible as black particulates in the residue from RT1. Analysis of the fractions confirmed that no quantifiable amount of catalyst **6** was lost through the membrane in M1. No catalyst was detectable in the solutions downstream of RT1 and M1 and the recycled solvent stream had no detectable presence of catalyst, hence the yield of catalyst from the retentate in RT1 should be quantitative with a theoretical catalyst purity of 0.82. However, only 0.52g of the catalyst was recovered from RT1, representing a 48% loss of catalyst though the catalyst purity increased from 0.50 to 0.63. The loss of catalyst can be attributed to absorption of the catalyst on the membrane. Absorption tests were performed by soaking 4 x 1cm^2 membrane coupons each into 1ml of THF solution containing 70mg of the catalyst for 3 days. It was estimated from these tests that 0.6g of catalyst were absorbed onto each gram of dry mass of membrane. The average weight of 4 randomly cut membrane coupon was 1.0g, therefore the loss of 0.49g of catalyst to adsorption was within expectations. A possible way to mitigate this issue is to reuse the membrane so that the membrane becomes saturated with the catalyst on the initial filtration so that future losses of catalyst will be minimal.

The diafiltration was ceased prematurely as a separation for the recovery of a 0.99 purity catalyst required in excess of 11 days. The long separation time required was a result of the low separation productivity in the first stage due to the low difference in separation difference between the product and the catalyst. This low productivity necessitated the use of copious amounts of diafiltering solvent for the separation in the first stage, but was reduced with the implementation of the second solvent recovery stage in M2. 6L of diafiltering solvent permeated through the membrane in M1 from T1 over the 3-day period but only 225ml of fresh THF was fed into the system from T0, which meant 96% of the diafiltering solvent used was recycled.

Another limitation with this setup is its non-robustness as the separation was dependent on the full rejection of the catalyst on the first DuraMem® 500 coupon. In a separate test, 300ml of a THF solution containing 10g of product and 1g of catalyst was diafiltered using the rig. A new batch of DuraMem® 500 membrane coupons which were used had a lower rejection of 0.97 for the catalyst. While there was little change in catalyst rejection (-3%), the loss of catalyst over time was significant.

At the end of the 7-day diafiltration most of the catalyst had actually permeated into M2, with no enrichment of the catalyst occurring in RT1 (See Table 3.6).

Table 3.6: Summary of mass balance at the start and the end of the 7-day diafiltration of a 300ml THF solution containing 10g of the product 2 and 1g of the catalyst 6 using the equipment shown in Figure 3.15

	0h		168h	
	Product mass / g	Catalyst mass / g	Product mass / g	Catalyst mass / g
T1	0.00	0.00	0.87	0.01
RT1	10.00	1.00	1.43	0.08
T2	0.00	0.00	0.07	0.00
M2	0.00	0.00	7.92	0.24
T3*	0.00	0.00	0.00	0.00
Total	10.00	1.00	10.28	0.33

* No retentate flux was produced from M2 into T3 in this run

These limitations are a consequence of the single stage setup for the catalyst retention stage and for the solvent recovery stage. These limitations are discussed in detail in Chapter 4 and an alternative membrane configuration is proposed in Chapter 5.

3.2.4.4 Effectiveness of recycled catalyst

The catalyst recovered from RT1 in the 3-day diafiltration was used in the reaction illustrated by Scheme 3.7. The nitrostyrene **1** was used and it was verified that catalyst **6** retained its activity and selectivity (See Entries 1 and 2 Table 3.7) despite the long filtration time required for separation. To ascertain that contamination of the catalyst by any residual product was not the cause of the observed consistency in catalytic activity, the recycled catalyst was also used to catalyse the Michael addition of **9** to dimethyl malonate. Again there was little change in the catalytic performance of the recycled catalysts (see Entries 3 and 4 in Table 3.7). Therefore **6** is compatible with this membrane recycling process.

Table 3.7: Comparison of activity and selectivity of fresh and recycled catalyst 6 in the catalysis of Michael addition.

Entry	Nitrostyrene	Conversion 24h[a] / %	Time[b] / day	Yield[c] / %	ee[d] / %
1	**1**	98	2	67	92
2	**1**	100*	1	75	93
3	**9**	90	3	89	94
4	**9**	93*	3	99	92

[*] Recycled catalyst, 17mg to account for theoretical catalyst purity of 0.82
[a] Determined by HPLC analysis under comparison with a naphthalene internal standard after 24h.
[b] Total time taken for the reactions using catalyst **6** (14mg), which were run with 0.4mmol of nitrostyrene and 3mol eq. of dimethyl malonate at -20°C until all nitrostyrene was consumed as determined by HPLC analysis at λ = 230nm.
[c] Isolated yield of product using preparative chromatography.
[d] Determined by chiral HPLC analysis.

3.2.5 Summary of results

Three different approaches to attaching an organocatalyst, O-desmethylquinidine, to a bulky anchor to increase its membrane retention were attempted, culminating in the successful synthesis of a new class of enlarged organocatalyst with polyalkylation. A combination of molecular weight increase and charge or hydroxyl group formation was more effective in increasing the retention of the catalyst. The enlarged catalyst with the phenolic hydroxyl group and basic quinuclidine nitrogen was effective in catalysis and catalysed the Michael addition more selectively than the incumbent catalyst. This catalyst was diafiltered in an attempt to separate it from the Michael addition product. The catalyst was purified over the 3-day diafiltration, and complete retention of the catalyst by the membrane was critical in a successful membrane recycling strategy for the catalyst. The catalyst was later reused and shown to be robust it was still catalytically effective after the diafiltration.

3.3 Materials and methods

3.3.1 Chemicals

AMS and MS were available at UCB Pharma SA. The bases $Ca(OH)_2$, $Mg(OH)_2$ and quinine were purchased from Sigma Aldrich and used without further purification.

The catalysts synthesis procedures and Michael addition reaction procedures are detailed in Section 8.2 of the Appendices.

3.3.2 Membranes

Desal 5 DK membranes were purchased from GE Water & Process Technologies. DuraMem® series membranes were purchase from MET (now Evonik-MET).

3.3.3 Membrane testing with recirculation experiments

Membrane testing were carried out on a METcell crossflow system (Evonik-MET, UK) illustrated in Figure 3.16. The OSN system was operated with a single flatsheet membrane coupon with an active filtration area of 54cm^2. The test solution was added into the retentate tank after membrane washing and RCP turned on to prime the pump. After priming the pump, the hotplate was turned on to maintain the temperature of the retentate in RT, with feedback from the resistance thermometer inserted into RT. Nitrogen gas from a gas bottle was fed into RT to provide pressure for the filtration. A proportional relief valve, PRV, was fitted in the gas line and calibrated such that it opens slightly to slowly relief nitrogen gas from the gas feed. This kept the pressure in RT constant at the desired pressure. Filtration was performed over different pressures by adjusting the PRV and gas supply into RT. The permeate flow from M1 was collected in a buffer tank, RBT. At the bottom of RBT was the feed tube for the metering pump. The metering pump was regulated by a PI controller implemented using LabView. The controller changed the flow rate of the pump in response to the level in RT. The level in RT was monitored with a weighing scale, which RT and the hotplate put on. Each recirculation at a different pressure was done for at least 2h or until the permeate metering pump flow stabilised. The retentate from RT was sampled from the drain valve, DV. Membrane flux was determined by collecting the permeate from M1 over a fixed time interval and verified with the metering pump flow. These samples were analysed on HPLC to determine solute concentration.

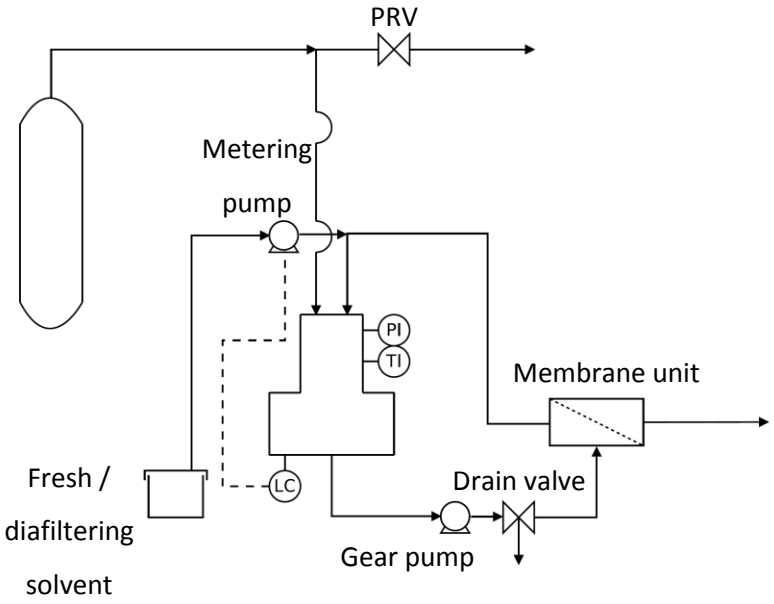

Figure 3.16: Schematic for constant volume diafiltration.

3.3.4 Constant volume diafiltration

Constant volume diafiltrations were later performed on binary solutions containing AMS and MS at concentrations of 0.025M each. Diafiltrations performed with no base added utilised Desal® 5 DK and DuraMem 200® membranes; DuraMem® 300 was not used as the retention of either solute was too low. Diafiltrations performed with $Mg(OH)_2$ added to increase the pH utilised Desal 5 DK, DuraMem® 200 and DuraMem® 300 membranes. The diafiltrations were performed using the procedure outlined by Székely et al. (2011).

3.3.5 Operation of membrane separation process

The membrane process was constructed according to the schematic in Figure 3.15. The operating procedure of the process can be classified into 1. startup; 2. operation of diafiltration; 3. shutdown of the process. Before startup, the membranes were rinsed with fresh THF by allowing the permeation of 300ml of THF through each membrane. This washed out the preservatives from the membranes. The Michael addition was performed batch wise in a separate vessel as the reaction temperature was low (-20˚C) and the total cycle time long (1 day).

Startup

During startup, the mixture to be separated was charged into RT1 and RCP was switched on to prime the gear pump. After the pump was primed, RT1 was pressurised to 18bar with bottled nitrogen gas. The pressure was maintained by allowing a slow flow of nitrogen through the pressure relief valve, which was calibrated to relief at 18bar. The hotplate which RT1 was on was used to regulate the temperature at a setpoint of 30˚C. The permeate from M1 was recycled back into T1 for recirculation back into RT1, with control for Pump 2 turned on to maintain a constant retentate level in RT1. This recirculation was performed overnight to condition the membrane and achieve steady membrane flux. After conditioning, samples of the retentate and permeate of the catalyst retention stage were taken to verify total retention of the catalyst by the membrane and permeation of the product through it.

On successful verification, the permeate flow from M1 was fed into T2 with the process set up as shown in Figure 3.15. The PI controllers for Pump 1 and Pump 3 were switched on to maintain the levels in T1 and T2. M2 was allowed to be filled with feed from T2 until the level of fluid in M2 overflowed from a port on top of M2. This port was then plugged with a swage cap to allow pressurisation of M2 while avoiding gas entrainment. The back pressure regulator, calibrated to relief at 10bar with nitrogen gas, was adjusted so that the pressure in M2 was maintained at 10bar.

Operation of diafiltration

The flow rates of Pumps 1, 2 and 3 were monitored along with the levels in (weights of) T1, RT1 and T2. Based on these outputs, the corresponding PI controllers were further fine-tuned to maintain the weights of these tanks within a range of ±1g and flowrate variations of the pumps within ±2ml min^{-1}.

Samples of the retentate from RT1 and M2 were taken every 24h to ascertain complete separation of the product from the catalyst retained in RT1. These samples were analysed using HPLC and the peaks of the product and catalysts were monitored at 230nm.

Shutdown

When separation was determined to be complete, Pumps 1, 2 and 3 were turned off. RT1 was depressurised by cutting the nitrogen feed and allowing the rest of the nitrogen to relief from RT1

until gauge pressure was at 0bar. The retentate from RT1 was drained out and RT1 was further rinsed with (3 x 250ml) of THF to flush out most of the residual retentate. This fraction was dried in vacuo to determine the amount of catalyst retained. The solution in T2, the retentate from M2 and the fluid in the concentrated product solution tank were collected separately and dried in vacuo to determine the amount of product removed from the reaction mixture. Finally the solution in T1 was evaporated to dryness and analysed to verify the mass balance around the whole system.

3.4 Conclusion

The selective addition of charge(s) to a solute, either through pH manipulation or polyalkylation, and the increase in molecular size of a solute using polyalklyation have been shown to improve the retention of the target solute, in agreement with predictions by the DSPM. However, these approaches were not always sufficient on their own to achieve full rejection of the solute to enable a complete separation with a single constant volume diafiltration stage due to the limitations of the diafiltration process. These limitations are discussed Chapter 4 while alternative membrane process configurations are proposed in Chapter 5.

4. Membrane Processes and Their Models

From the membrane processes reviewed in Chapter 1, it is evident that OSN can be widely applied in the pharmaceutical industry. However, their use to facilitate the chemical synthesis of API industrially has not been reported. The limitations of OSN processes, identified by considering performance based on their process models, might be able to explain the dearth of industrial examples.

In the first part of this chapter, the simpler solvent recovery membrane process models are covered. In these cases, the models only consider a single solute for simplicity. Subsequently, solvent exchange and solute fractionation are examined together because their models can be used interchangeably.

4.1 Solvent Recovery

Solvent recovery in the pharmaceutical industry is often performed in conjunction with solute concentration as the solutes are usually desired and need to be recovered (Rundquist et al., 2012a ; Rundquist et al., 2012b). The prevalence of distillation for solvent recovery can be attributed to the typically high volatility difference between the solute and solvent which allows for easy recovery of pure solvent and minimal solute loss. Hence an OSN alternative needs to possess a similar capacity for pure solvent recovery and allow only minimal solute loss during concentration to compete with distillation.

4.1.1 Batch concentration

The simplest setup (Figure 4.1) for solvent recovery involves the filtration of a solution with a membrane that can retain the solute(s) in solution until the solute concentration reaches a target concentration level, or when the desired amount of solvent has permeated through the membrane (Darvishmanesh et al., 2011; Geens et al., 2007; Rundquist et al., 2012b).

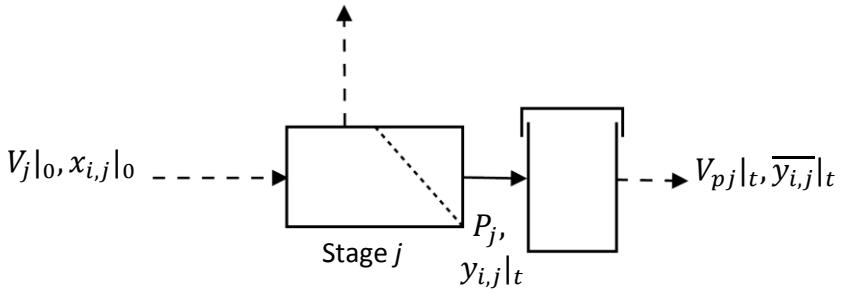

Figure 4.1: Schematic illustrating batch concentration. For this concentration stage *j*, the retentate volume is reduced from $V_j|_0$ to $V_j|_t$ while the concentration of solute *i* rises from $x_{i,j}|_0$ to $x_{i,j}|_t$ over the filtration time *t*. This produces a permeate stream (recovered solvent stream) of volume $V_{Pj}|_t$ with a concentration of $\overline{y_{i,j}}|_t$ at the end of the filtration cycle. The dotted arrows denote batch transfer of fluids.

When the solute rejection across the membrane is lower than unity, the solute concentration in the permeate changes over the filtration time. Suppose for a moment that the solution in the retentate and the exiting permeate are always well-mixed and that the rejection of the solute remains constant throughout the filtration time, t. In this case, the concentration of the solute i ($i = A, B, C$ …) in the permeate from diafiltration stage j ($j = 0,1, \dots, n$) follows

$$y_{i,j}|_t = (1 - R_{i,j})x_{i,j}|_t \qquad \textbf{Equation 4.1}$$

Hence the solute concentration in the permeate stream increases over time as the solute concentration in the retentate increases. Determination of the exact permeate concentration at the end of the batch concentration requires detailed understanding of the process dynamics in the retentate. This is challenging as evolution of solute concentration over the filtration time is uncertain. The process model can be simplified if the concentration of solute in the retentate is assumed to increase linearly over time, as illustrated by Figure 4.2. With the further assumption that the system has both a perfect flow controller and a perfect actuator that can maintain constant permeate flux and solute rejection over the filtration time, the concentration of solute *i* in the retentate of stage *j* can be expressed as a first order equation (Equation 4.2) with respect to filtration time, t.

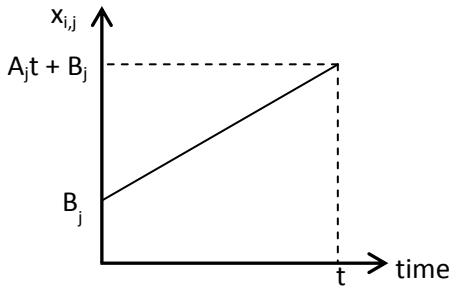

Figure 4.2: Change in retentate concentration, from B_j to $A_jt + B_j$, in stage *j*, assuming a linear increase in retentate concentration over filtration time, *t*

$$x_{i,j}|_t = A_j t + B_j \qquad \textbf{Equation 4.2}$$

The recovered solvent from the permeate stream will have a solute *i* concentration that is an average of the permeate collected over the total filtration time. A mass balance analysis of the loss of solute *i* from the retentate and its relationship with the solute in the permeate is shown in Equation 4.3.

$$V_j|_0 x_{i,j}|_0 - V_j|_t x_{i,j}|_t = \int_0^t P_j(1 - R_{i,j}) x_{i,j} dt$$
$$= P_j(1 - R_{i,j}) \int_0^t A_j t + B_j dt \qquad \textbf{Equation 4.3}$$

Equation 4.3 can be further simplified to

$$Loss\ of\ solute\ i = P_j(1 - R_{i,j}) \left(\frac{A_j}{2} t^2 + B_j t\right) \qquad \textbf{Equation 4.4}$$

By dividing this amount of solute by the total volume of permeate collected over the filtration time, the concentration of solute *i* in the recovered solvent can be expressed by

$$\overline{y_{i,j}}|_t = (1 - R_{i,j}) \left(\frac{A_j}{2} t + B_j\right) \qquad \textbf{Equation 4.5}$$

The stage cut, which is defined as the ratio of the solvent volume recovered and the initial solution volume being filtered (see Equation 4.6), determines the amount of the recovered solvent. A high stage cut would result in a high solvent recovery rate and vice versa.

$$\theta = \frac{P_j t}{V_j|_0} = \frac{V_{pj}|_t}{V_j|_0} \qquad \textbf{Equation 4.6}$$

The solute *i* ($i = A, B, C, \dots$) balance over the process is

$$V_j|_o x_{i,j}|_0 = V_j|_t x_{i,j}|_t + V_{pj}|_t \overline{y_{i,j}}|_t \qquad \textbf{Equation 4.7}$$

While the solvent flow balance over the process is

$$V_j|_o = V_j|_t + V_{pj}|_t \qquad \textbf{Equation 4.8}$$

Combining the solute balance (Equation 4.7) and material balance (Equation 4.8) equations and rearranging would yield

$$\frac{V_{pj}|_t}{V_j|_t} = \frac{x_{i,j}|_0 - x_{i,j}|_t}{\overline{y_{i,j}}|_t - x_{i,j}|_0} \qquad \textbf{Equation 4.9}$$

Also by combining the stage cut equation (Equation 4.6) and the flow balance equation (Equation 4.8) with Equation 4.9 and rearranging, an alternative expression for stage cut can be obtained to solve this set of equations.

$$\theta = \frac{\frac{V_{pj}|_t}{V_j|_t}}{1 + \frac{V_{pj}|_t}{V_j|_t}} \qquad \textbf{Equation 4.10}$$

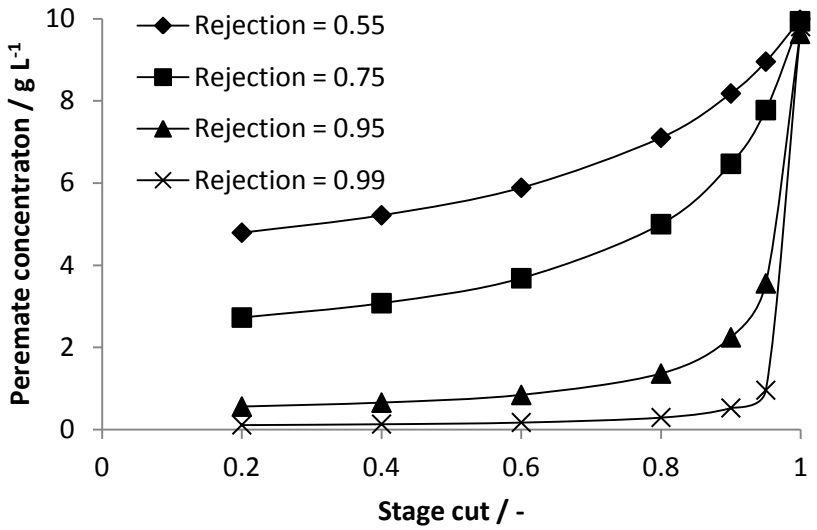

Figure 4.3: Solute concentration in recovered solvent when using membranes in batch concentration mode for solvent recovery from a solution containing 10g L^{-1} of a solute. The rejection values refer to the single pass rejection of these membranes. As more solvent is recovered (higher stage cut), the concentration increases, making pure solvent recovery a challenge at high recovery rates.

The limitations of the batch concentration process became apparent when simulations were performed, at various stage cuts and membrane rejections, for the batch concentration of a solution containing 10g L^{-1} of solute. The results are illustrated in Figure 4.3. When solvent recovery rates were increased, the amount of solute in the recovered permeate increased. While this increase was delayed as the single pass rejection approached unity, the recovery of high purity solvents with the process was limited to high rejection membranes, making the process inflexible. Do note that constraints imposed by elevated osmotic pressure, excessive concentration polarisation and the solubility limit of the solute were neglected in these simulations to illustrate the challenges faced when trying to achieve high recovery rates for pure solvent.

4.1.1.1 Batch permeate multipass cascade

When the single pass rejection of the membrane is too low, the permeate from a batch concentration stage can be sent to further concentration stages to produce an increasingly dilute permeate (Katraro et al., 1997; Rundquist et al., 2012b). A series of such batch concentration stages forms a batch permeate multipass cascade. Schematically, the permeate stream from stage *j* is sent

for further filtration in stage *j + 1* until the desired permeate solute concentration, $\overline{y_{i,n}}$, from the final stage is achieved (see Figure 4.4).

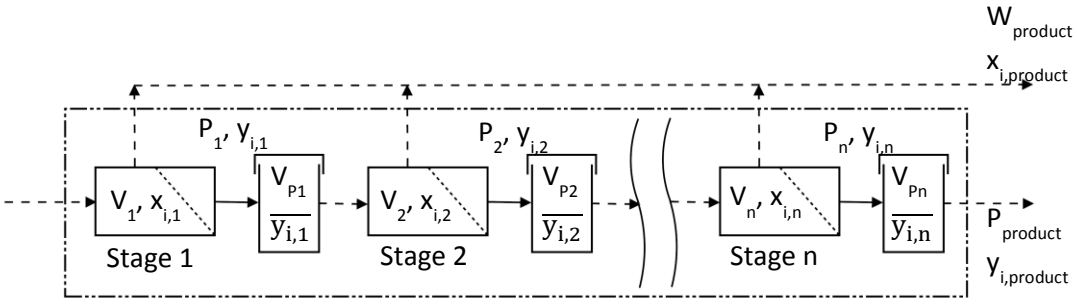

Figure 4.4: Schematic of a batch permeate multipass cascade. For every stage *j*, the retentate volume is reduced from $V_j|_0$ to $V_j|_t$ while the concentration rises from $x_{i,j}|_0$ to $x_{i,j}|_t$ over the filtration time *t*. This produces a permeate stream from each stage of volume $V_{Pj}|_t$ with a concentration of $\overline{y_{i,j}}|_t$ at the end of the filtration cycle. In this scenario $y_{i,product} = \overline{y_{i,n}}|_t$. The dotted arrow lines denote batch transfer of fluids.

As this cascade is an expansion of the batch concentration nanofiltration, Equation 4.2 and Equation 4.5 can be used to describe the evolution of solute concentration in each stage. Equation 4.9 and Equation 4.10 were used to determine the solute balance in each stage.

If a fixed stage cut was used in each stage, the amount of permeate at the end of the filtration in each stage can be expressed, with respect to the initial retentate volume, by

$$V_n|_t = (1-\theta)^n V_1|_0 \qquad \textbf{Equation 4.11}$$

The concentration of the resulting retentate, where *t* is the *constant* filtration time for each stage, can be expressed as

$$x_{i,product} = \frac{(1-\theta)x_{i,1}|_t + (1-\theta)^2 x_{i,2}|_t + \ldots + (1-\theta)^n x_{i,n}|_t}{(1-\theta) + (1-\theta)^2 + \ldots + (1-\theta)^n} \qquad \textbf{Equation 4.12}$$

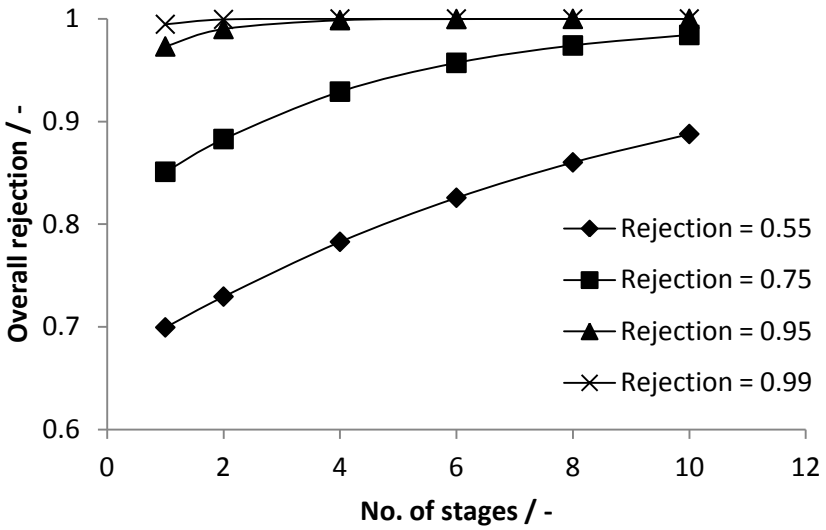

Figure 4.5: Relationship between overall rejection of the batch permeate multipass cascade and the number of stages in this cascade. Simulations were performed for a high stage cut of 0.95 to maximise solvent recovery. The overall rejection of the cascade increased with the increase in number of stages.

The performance of the cascade was quantified with the overall rejection, which is represented by Equation 4.13.

$$R_{i,o} = 1 - \frac{\overline{y_{i,n}}|_t}{x_{i,product}} \qquad \textbf{Equation 4.13}$$

Simulations of the cascade for the treatment of a 10g L^{-1} solution, with a high stage cut of 0.95 to maximise solvent recovery and assuming the solute is soluble at all concentrations, showed that the addition of stages increased the overall rejection of the cascade (Figure 4.5). At first glance, this approach seems feasible as a workaround for insufficient membrane rejection in pure solvent recovery as the process scaled well with the increase in the number of stages.

Further simulations of a 3-stage batch permeate multipass cascade performance at different stage cuts showed that the overall rejection of the cascade decreased as the stage cut approaches unity (see Figure 4.6), which was a minor impediment to the use of this cascade. The cascade also had a low capacity for solute enrichment in the retentate (see Figure 4.7) at stage cuts below 0.6. This meant that the operation of the cascade with the dual aims of high overall rejection and high solute

enrichment, typically required for maximal solvent recovery (Katraro et al., 1997; Rundquist et al., 2012b), is not attainable unless the membranes reject the solute highly.

Furthermore, such a batch system would become unwieldy as the amount of solvent treated and number of stages required increase. The sizes of all the buffer tanks required between each stage increases proportionally to the volume of solvent treated, while each additional stage adds an additional cycle and its associated time to the whole process.

The complexity of designing such a cascade is also an issue. If every cascade stage is sized identically, the first stage will take most time for filtration and will be the rate limiting step if the stage cut for every stage is not unity. It should be noted that each additional stage also decreases the amount of recovered solvent, with θ^n of the initial solvent volume recovered at the end of *n* stages, limiting the number of stages that can be added if high solvent recovery rate is required.

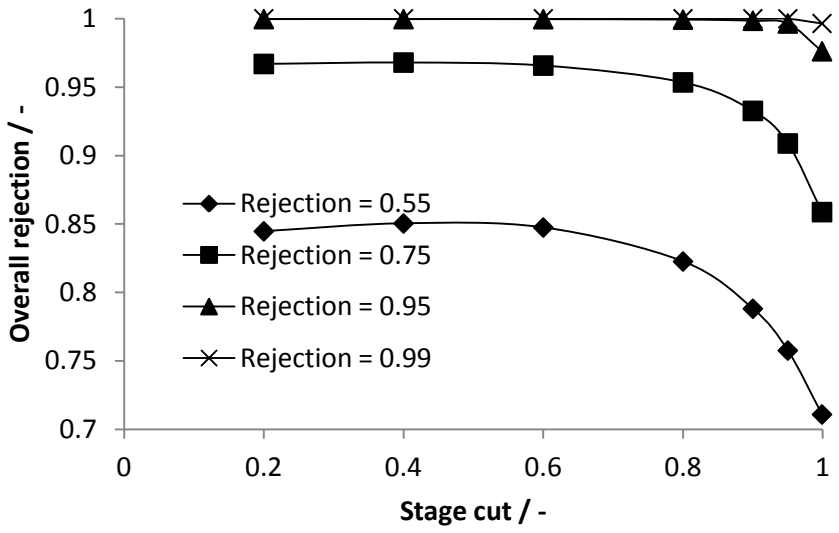

Figure 4.6. Relationship between overall rejection of a 3-stage batch permeate multipass cascade and the stage cut for each stage. The overall rejection of the cascade decreased as the stage cut for each membrane stage approached unity. Hence a cascade aiming for high overall rejection would operate at low to moderate stage cuts.

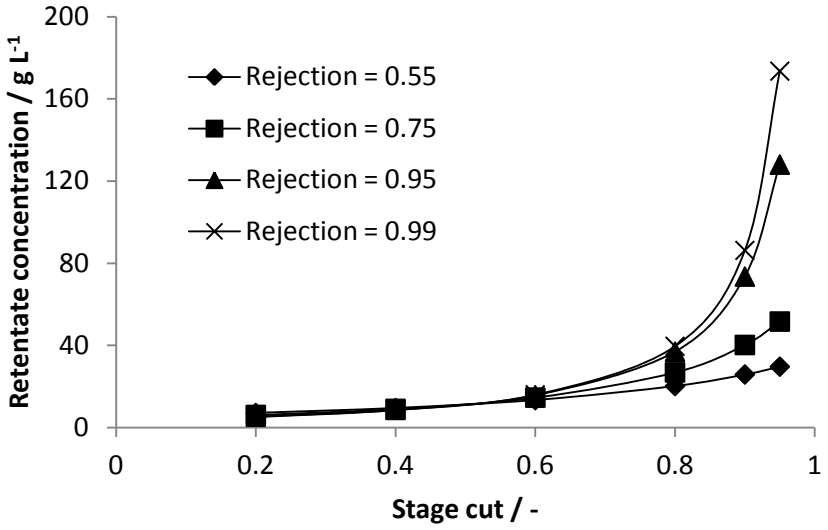

Figure 4.7: Relationship between stage cut of each stage and the concentration of the product retentate from the 3-stage batch permeate multipass cascade. A stage cut below 0.6 limits the capacity of the cascade for the concentration of solute in the retentate. Therefore the conflicting aims of high overall rejection and concentration of solutes cannot be achieved simultaneously unless the rejection is high.

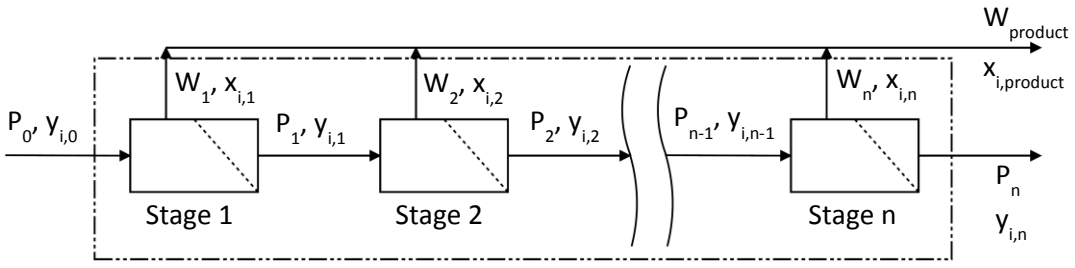

Figure 4.8. Schematic of a continuous permeate multipass cascade. In each stage, the proportion of feed solution filtered is based on the stage cut; a higher stage cut results in a higher proportion of solution filtered. The resulting permeate from each stage is channelled to successive membrane stages for further rectifying. $x_{i,product}$ is equivalent to the average concentration of all the retentate streams and $y_{i,product} = y_{i,n}$.

4.1.2 Continuous concentration

The use of continuous membrane filtration cascade processes has also been explored for solvent recovery (Abejon et al., 2012; Caus et al., 2009). In the simplest fashion, the batch permeate multipass cascade can also be operated continuously as shown in Figure 4.8, with the permeate from stage *j* sent to stage *j + 1* until the desired solute concentration in the permeate product stream from stage *n* ($y_{i,n} = y_{i,product}$) is achieved. The retentate streams from all the stages can be collected together to form the concentrate product stream.

For this continuous permeate multipass cascade, the flow balance over each stage can be summarised by

$$P_{j-1} = W_j + P_j = \big(1 - \theta_j\big)P_{j-1} + \theta_j P_{j-1} \qquad \textbf{Equation 4.14}$$

Where θ_j is the stage cut of stage *j* ($j = 0,1, \dots, n$).

$$\theta_j = \frac{P_j}{P_{j-1}}, \qquad 0 \leq \theta_j \leq 1 \qquad \textbf{Equation 4.15}$$

Therefore, the material balance over each stage can be expressed as

$$P_{j-1}y_{i,j-1} = \big(1 - \theta_j\big)P_{j-1}x_{i,j} + \theta_j P_{j-1}y_{i,j} \qquad \textbf{Equation 4.16}$$

Partitioning of solute across the membrane at each stage is dependent on membrane performance and operating conditions. If the retentate in each membrane unit is assumed to be well-mixed, the partitioning of the solute can be expressed as

$$y_{i,j} = (1 - R_{i,j})x_{i,j} \qquad \textbf{Equation 4.17}$$

Equation 4.16 and Equation 4.17 can be combined and rearranged to give

$$x_j = \frac{y_{i,j-1}}{(1 - \theta_j) + \theta_j(1 - R_{i,j})} \qquad \textbf{Equation 4.18}$$

This can be solved to obtain the concentration of solute in the retentate from stage *j*, while Equation 4.17 can be solved to obtain solute concentration in the permeate from the same stage.

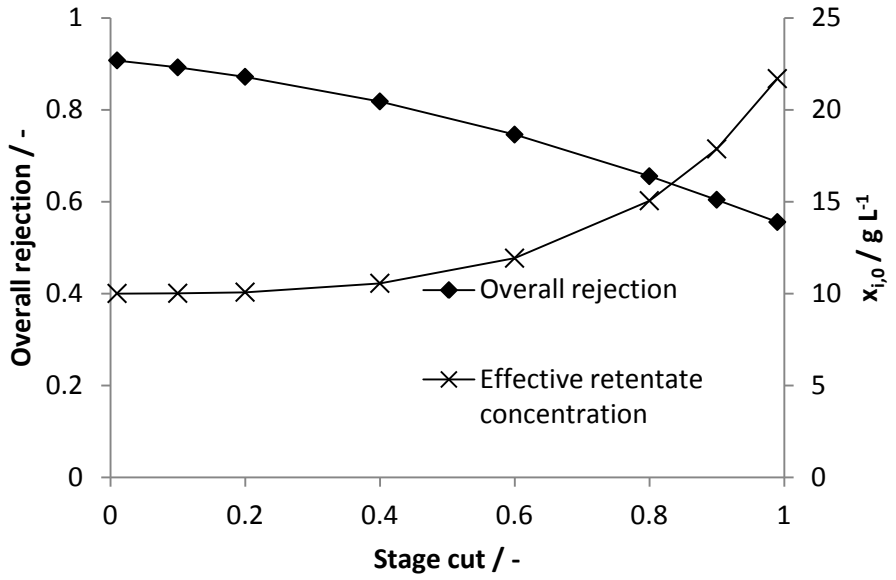

Figure 4.9: Relationship between overall rejection of the continuous permeate stage system and the stage cut in each membrane stage. Note that the overall rejection decreased with increasing stage cut, while the concentration of the retentate increased with stage cut.

Meanwhile the solute concentration in the retentate stream of the cascade can be expressed as

$$x_{i,product} = \frac{W_1 x_{i,1} + W_2 x_{i,2} + \cdots + W_n x_{i,n}}{W_1 + W_2 + \cdots + W_n} \qquad \textbf{Equation 4.19}$$

Hence the overall rejection over this cascade can be represented by

$$R_{i,o} = 1 - \frac{y_{i,n}}{x_{i,product}} \qquad \textbf{Equation 4.20}$$

The main operating parameter for this cascade is the stage cut for each membrane stage. The cascade was simulated for the treatment of a 10g L^{-1} solution, at different stage cuts and with a single pass rejection of 0.55, and it was evident from Figure 4.9 that the cascade had limited capacity for concentration of the retentate stream though it had a high theoretical limit for overall rejection of 0.91 when the stage cut approached zero. The cascade barely concentrated the solution at stage

cuts below 0.6. On the other hand, the overall rejection dropped rapidly toward the single pass rejection of 0.55 at stage cuts above 0.8.

A variant of this cascade was proposed firstly by Caus et al. (2009) and then by Abejon et al. (2012), where the retentate from stage *j + 1* is recycled back into stage *j*, with the exception of stage *n* where no further stages were available downstream to provide the recycle (see Figure 4.10). This new configuration also made it possible for all stages, except the final one, to be sized identically.

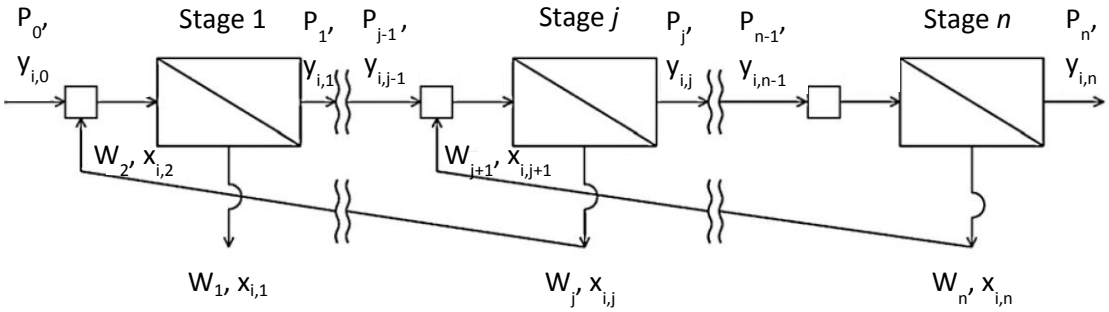

Figure 4.10: Schematic of cascade by Caus et al. (2009) and Abejon et al. (2012). Adapted from work by Abejon et al. (2012)

For this cascade, the flow balance over the cascade from stage *j* can be expressed with

$$P_{j-1} = W_j + P_n \qquad \textbf{Equation 4.21}$$

The material balance in this cascade follows the general formula

$$P_{j-1} y_{i,j-1} = W_j x_{i,j} + P_n y_{i,n} \qquad \textbf{Equation 4.22}$$

This can be rearranged to

$$x_{i,j} = \frac{P_{j-1}}{W_j} y_{i,j-1} - \frac{P_n}{W_j} y_{i,n}$$ **Equation 4.23**

The partitioning of solute can be assumed to follow Equation 4.17.

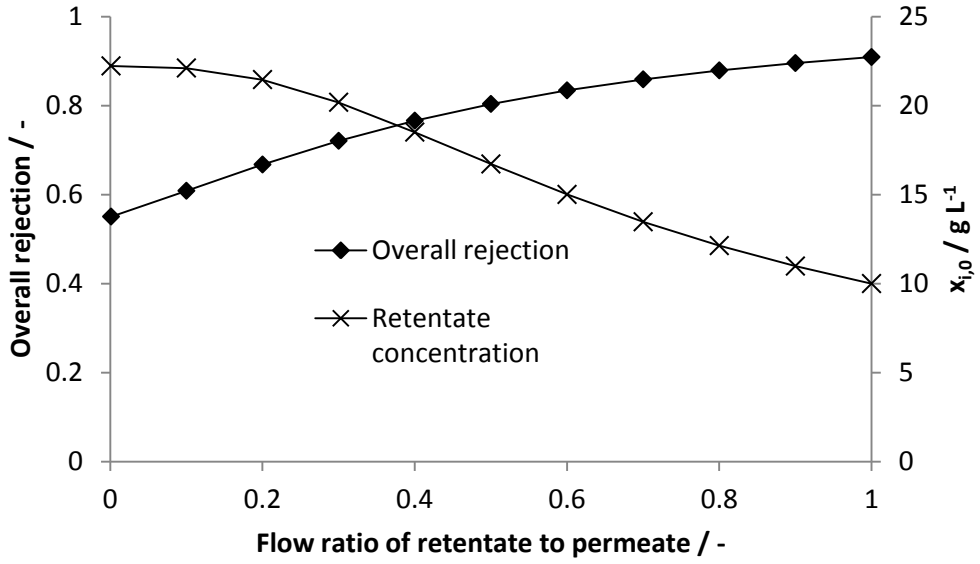

Figure 4.11: Relationship between overall rejection of the cascade system proposed by Caus et al. (2009) and Abejon et al. (2012) and the ratio between the recycled retentate and permeate flow. While the overall rejection increases with the ratio of flows, the concentration of the retentate decreased with the ratio causing little enrichment of the solute at high rejections.

The recycle ratio in this cascade, defined as the flow ratio between the retentate sent to stage *j – 1* from stage *j* and the permeate sent from stage *j – 1* to to stage *j*, with the exception of the final stage *n* can be expressed as

$$R = \frac{W_j}{P_{j-1}}, j \neq n+1$$ **Equation 4.24**

Suppose the permeate flux for all stages, less the final stage, are constant and the solute rejection in all stages are identical. Simulations were performed for such a cascade (see Figure 4.11), with the single stage membrane rejection set at 0.55, to elucidate the depedence of the cascade's performance on the recycle ratio in this cascade. While total recycle of the permeate was able to bring the overall rejection of this cascade to a maximum of 0.91, the concentration of the resulting

retentate fell towards the feed concentration of 10g L^{-1}, resulting in very little enrichment of the solute in the retentate. To achieve a maximum enrichment of the solute to 22.2g L^{-1}, there should be no permeate recycled. However, in this case the rejection in the cascade drops to the single stage rejection of 0.55. Hence it is evident that this cascade has a limited solute concentration capacity when trying to attain high overall rejections, unless the single pass rejection is at unity.

4.2 Solvent Exchange and Solute Fractionation

Solvent exchange is a routine unit operation in the pharmaceutical industry as many sequential reactions are carried out in different organic solvents (Lin & Livingston, 2007). The solutes, of lower volatility, are retained in the reaction mixture while the solvent, of higher volatility, is removed; another solvent is routinely added into the mixture to increase the solvent content of the replacing solvent.

Solute fractionation, on the other hand, can be critical to the success of the synthesis of an active pharmaceutical ingredient (API). The processes commonly used for solute fractionation include distillation, adsorption-desorption, solvent extraction, membrane-assisted liquid-liquid extraction (Eldrige, 1993), fractional crystallisation (Sherwood & Pigford, 1952) and chromatography (Sereewatthanawut et al., 2010). These processes involve the separation of a solute that has a higher affinity for a phase from another solute with a lower affinity for that phase. When the affinity differences in these processes prove insufficient, nanofiltration might be used as an alternative tool to induce an adequate separation driving force.

The process models for solvent exchange and solute fractionation can be treated similarly as at least 3 species need to be processed for these equations. Arguably, these processes are harder to model than the solvent recovery processes.

4.2.1 Discontinuous batch diafiltration

Solvent exchange with discontinuous batch diafiltration is analogous to the “put-and-take” distillation commonly used for solvent exchange in the pharmaceutical industry. In both cases, a solution containing the reaction mixture is first concentrated by a batch removal of solvent, using either a batch concentration membrane process described in Section 4.1.1 or distillation. Secondly, the replacing solvent is added to the concentrated solution to dilute it. These 2 steps are repeated

until the desired solvent switch is achieved. While the membrane process can potentially realise energy savings, distillation is well-established and simpler to use. Solvent switch with distillation can be stopped unambiguously when the desired vapour temperature is achieved. Furthermore the solutes in the reaction mixture tend to be a lot less volatile than the solvent, minimising the loss of the desired solute during the concentration phase.

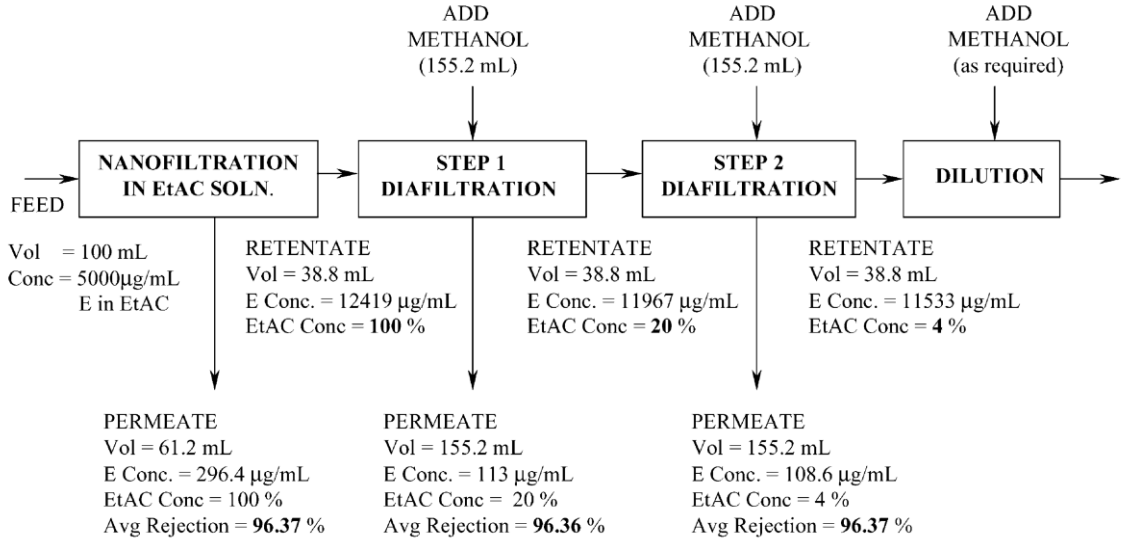

Figure 4.12: Solvent exchange procedure performed by Sheth et al. (2003).

To illustrate a working example of a discontinuous batch diafiltration, a process model for the process used by Sheth et al. (2003) (see Figure 4.12) was developed. Firstly an initial batch concentration process was used to remove some solvents. The batch concentration equations can be used to describe the evolution of solute concentration in the retentate during the batch concentration step. Hence Equation 4.1 can be used to describe the partitioning of the solute, Equation 4.2 for the concentration change of solute in the retentate, Equation 4.5 the change in solute concentration in collected permeate and Equation 4.9 for the description of the relationship between the volume ratio of the permeate and retentate after the batch concentration.

When rediluting the solution for the subsequent concentration, the retentate was replenished to its original volume with a replacing solvent. The amount of solvent added after every stage (step) *j* of

the diafiltration was $V_{pj}|_t$. By rearranging Equation 4.9, an equation to determine the concentration of solute in retentate tank can be obtained

$$x_{i,j+1}|_0 = \frac{x_{i,j}|_t V_j|_t}{V_{j+1}|_0} \qquad \textbf{Equation 4.25}$$

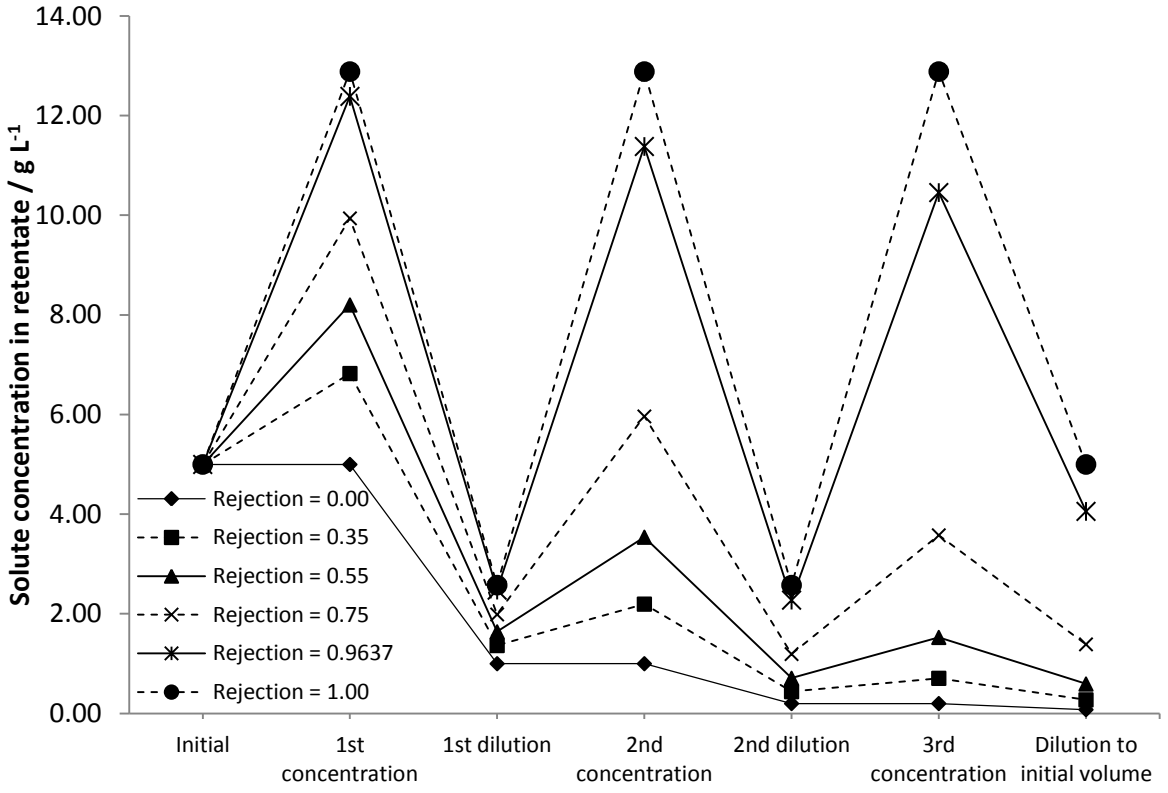

Figure 4.13: Changes in concentration of solute in the retentate during the solvent exchange cycle as performed by Sheth et al. (2003).

The volumes and rejection values from the solvent exchange cycle described by Sheth et al. (2003) were used in this equation set for validation. The rejection of the solute was also varied to illustrate the influence of solute rejection on the effect of the solvent exchange / solute removal.

The loss of the solute, using the rejection of 0.9637 as reported by Sheth et al. (2003), was estimated at 18.8% compared to the 10.9% reported by them. While not spot on, this was of the same order of

magnitude and this model should give a good idea of the performance of discontinuous diafiltration. As seen in Figure 4.13 the changes in solute concentration were larger when the rejections of the solute were lower. On the other hand, the loss of solute in such a cycle decreases exponentially with an increase in the rejection of the solute (see Figure 4.14). In the case of solvent exchange, where the rejections of the solvents are often assumed to be zero (Lin & Livingston, 2007; Rundquist et al., 2012a), it is apparent that a successful solvent switch require the use of a membrane which rejects the desired solute very close to unity.

This process has not been used for solute fractionation purposes in organic solvents yet, though conceptually a high yield fractionation should see high rejection of the desired solute by the membrane and low rejection of the undesired solute (see Figure 4.14).

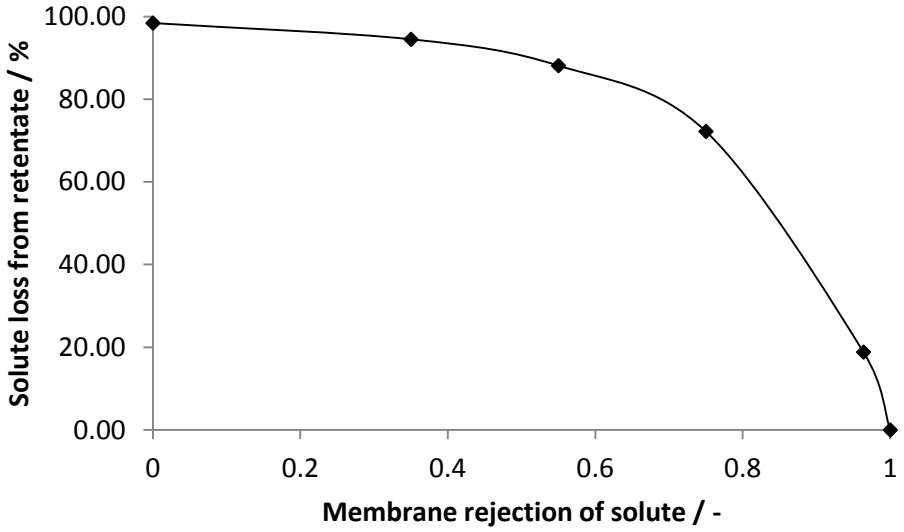

Figure 4.14: Solute loss from the retentate, when using the procedure depicted in Figure 4.12, as a function of the rejection of the solute.

The need for a high rejection membrane was further highlighted when the solute concentration in the permeate, from simulation of the process, was examined (see Figure 4.15). When rejection was below unity, the more retained solute was always present in the permeate. In chromatography parlance, co-elution of the more retained solute occurred. Hence full fractionation of the desired solute from the rest of the solutes is impossible with such a process unless the desired compound is completely retained by the membrane. The requirement for full rejection means the process is not robust as even a slight deviation from total rejection can cause co-elution and decrease the

efficiency of the separation. The sensitivity of the process to membrane retention of the solute also means that it is a rigid process, making implementation in the typical multipurpose pharmaceutical manufacturing plant a challenge.

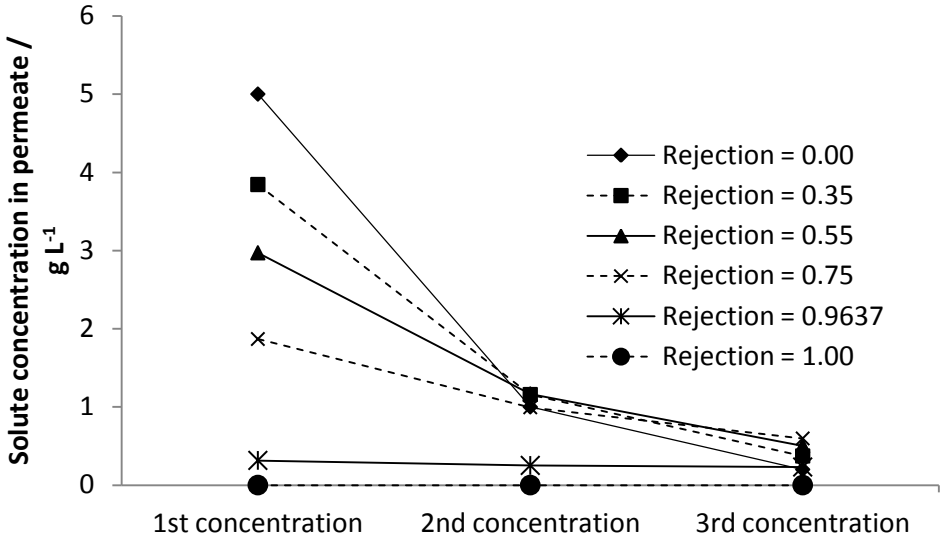

Figure 4.15: Solute concentration in the permeate during the batch concentration steps for the solvent switching of a 5g L^{-1} solution. Only when rejection was unity was there no solute present in the permeate.

4.2.2 Constant Volume Diafiltration

The elevated osmotic pressures in discontinuous diafiltration at high solute concentrations have led to the adoption of constant volume diafiltration (Da Silva et al., 2008). Constant volume diafiltration is the state of the art in OSN processes for solute fractionation (Rundquist et al., 2012b; Sereewatthanaut et al., 2010; So et al., 2010; Székely et al, 2011; Vanneste et al., 2012). In constant volume diafiltration, the membrane is used to retain a compound preferentially while pressure driven solvent flow causes the permeation of the less retained solute(s). The fluid level in the retentate tank is kept constant by a flow of diafiltering fluid into it. Past work has shown that the preferentially retained solute will not always be retained completely (Darvishmanesh et al., 2011; Geens et al., 2007; Rundquist et al., 2012b), hence product purification often occurs in the retentate tank; co-elution makes product purification in the permeate stream impossible. Constant volume diafiltration is simple to use and understand. The solute concentration in the retentate follows the

general formula in Equation 3.5 (Mulder, 1996; Sereewatthanawut et al., 2010) when rejection of the solute is assumed to be constant over time. For easy reference, this is rewritten below.

$$x_{i,j}|_t = x_{i,j}|_0 e^{-N|_t(1-R_{i,j})} \quad \textbf{Equation 4.26}$$

Equation 4.26 suggests that an increased rejection leads to a slower decrease in the concentration of the solute in the retentate over the number of diafiltration volumes. Hence a solute with a higher rejection will be enriched in the retentate over a solute with a lower rejection.

Consider a case where A, a more permeable solute, and C, a more retained solute are separated using constant volume diafiltration. The following 4 equations can be used to quantify the performance of the separation in stage *j*. Firstly, the purity of C enriched in the retentate produced by the diafiltration can be determined using Equation 4.27.

$$X_{C,j}|_t = \frac{x_{C,j}|_t}{x_{C,j}|_t + x_{A,j}|_t} \quad \textbf{Equation 4.27}$$

The yield of C obtained in the retentate is

$$Yield_{C,j}|_t = \frac{x_{C,j}|_t}{x_{C,j}|_0} \quad \textbf{Equation 4.28}$$

The purity of A produced, produced in the permeate stream, can be expressed as

$$Y_{A,j}|_t = \frac{x_{A,j}|_0 - x_{A,d}|_t}{(x_{A,j}|_0 - x_{A,j}|_t) + (x_{C,j}|_0 - x_{C,j}|_t)} \quad \textbf{Equation 4.29}$$

While the yield of A in the permeate stream can be determined by

$$Yield_{A,j}|_t = \frac{x_{A,j}|_0 - x_{A,j}|_t}{x_{A,j}|_0} \quad \textbf{Equation 4.30}$$

Predictions of constant volume diafiltration performance have often been performed using Equation 4.26 and high rejection of the more retained solute have often been cited as a decisive factor in enabling a successful separation (So et al., 2010; Székely et al., 2011) while low rejections of the less permeable product were desired. The use of solute rejection for the prediction of diafiltration

performance, however, is not intuitive. When examining separation processes such as distillation and liquid-liquid extraction, one will notice these process' selectivities are expressed in terms of the partitioning of one solute over the another into another phase. Adapting such an approach in constant volume diafiltration, a selectivity term can be formed using the relative permeability of solute A over solute C into the permeate. This term has been used by a number of groups as a measure of the driving force for solute fractionation through membranes (Caus et al., 2009; Ghosh, 2003; Gunderson et al., 2007; Lightfoot et al., 2008; Mayani et al., 2010), and is termed the relative permeation factor in this work. The relative permeation factor of A over C in a membrane stage *j* is

$$\alpha_{A/C,j} = \frac{y_{A,j}/x_{A,j}}{y_{C,j}/x_{C,j}} = \frac{1 - R_{A,j}}{1 - R_{C,j}} \qquad \textbf{Equation 4.31}$$

The use of this term was demonstrated by simulating the diafiltration of a solution containing A and C, from a C purity of 0.60 to 0.80. The rejections values for A and C were manipulated in the simulations. Simulations with the same relative permeation factors gave identical separation performance and different process productivity (see No. 1 – 4, Table 4.1). The separation performance was determined by the yield of A, the yield of C and the purity of A in the permeate; the process productivity was determined by the number of diafiltration volumes required for the separation. Rejection values were unsuitable for the prediction of separation performance; simulations with different pairs of rejection values that had the same relative rejection differences gave vastly different separation performances, though they had similar productivities (see No. 5 – 8, Table 4.1). It appears that rejection values could only predict process productivity.

Constant volume diafiltration has 2 main challenges. Firstly, it requires the use of considerable amounts of fresh solvent for total purification (Sereewatthanawut et al, 2010). While a solvent recovery stage can significantly decrease solvent usage, energy has to be expended to implement this recycle.

Table 4.1: Summary of effects various solutes' rejections on the separation performance of a constant volume diafiltration process in purifying a feed with Compound C purity of 0.60 to 0.80. Similar to Table 1, No. 1 – 4 had increasing difference in rejections between C and A but had the same relative permeation factor of A over C; No. 5 – 8 had the same difference in rejections between C and A but decreasing relative permeation factor of A over C.

No.	$R_{C,s}$ / -	$R_{A,s}$ / -	$(R_{C,s} - R_{A,s})$/ -	$\alpha_{A/C,s}$ / -	$N\|_t$ / -	$Yield_C$/ -	$Yield_A$/ -	$Y_{A,F}$/ -
1	0.9999	0.9990	0.0009	10.00	1090	0.897	0.664	0.811
2	0.9990	0.9900	0.0090	10.00	109	0.897	0.664	0.811
3	0.9900	0.9000	0.0900	10.00	10.9	0.897	0.664	0.811
4	0.9000	0.0000	0.9000	10.00	1.09	0.897	0.664	0.811
5	0.9000	0.3000	0.6000	7.000	1.63	0.849	0.682	0.751
6	0.8000	0.2000	0.6000	4.000	1.63	0.721	0.730	0.636
7	0.7000	0.1000	0.6000	3.000	1.63	0.612	0.770	0.570
8	0.6000	0.0000	0.6000	2.500	1.63	0.520	0.805	0.528

Secondly, diafiltration is an inefficient process for the removal of trace amounts of permeable solutes. This inefficiency is apparent when one tries to achieve high purity separation using constant volume diafiltration. Suppose a purification of a binary solution containing 10g L^{-1} of Compound C (with a rejection of 0.99) and 10g L^{-1} of Compound A (with a rejection of 0.9) was performed. If the concentrations of these 2 solutes in the retentate were plotted over the number of diafiltration volumes (Figure 4.16), one would notice that the rate of increase in the purity of Compound C in the retentate would decrease over time. This decrease in diafiltration productivity as quantified using the marginal output of diafiltration volumes (Equation 4.32), which was defined as the increase in purity of the less permeable solute (C) in the retentate per to a unit increase in diafiltration volume, decreases towards zero with increasing purity of C (See Figure 4.17).

$$\mathrm{MPD}_j = \frac{\Delta X_{C,j}}{\Delta N} \qquad \textbf{Equation 4.32}$$

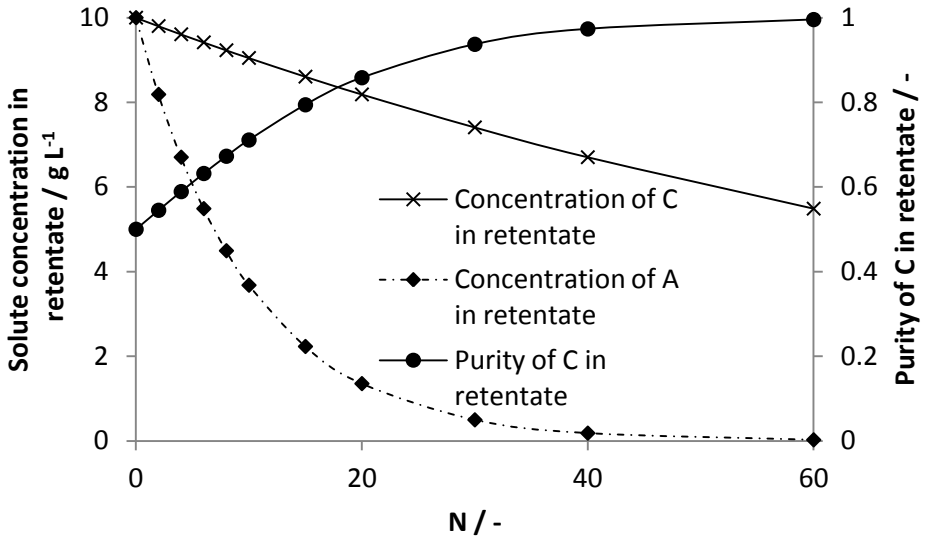

Figure 4.16: Concentration profile of retentate when performing constant volume diafiltration to purify Compound C from a solution containing 10g L^{-1} of Compound A and 10g L^{-1} Compound C. The rejection of Compound A was defined as 0.90 and Compound C as 0.99. Note the diminishing effect of increasing diafiltration volumes as the number of diafiltration volumes increases.

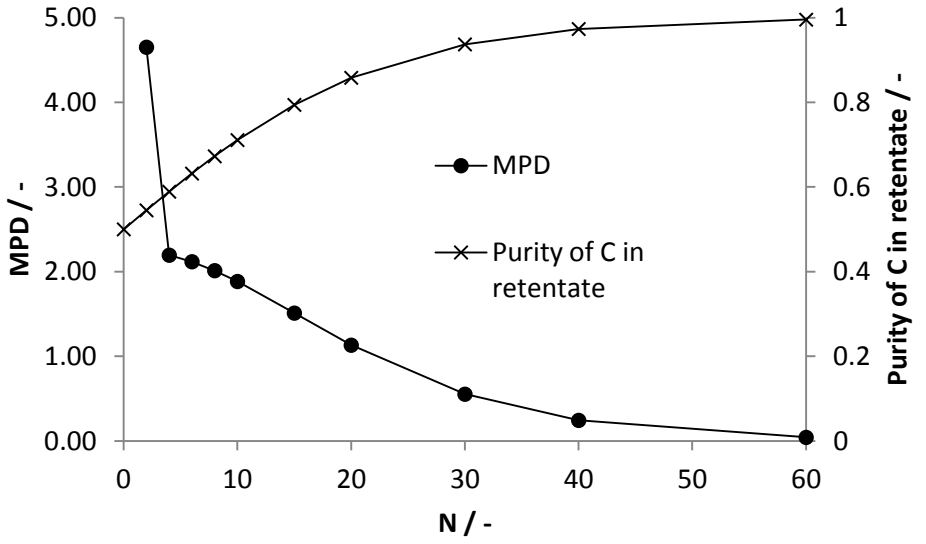

Figure 4.17: Change in the effect of increasing diafiltration volumes in purifying Compound C in the retentate. Note the increasing inefficiency of constant volume diafiltration at high Compound C purity.

The high solvent usage in diafiltration is partly a consequence of the decreasing diafiltration productivity at increasingly high purities. The concentration and amount of retained solute, Compound C, will constantly decay throughout the diafiltration process as long as the rejection of C is less than unity. Hence the decreasing productivity at high Compound C purity will contribute to an increased loss of C at high C purities. While hybrid processes (Pink et al., 2008; Székely et al., 2011; Székely et al., 2012) can decrease solvent usage and increase diafiltration productivity by circumventing the need to perform diafiltration to high purities, these processes involve the use of an irreversible adsorption step that is detrimental to the total process yield of C.

When the rejection of the desired solute is not unity, the solute will also co-elute into the permeate stream, making complete separation of the less permeable and more permeable solute impossible with this process.

4.2.3 Continuous solvent exchange and fractionation

Addressing the challenges in constant volume diafiltration would require maximising depletion of the diafiltering fluid capacity while increasing the removal of the more permeable species. Barring chemical or physical transformation of the solute and the use of a different membrane, a change in process configuration might just be able to achieve that.

While continuous solute fractionation processes have not been demonstrated for organic solvents, Lightfoot & co-workers (Gunderson et al., 2007; Lightfoot, 2006; Lightfoot et al., 2008) and Ghosh (2003) have been particularly prolific in the use of membrane cascades for the fractionation of solutes. They developed a process model for such a cascade, by approximating each membrane stage as a constant volume diafiltration unit. Mayani et al. (2010) brought this idea to fruition by demonstrating the use of a cascade to fractionate lysozyme from other proteins. Their cascade design, however, involves the use of differently sized stages making modular and flexible design of such processes for the pharmaceutical industry challenging. Barker & Till (1992) were able to use a modular system for dextran fractionation, however, their system was batch operated.

4.3 Conclusion

The process models for commonly used membrane processes were reviewed to determine the operational limits of the processes. While examples for the use of single stage batch membrane

processes exist, meaningful deployment of such processes relies on the complete or near-complete retention of the desirable solute. As such these processes are not robust, with slight deviation from total rejection likely to cause failure in separation. Furthermore single stage diafiltration processes are not productive due to the high diafiltering solvent usage for high purity solute fractionation and solvent exchange. Continuous membrane processes developed in response to the limitations of the single stage batch processes have their merits in improving solute fractionation and solvent exchange. However, these processes either inherently do not have the capability to perform the required separation function, or are hard to fit into the typical multipurpose pharmaceutical manufacturing plant due to their non-modular design.

5. Membrane Cascades

Chapter 4 lists the limitations of batch membrane processes and the attempts made to operate these processes continuously in response to these constraints. Many, if not most, of the membrane processes listed were not modular in design due to the different stage sizing. The design of alternative membrane processes, that are flexible and robust, is imperative for the wider adoption of such processes in the typical multipurpose pharmaceutical manufacturing plant. More importantly, there has to be a high level of confidence that the processes can be used for purification even when slight deviations in membrane performance occur.

A new pure solvent recovery and solute concentration membrane process is presented in the first part of this Chapter in response to limited concentration capabilities and rigid design of the existing solvent recovery membrane processes.

In the later part of the Chapter, a membrane cascade process for solvent switching / solute fractionation is presented, in response to the inherently unproductive separation capabilities of batch diafiltration processes.

5.1 Solvent Recovery and Solute Concentration

As noted in Chapter 4, batch solvent recovery membrane processes and their continuous counterparts in literature are unable to perform solute enrichment and pure solvent recovery concurrently unless the membranes used reject the solute in question close to unity. The constraint of high rejection limits the scope for multipurpose usage of these processes, hence impeding their use in pharmaceutical manufacturing. Therefore a new process which can perform solute enrichment and solvent recovery with a wide variety of membrane rejections, while being flexible and modular in nature, needs to be developed.

5.1.1 Case study and process development

In one of the possible routes for the production of a small developmental API molecule (approximately 300Da) at UCB Pharma, a continuous chiral chromatographic process is used to separate the API from its racemic mixture. The chromatography employs a solvent mixture,

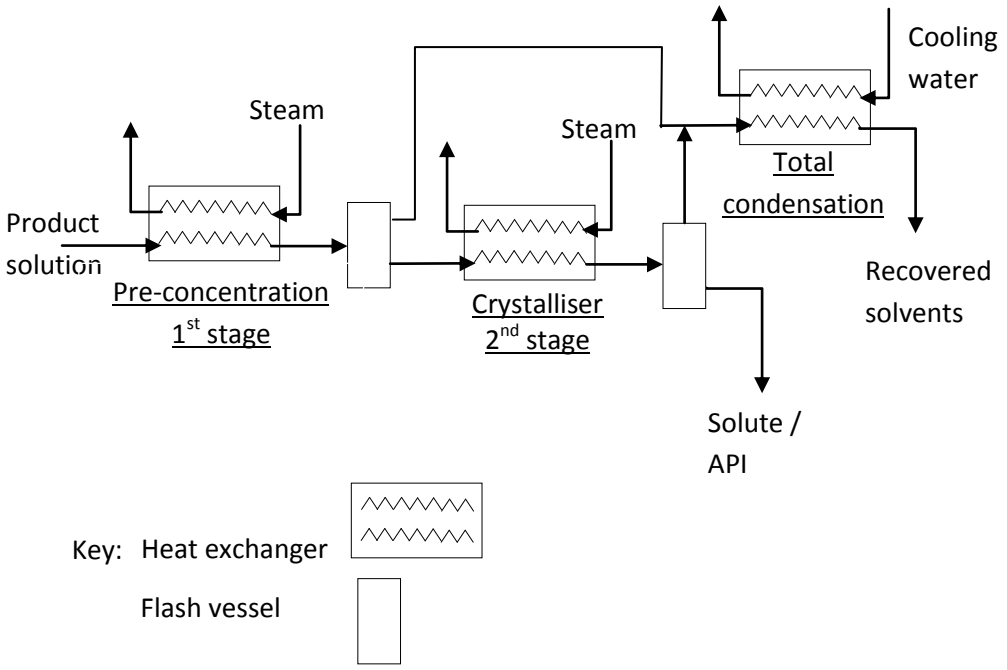

Figure 5.1: Schematic for solvent recovery of the eluent (product solution) from the continuous chromatography process used in the production of the API.

containing methanol and ethyl acetate, as the mobile phase. As large amounts of mobile phase are utilised, they need to be recovered after the separation. The recovery process involves 2 stages. Firstly the product solution, containing either the API or its enantiomer at 10g L^{-1} in concentration, is pre-concentrated with an evaporator to 90g L^{-1}. The resulting vapour stream is then be sent to a total condenser to recover the solvent, which is continuously recycled back into the chromatographic process. Secondly, the product concentrate from the evaporator is sent to a crystalliser where the remaining solvent is evaporated, with the vapours once again sent to a total condenser for solvent recovery. The recovered solvent cannot contain more than 0.005g L^{-1} of solute to minimise impurity effects on the chromatographic separation.

The phase changes in evaporation and condensation require the input of significant amount of energy, even if heat integration can be used to reduce the energy requirement. Furthermore, the higher volatility of methanol relative to ethyl acetate in the mobile phase means the mobile phase composition changes as the product solution is concentrated. The solution becomes less polar as it gets concentrated via evaporation. A consequence is a decrease of API solubility, which is mitigated by heating the concentrate to elevated temperatures to prevent premature crystallization.

The use of a membrane process to replace the first pre-concentration stage was an attractive proposition as the elimination of phase changes may lead to significant energy savings, acting as a hedge against the energy price volatility that has characterised the last decade (Kojima, 2009). Furthermore, if the membranes do not discriminate between the solvents, the API can be kept in solution without addition heating to maintain API solubility.

The limited solute concentration capacity of membrane processes in literature can be addressed with the addition of a stripping section to provide additional solute enrichment capacity. A membrane cascade analog of a distillation column was designed, with a McCabe-Thiele approach used to formulate an easy to use process model for the cascade. The partial molar volume of the solute was neglected. This cascade is illustrated in Figure 5.2. At steady state, the material balance over such a cascade can be split into 3 parts: the part above the feed stage, where the behaviour in each unit is described by the top operating line(s); the part below the feed stage, where the units' performances are represented with the bottom operating line(s); and the feed stage.

The material balance in the rectifying section above the feed stage follows the general formula below, where *i* ($i = A, B, C, \dots$) refers to the solute and *j* ($j = 0,1, \dots, n$) refers to the stage number.

$$P_{j-1}y_{i,j-1} = W_j x_{i,j} + P_p y_{i,p} \qquad \textbf{Equation 5.1}$$

While in the stripping section below the feed, the material balance follows

$$W_{j+1}x_{i,j+1} = P_j y_{i,j} + W_1 x_{i,1} \qquad \textbf{Equation 5.2}$$

Solute *i* partitions across the membrane as a function of its rejection by the membrane.

$$y_{i,j} = \left(1 - R_{i,j}\right)x_{i,j} \qquad \textbf{Equation 5.3}$$

Rearranging Equation 5.1, an equation for the operating line(s) above the feed can be obtained

$$y_{i,j-1} = \frac{W_j}{P_{j-1}} x_{i,j} + \frac{P_p}{P_{j-1}} y_{i,p} \qquad \textbf{Equation 5.4}$$

In a similar fashion, Equation 5.2 can be rearranged to an expression for the bottom operating line(s)

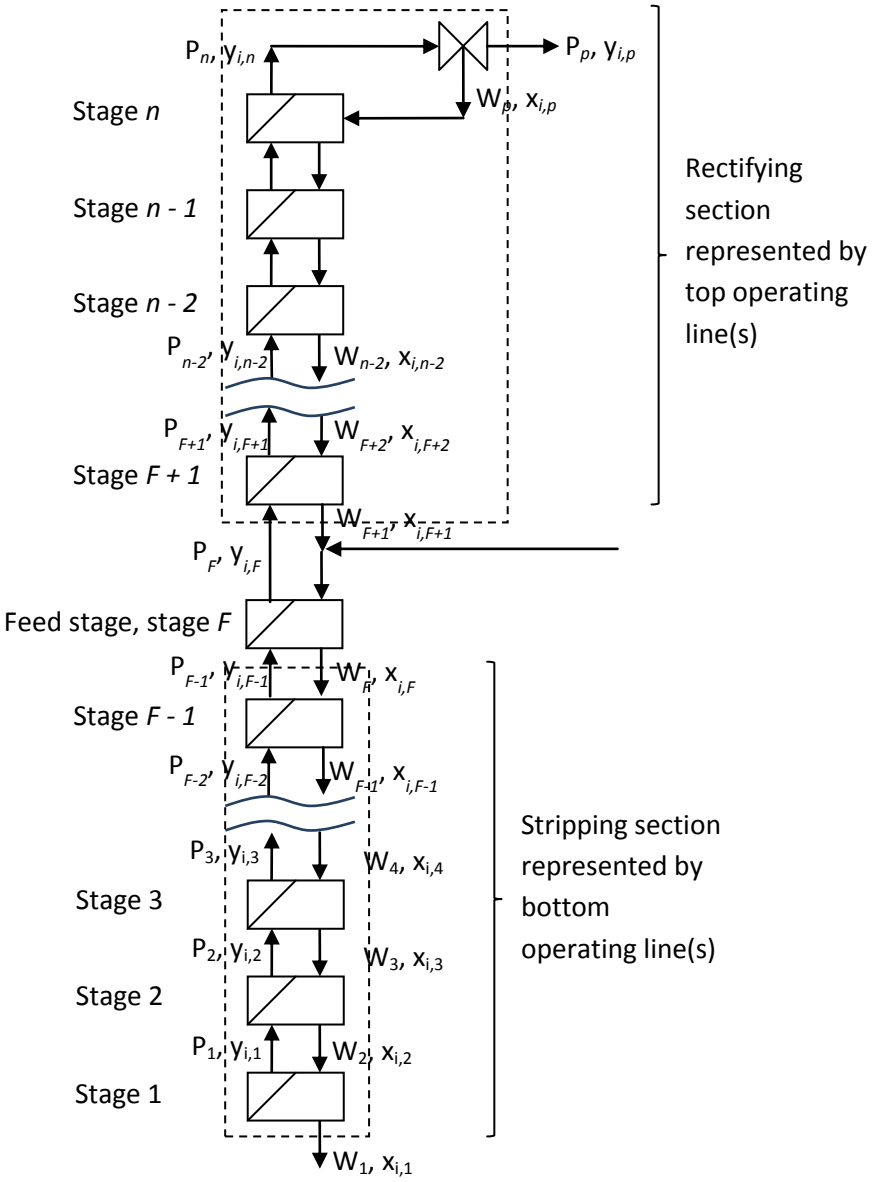

Figure 5.2. Schematic of a multipass membrane cascade with n stages. Cascade stages in the rectifying section decrease solute content in the recovered solvent while stages in the stripping section enrich solute content in the concentrate stream. In this cascade, $x_{i,product} = x_{i,1}$ **and** $y_{i,product} = y_{i,p}$

$$y_{i,j} = \frac{W_{j+1}}{P_j} x_{i,j+1} - \frac{W_1}{P_j} x_{i,1}$$ **Equation 5.5**

The stage into which the feed enters is termed the feed stage. At this stage, the top and bottom operating lines intersect. The material balance over this stage can be expressed by both a top operating line equation (Equation 5.4) and a bottom operating line equation. The analysis of the bottom operating line for this stage requires the inclusion of the additional F and $z_{i,F}$ terms. Rearrangement of this analysis yields Equation 5.6.

$$y_{i,F} = \frac{W_{F+1}}{P_F} x_{i,F+1} + \frac{F}{P_F} z_{i,F} - \frac{W_1}{P_F} x_{i,1}$$ **Equation 5.6**

The overall rejection in this cascade, as a measure of its performance, can be expressed as

$$R_{i,o} = 1 - \frac{y_{i,p}}{x_{i,1}}$$ **Equation 5.7**

5.1.1.1 Degree-of-freedom analysis

Degree of freedom analysis was performed around the cascade to determine potential controllable parameters for the cascade's operation. For each membrane stage *j*, the typically known parameters are P_{j-1} (except for stage 1), W_{j+1}, $y_{i,j-1}$, $x_{i,j+1}$, p_j and T. The unknown variables are P_j, W_j, $y_{i,j}$ and $x_{i,j}$.

The permeate flow from each membrane stage is known to be a function of effective transmembrane pressure across the membrane and stage temperature.

$$P_j = f(p_j, T)$$ **Equation 5.8**

Similarly, the membrane rejection is a function of the effective transmembrane pressure and stage temperature. Consequentially it is a function of membrane flux.

$$R_{i,j} = h(P_j)$$ **Equation 5.9**

Hence Equation 5.3 can thus be expressed as

$$y_{i,j} = \big(1 - h(p_j, T)\big)x_{i,j}$$ **Equation 5.10**

The flow balance around each membrane stage can be expressed as

$$W_j + P_j = W_{j+1} + P_{j-1} \qquad j > 1$$

$$W_j + P_j = W_{j+1} \qquad j = 1$$ **Equation 5.11**

While the solute balance around each membrane stage follows

$$W_j x_{i,j} + P_j y_{i,j} = W_{j+1} x_{i,j+1} + P_{j-1}\, y_{i,j-1} \qquad j > 1$$

$$W_j x_{i,j} + P_j y_{i,j} = W_{j+1} x_{i,j+1} \qquad j = 1$$ **Equation 5.12**

Equations 5.8, 5.10 – 5.12 are 4 independent equations which can be solved to determine the 4 unknown variables for membrane stage *j.* In this scenario, the steady state operation of each stage would rely firstly on control of temperature and secondly on control of either the transmembrane pressure in each stage or the permeate flux from each stage.

Once steady state operation of every individual stage is achieved, steady state operation of the cascade becomes possible. The flow and composition of the feed stream are usually known during design of the cascade hence F and $z_{i,F}$ are known parameters. The unknown variables on the other hand are P_p, W_1, R, $y_{i,p}$ and $x_{i,1}$. In this cascade design, the recycle ratio is defined by

$$R = \frac{W_p}{P_p}$$ **Equation 5.13**

The cascade at steady state will run with a known permeate flow, therefore

$$W_p + P_p = P_n$$ **Equation 5.14**

The flow balance over the whole cascade is represented by

$$F = W_1 + P_p \qquad \textbf{Equation 5.15}$$

And the solute balance by

$$Fz_{i,F} = W_1 x_{i,1} + P_p y_{i,p} \qquad \textbf{Equation 5.16}$$

With 4 independent equations and 5 variables, there is still one degree of freedom. Either $y_{i,p}$ or $x_{i,1}$ must be specified to solve this equation set. To prevent crystallisation in the concentrate stream, $x_{i,1}$ should be fixed. From this analysis, it is apparent that the manipulation of the recycle ratio with the fixing of the product retentate concentration would suffice to control cascade performance.

5.1.2 Factors affecting multipass membrane cascade performance

The illustration of the cascade performance using a McCabe-Thiele approach gives better clarity on how the system will perform in response to changes in

1. The number of stages;
2. The partitioning of the solute across the membrane;
3. The ratio of retentate flow fed into and permeate flow from each stage.

Consider such a 3-stage membrane cascade where a 10g L^{-1} feed is fed into the 2nd stage to produce a concentrate stream of 20g L^{-1}. One can produce a McCabe-Thiele diagram with a single top operating line intersecting a bottom operating line as shown in Figure 5.3. An examination of 5.3(a) reveals that an increase in the number of stages above the feed will decrease solute concentration in the recovered solvent stream, increasing the capacity for solvent purification. On the other hand, an increase in the number of stages below the feed will increase the solute concentration in the concentrate stream, amplifying the cascade's solute enrichment capability.

The effect of solute partitioning across the membrane can be seen when comparing 5.3(a), where the membranes had a single pass rejection of 0.55, and 5.3(b), where the same rejection was 0.80. The cascade depicted in 5.3(b) is able to produce a recovered solvent stream of 0.55g L^{-1}, which is

more dilute than the 3.13g L^{-1} produced in 5.3(a). Effectively, the cascade represented by 5.3(b) has a higher overall rejection of 0.97 compared to 0.84 in 5.3(a).

The consequence of increasing the recycle ratio from 1.2 in 5.3(b) to 10.0 in 5.3(c) is an increase in ratio of retentate fed into, and permeate from, each stage. Overall this will lead to an increase in the gradients for the operating lines in 5.3(c) relative to 5.3(b) and effectively lead to the production of a much more dilute recovered solvent stream (0.23g L^{-1} compared to 0.55g L^{-1}) in 5.3(c) than in 5.3(b).

5.1.3 Comparison of cascades

By changing the recycle ratio in this cascade, the overall rejection can be modified. Simulations were performed for a 3-stage membrane cascade, with a single stage rejection of 0.55, for the concentration of a 10g L^{-1} feed to 30g L^{-1}. An increase in recycle ratio increased the overall rejection in this cascade up to a theoretical maximum of 0.91 when all the permeate was recycled (total recycle; see Figure 5.4). While this maximum overall rejection was identical to the continuous solvent recovery cascades (see Section 4.1.2) and higher than the batch concentration cascade (0.85; see Section 4.1.1.1), this cascade also had a higher capacity for solute concentration than the continuous concentration cascades (maximum retentate concentration of under 23g L^{-1}) due to the inclusion of the stripping section.

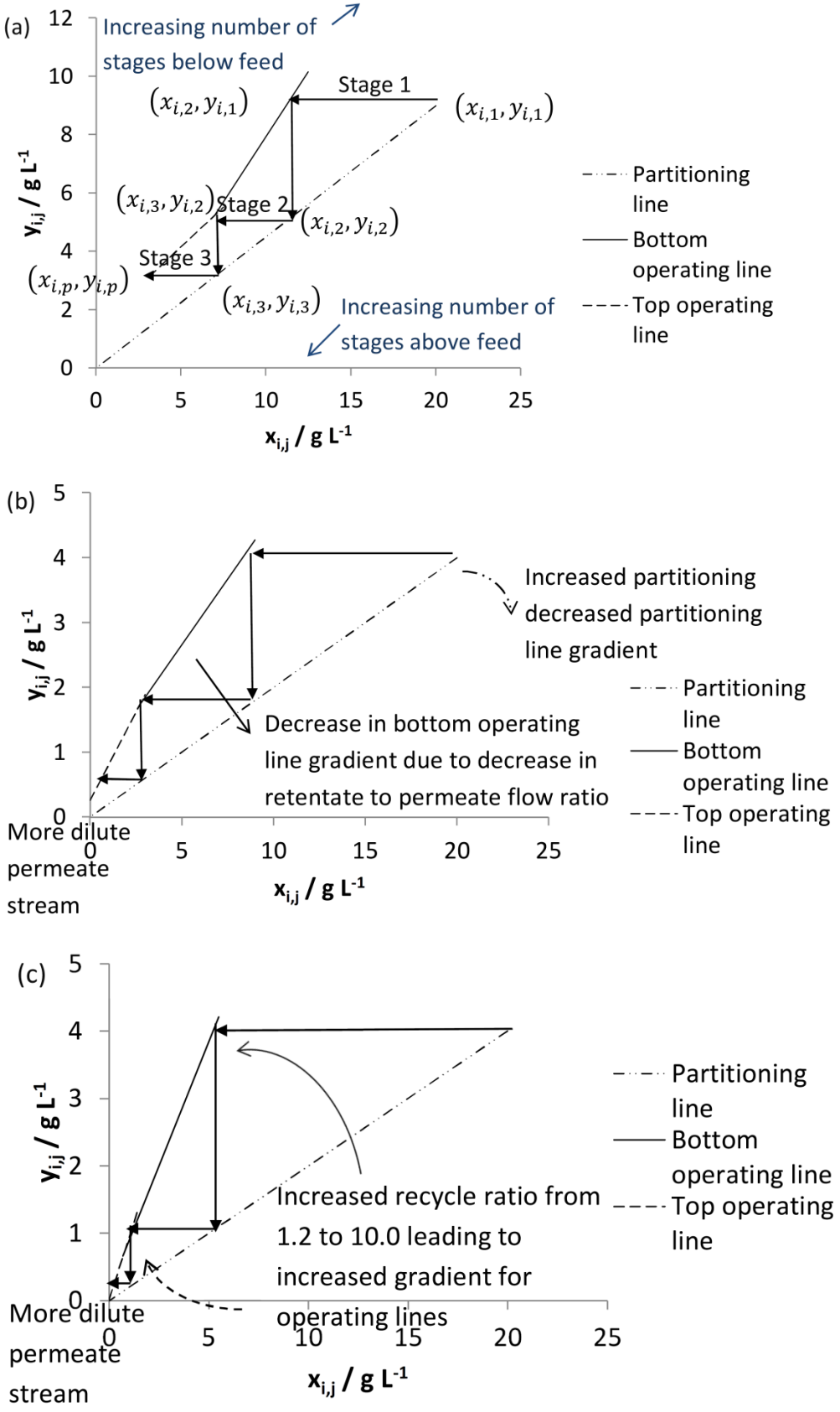
(a)
Increasing number of stages below feed
Stage 1
Stage 2
Stage 3
$(x_{i,1}, y_{i,1})$
$(x_{i,2}, y_{i,1})$
$(x_{i,2}, y_{i,2})$
$(x_{i,3}, y_{i,2})$
$(x_{i,3}, y_{i,3})$
$(x_{i,p}, y_{i,p})$
Increasing number of stages above feed
Partitioning line
Bottom operating line
Top operating line
$y_{i,j}$ / g L^{-1}
$x_{i,j}$ / g L^{-1}
(b)
Increased partitioning decreased partitioning line gradient
Decrease in bottom operating line gradient due to decrease in retentate to permeate flow ratio
More dilute permeate stream
(c)
Increased recycle ratio from 1.2 to 10.0 leading to increased gradient for operating lines
More dilute permeate stream

Figure 5.3. (a) Graphical representation of a 3–stage multipass membrane cascade with a recycle ratio of 1.2, with each stage possessing a single pass rejection of 0.55, used to concentrate a solution from 10g L^{-1} to 20g L^{-1}. (b) Depiction of the membrane cascade, employing membranes with single pass rejection of 0.80 and operating at a recycle ratio of 1.2, used for the same application. Each step change led to a larger change in permeate concentration in that stage, improving recovered solvent quality. (c) Illustration of the same membrane cascade depicted in 5(b), however with a recycle ratio of 10. Increase in recycle ratio led to increases in operating lines' gradients. Consequentially, this led to an improvement in recovered solvent quality.

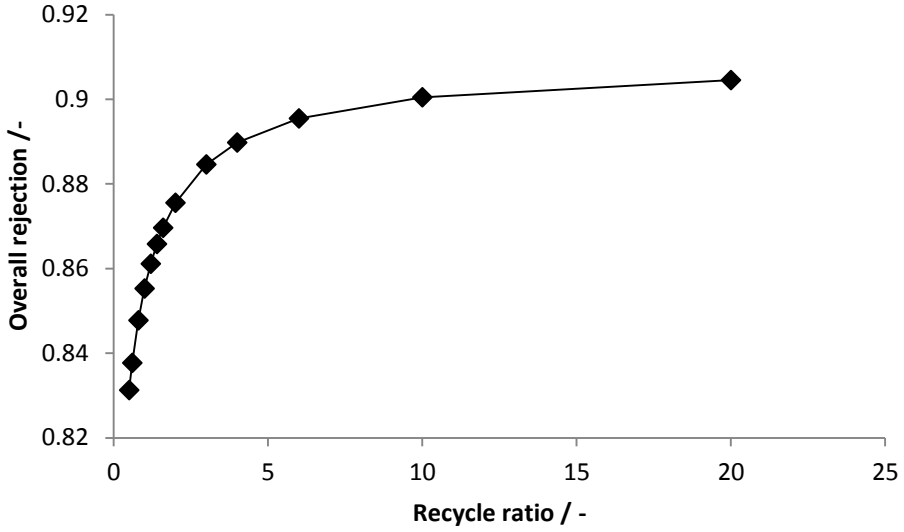

Figure 5.4: Relationship between overall rejection in the multipass membrane cascade and the recycle ratio in the cascade. Note that the overall rejection increased with recycle ratio to a theoretical maximum of 0.91 approached at infinite recycle ratio (total recycle).

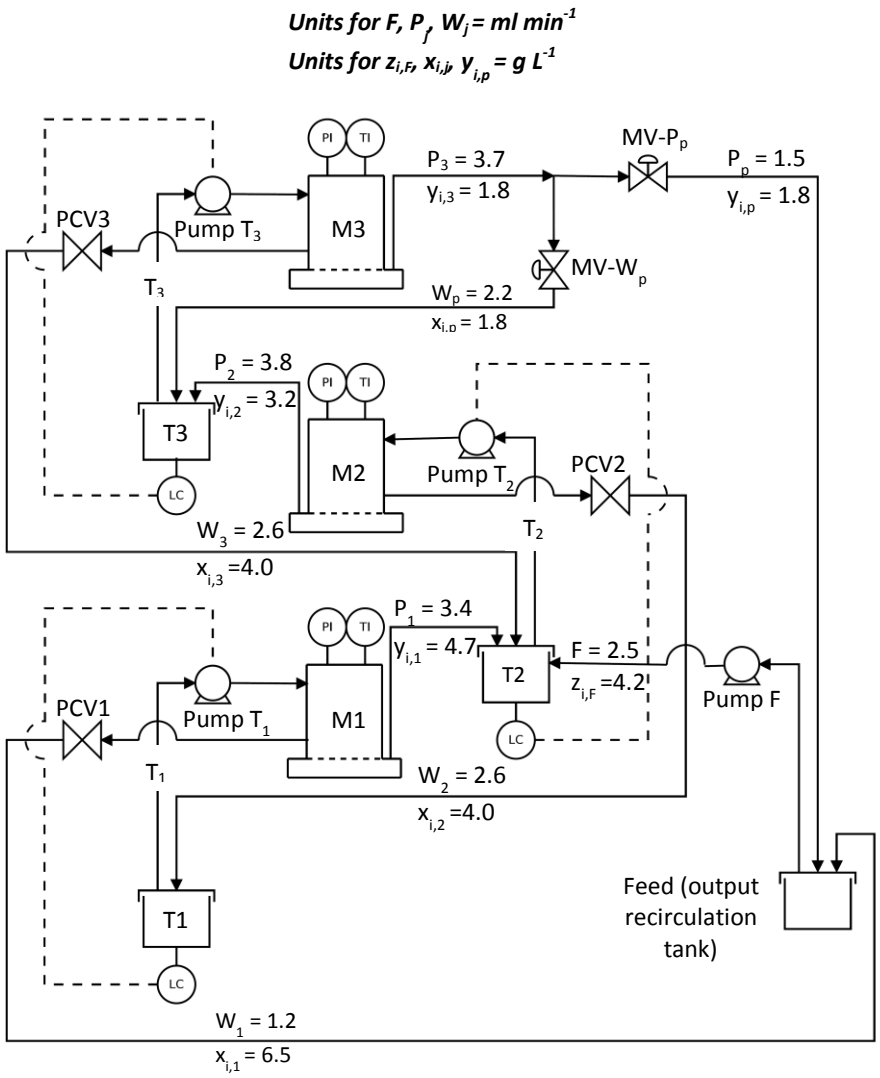

Figure 5.5: Process flow diagram of the 3-stage membrane cascade. M1, M2 and M3 refer to membrane units holding flatsheet membrane coupons. T1, T2 and T3 refer to buffer tanks on weighing scales connected to a computer running a LabView code for the implementation of a level controller. The numbers correspond to the membrane stage they fed into. The dotted lines denote the control loop used for control to maintain steady state operation of the cascade. LC = level controller, MV = metering valve, PI = pressure indicator, PCV = pressure control valve, TI = temperature indicator. Numbers beside the flow and concentration label in each line correspond to the flow and concentration of that line determined via sampling after running the cascade for 141h (Sample 4). The units are ml min^{-1} for flow and g L^{-1} for concentration.

5.1.4 Results and discussions

The favourable simulated performance of the cascade motivated the construction of a 3-stage membrane cascade to demonstrate its feasibility. This cascade was operated over 141h. The permeate and retentate from the cascade were mixed to form the feed stream and recirculated back into the cascade. The feed stream was fed into the 2nd stage to demonstrate operation of both the rectifying section and the stripping section. The schematic of the cascade is shown in Figure 5.5.

5.1.4.1 General observations

Initially, DuraMem® 300 membrane coupons were used in the membrane units. However, the low fluxes (20-23 L m^{-2} h^{-1}, corresponding to permeate flows of 1.8-2.1ml min^{-1}) through these coupons made flow control of the recycle difficult. At times there was not enough back pressure, causing flow through only one of the metering valves. Therefore PuraMem® S membrane coupons, which had higher fluxes (36-46 L m^{-2} h^{-1}, corresponding to permeate flows of 3.2-4.2ml min^{-1}) were used instead.

Due to the large system volume relative to the flow rates in the system (leading to long residence times) and the number of stages, the time it took for the cascade to reach steady state was very long. In the case of this cascade, the flows stabilised about 20h after starting up the system. A similar observation was noted by Lin & Livingston (2007). This stabilisation time can be reduced by decreasing the ratios of system volume to flow rates. However, due to equipment constraints, this was not possible for this work.

Whilst the single stage rejection of the membrane units were low and never higher than 59%, the overall rejection of the whole cascade was much higher, ranging from 73-83%. The consistency of the overall cascade performance was remarkable despite the large variation in the single stage rejection over time. This suggests that a cascade system is inherently more reliable than a single stage system in maintaining system performance.

5.1.4.2 Solvent partitioning over the membrane

Initial filtration of only the solvent mixture was performed to ascertain if the two different solvents permeated through the membrane at significantly different rates.

Single stage membrane filtration recirculation experiments were performed as described in Section 3.3.1. The filtration of the solvent mixture was shown not to produce significant solvent partitioning, with the rejection of methanol being relatively constant at all pressures tested (See Table 5.1). A membrane cascade, employing PuraMem® S membranes, was designed for the concurrent production of a recovered solvent stream, with not more than 0.005g L^{-1} of solute, and a concentrate stream, with 90g L^{-1} of solute, from a feed stream containing 10g L^{-1} of solute. The design required 14 stages and a methanol rejection of 8% was predicted to give a methanol concentration of 8.5wt% in the permeate stream and 12.1wt% in the retentate stream from a feed concentration of 8.9wt%.

Table 5.1: Single-pass methanol rejection at various pressures over the membranes to be employed in the cascade

Pressure / bar	MeOH rejection PuraMem® S	MeOH rejection DuraMem®300
10	0.069	0.016
20	0.076	-0.12
30	0.051	-0.19

Furthermore, initial operation of the 3-stage membrane cascade employing DuraMem® 300 membranes at 30bar was shown to not significantly accentuate any slight solvent partitioning (see Table 5.2). As a result, changes in solvent composition should not be of concern during operation of the cascade. This is significant because the solvent composition is critical to API solvation, ensuring premature precipitation of the API will not be an issue when using the cascade.

Table 5.2. Partitioning of methanol when using a 3-stage membrane cascade employing DuraMem® 300 membranes. Pressure in each stage maintained at 30bar.

Sample	Operating Time	$R_{MeOH,1}$ / -	$R_{MeOH,2}$ / -	$R_{MeOH,3}$ / -	$R_{MeOH,o}$ / -	$z_{MeOH,F}$ / wt%	$x_{MeOH,1}$ / wt%	$y_{MeOH,p}$ / wt%
A	5h	-0.034	-0.003	0.069	-0.120	9.09	7.41	8.27
B	29h	-0.067	-0.032	-0.028	-0.060	9.19	6.71	7.15

5.1.4.3 Control issues

There was an issue with the consistency of solute rejection in each unit, which seemed to be linked to the control of permeate flow from each stage. Pressure was controlled, instead of retentate flow and permeate flow, in each unit. As a result, there were runs where the retentate flow from the *(j +*

1)th unit and/or permeate flow from the *(j - 1)*th stage were/was too low. Consequently, the feed flow into the *j*th unit (T_1 , T_2 and T_3; See Table 5.3) had to be lowered to maintain the setpoint level in the buffer tank. At a certain feed flow level, the flow was insufficient in maintaining the pressure set by the pressure control valve while at the same time was not low enough to cause a pressure decrease below the threshold pressure for the control valve to close. Hence the membrane unit was unable to repressurise to the set pressure and this sustained reduction in pressure led to a decrease in the rejection of API along with the permeate flux in that unit. To implement a more effective embodiment of this cascade, it might be prudent to use a flow controller to control the permeate fluxes in each membrane stage instead. This will allow control of fluxes in each stage directly and more effectively, albeit with higher equipment costs.

5.1.4.4 Effect of solute partitioning

When comparing the samples 1 and 2 with sample 4 (see Table 5.3), one will notice that the higher single pass rejection in stage 2 in samples 1 and 2 (0.56 and 0.57 compared to 0.37) resulted in a higher overall rejection in these samples (0.81 and 0.80 compared to 0.73). Therefore it has been demonstrated that a higher single pass rejection will increase the overall rejection and improve the separation performance of the cascade.

5.1.4.5 Effect of increasing recycle ratio

The increase of the recycle ratio increased the overall rejection of the cascade as shown in Figure 5.6. In samples 1 and 2 (operating time of 20h and 43h, respectively), where the recycle ratios were 1.3, the overall rejections were 0.81 and 0.80, respectively. An increase of recycle ratio to 4.10 in sample 3 (operating time 70h) increased this rejection to 0.87. This was, however, achieved at the expense of the capacity which the cascade could treat. Whereas in samples 1 and 2, 1.8ml min^{-1} and 1.7ml min^{-1} of recovered solvent streams were produced, in sample 3 only 0.8ml min^{-1} of recovered solvent was produced.

Table 5.3: Relationship between the feed pumps' flow rates with the permeate flux and API rejection in each stage. Note the lower single pass rejection of the API ($R_{A,j}$) in some stages, which corresponded to lower fluxes (f_j) from those stages and lower pump flow rates into those stage

Sample	Operating Time	T_1 / ml min^{-1}	f_1 / L m^{-2} h^{-1}	$R_{API,1}$ / -	T_2 / ml min^{-1}	f_2 / L m^{-2} h^{-1}	$R_{API,2}$ / -	T_3 / ml min^{-1}	f_3 / L m^{-2} h^{-1}	$R_{API,3}$ / -	$R_{API,o}$ / -	R / -
1	20h	3.32	36	0.22	7.30	44	0.56	5.74	46	0.58	0.81	1.3
2	43h	3.94	37	0.27	7.84	43	0.57	5.99	44	0.52	0.80	1.3
3	70h	5.21	42	0.55	9.10	43	0.59	6.95	45	0.58	0.87	4.1
4	141h	4.61	38	0.28	8.44	43	0.37	6.22	41	0.55	0.73	1.5

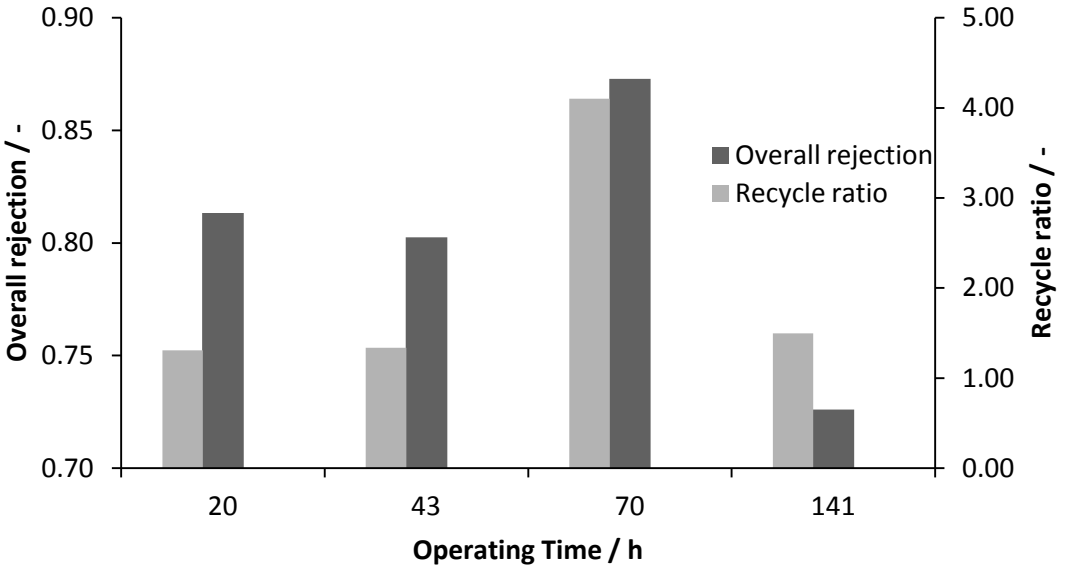

Figure 5.6. Dependence of overall rejection on the recycle ratio in the cascade. There was a strong correlation between the overall rejection and recycle ratio. An increase in recycle ratio produced an increase in the overall rejection in the cascade.

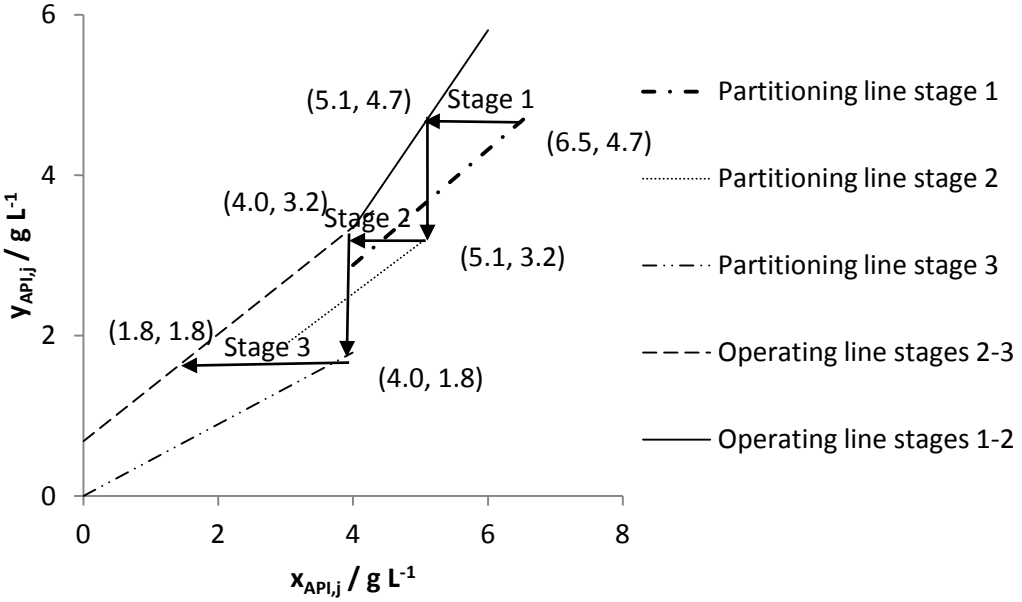

Figure 5.7: Graphical illustration of the cascade operation on a McCabe-Thiele type graph for sample 4. Refer to Figure 5.5 for the corresponding flows and concentration in that sample set.

5.1.4.6 Process model validation

Figure 5.7 illustrates the behaviour of the cascade in sample 4 (refer to Figure 5.5 for concentration and flow numbers). In general, the operating lines have a gradient of $\frac{W_{j+1}}{P_j}$ while the partitioning lines have a gradient of $\left(1 - R_{i,j}\right)$. The cascade aims to produce both a high purity solvent stream (low concentration in permeate, y-axis) and a high concentration retentate stream (high value on the x-axis). Operating lines with steeper gradients will therefore perform the separation with a lower number of stages while partitioning lines with gentler gradients have the same effect. As a result, a large difference between the gradients of the operating line and the partitioning line decreases the effort required for the separation. On the other hand, if the operating line and the partitioning line intersect, that intersection is a pinch point where the solute concentration in both the retentate and the permeate will change no further no matter the number of stages put in place. In such a cascade, it is impossible for the concentrations of the retentate and the permeate at that pinch point to be achieved.

The equation set for the multipass membrane cascade was solved for each sampled run by plugging in experimental values for pump, permeate and retentate flows (see Table 5.4); the solute concentration in the feed, $z_{API,F}$, (see Table 5.5) and the rejection values in each stage (see Table 5.3). The model was fitted to experimental data by determining the least sum of squared residuals between the experimental solute concentration values and the process model predicted values. A more detailed description is given in Appendix 8.4. As seen in Table 5.6, the predicted concentrations were in agreement with the actual concentrations. The magnitudes of difference between the predicted concentrations and the experimentally determined concentrations were all either equal to or below 30%.

Table 5.4: Flow table showing flows sampled and recorded during cascade operation.

Sample	Operating Time	Measured Flows / ml min^{-1}		Pump Flows / ml min^{-1}				Inferred Flows / ml min^{-1}					
		W_1	P_p	T_1	T_2	T_3	F	P_1	P_2	P_3	W_2	W_3	W_p
1	20h	0.1	1.8	3.32	7.30	5.74	2.50	3.2	4.0	4.2	3.3	1.6	2.4
2	43h	0.6	1.7	3.94	7.84	5.99	2.50	3.3	3.9	4.0	3.9	2.0	2.3
3	70h	1.5	0.8	5.21	9.10	6.95	2.50	3.7	3.9	4.1	5.2	2.9	3.3
4	141h	1.2	1.5	4.61	8.44	6.22	2.50	3.4	3.8	3.7	4.6	2.6	2.2

Table 5.5: Concentration table showing sampled concentrations of API during operation of the cascade.

Sample	Operating Time	API concentration / g L^{-1}							
		$z_{API,F}$	$x_{API,1}$	$y_{API,1}$	$x_{API,2}$	$y_{API,2}$	$x_{API,3}$	$x_{API,p}$	$y_{API,p}$
1	20h	3.3	7.4	5.7	5.9	2.6	3.3	1.4	1.4
2	43h	3.5	7.7	5.7	5.9	2.5	3.1	1.4	1.5
3	70h	5.9	7.9	3.5	4.9	2.0	2.4	1.0	1.0
4	141h	4.2	6.5	4.7	5.1	3.2	4.0	1.8	1.8

Table 5.6: Relative convergence of the calculated solute concentration values and the actual sample concentration values.

Sample	Percentage difference between predicted concentration and actual concentration						
	$x_{API,1}$	$y_{API,1}$	$x_{API,2}$	$y_{API,2}$	$x_{API,3}$	$x_{API,p}$	$y_{API,p}$
1	-17	-17	-8.0	-8.0	-10	-11	-10
2	16	16	11	11	22	30	22
3	20	20	2.4	2.4	4.0	4.6	4.0
4	-0.21	-0.21	1.6	1.6	-1.9	-4.6	-1.9

5.1.4.7 Economic feasibility

An evaluation of the economic feasibility of using the cascade to replace the first solvent recovery stage described in this case study, for the concentration of the API solution from 10g L^{-1} to 90g L^{-1} while producing a very pure recovered solvent stream containing not more than 0.005g L^{-1} API, was performed. While optimisation techniques are known (Gassner & Marechal, 2010; Voros et al. 1997), they were not implemented. Given the relatively short product lifecycle in a non-generic API producer, focus was placed instead on designing a cascade that is highly modular and flexible for multipurpose usage. Hence all the stages in the cascade were sized identically and operated with the same permeate flow and rejection. The position of permeate recycle was fixed in the last stage for simplicity. The feed was located at the stage that possessed a retentate concentration which had the lowest difference with the feed concentration to operate close to idealised cascade conditions where minimum work was required for the separation (McCandless, 1994; McCandless, 1999).

Experimental rejections of the API at the test pressures were used in the simulations. Initial simulations were performed for 2 variables, R = 1 and 3 and P = 10bar and 30bar. The linear regression of the annualised cost for these simulations suggests that the annualised cost will be minimised at maximum pressure where the single pass rejection was the highest at 0.71. This was in line with expectations given the high cost of the membranes. Note that publication of the price of the membranes has been restricted by the manufacturer Evonik-MET. Since it was not possible to obtain data for rejection at higher pressures given the capacity limitation of pumps at UCB Pharma SA, a sensitivity analysis was performed for various recycle ratios at 30bar.

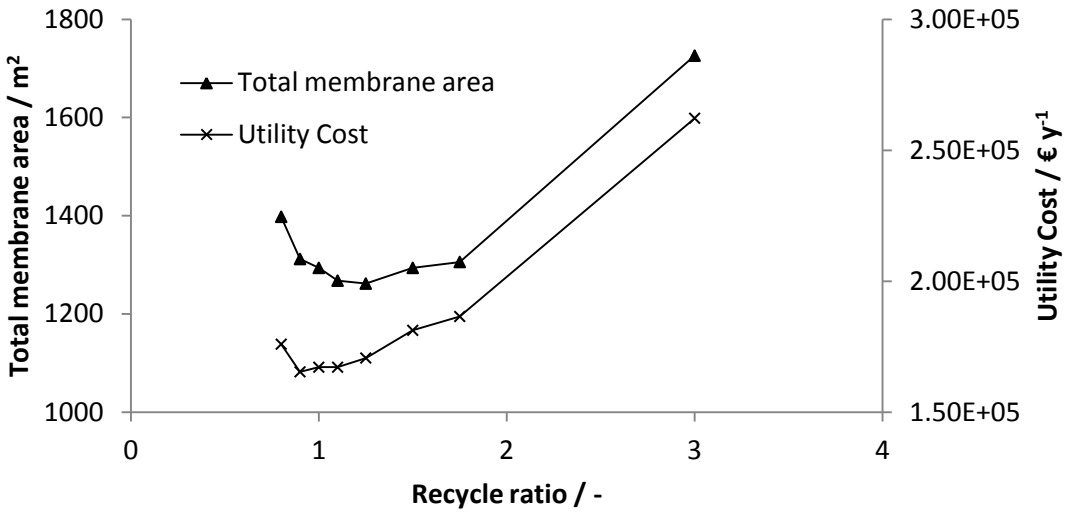

Figure 5.8: Relationship between total membrane area required and utility cost (operating cost) of the cascade with the recycle ratio of the cascade. Simulations were performed using single pass rejection of API at 30bar across a PuraMem® S membrane.

The relatively high cost of the membrane modules meant the total membrane area required correlated very well with the capital expenditure of such a process, and an optimal cascade design would require the minimisation of membrane area required. While the minimum utility cost occurred at around R = 0.9, the minimum for membrane area requirement occurred at R = 1.2. At R = 1.2, total utility cost was estimated to be €170k/year for 1.5E6 kWh y^{-1} of electricity (Refer to Figure 5.8). This translated to a cost increase of about €20k/year for a process that used about half the energy used in flash-condensation, due to the switch to electricity which is more costly than gas. The challenge in producing additional energy saving in the membrane cascade arose from the inability to perform integration of electrical energy used in the pumps. Unless there are specific needs for non-thermal treatment when recovering the solvents, it is unlikely to be an attractive option.

It would appear that membranes with better rejection properties are required to make such cascades competitive with traditional processes. To give a perspective on how membrane rejection will affect the design of the cascade, simulations were performed with the assumption that single pass solute rejection could be changed independently (for example by changing the solute used). In these simulations, 10g L^{-1} of solution was once again treated to form a concentrate stream of 90g L^{-1} and recovered solvent stream of not more than 0.005g L^{-1}. For each solute rejection, the optimal recycle ratio was changed to minimise utility cost. The results, as summarised in Table 5.7, show that

even a slight increase of single pass rejection to 0.800 brought the operating cost down to a level competitive with the flash-condensation process described in Section 5.1.1, which was predicted at UCB Pharma to have a utility cost of €150k per year. More importantly, this set of simulations shows that the cascade can provide significant cost savings without requiring the use of too much membrane area even if the rejection across the membrane is not complete. Therefore it is clear that the use of the cascade can be very attractive if tight membranes with high fluxes were developed.

Table 5.7: Dependence of the multipass membrane cascade performance on solute rejection. As single pass rejection of the solute ($R_{i,j}$) increases, a lower recycle ratio (R) is required for the permeate product stream to meet specification. In turn fewer stages will be required for the separation leading to a decrease in cascade sizing and utility requirement.

$R_{i,j}$ / -	Optimal R / -	No. of stages required / -	Feed stage / -	Pump power / kW	Membrane area required / m^2	Utility cost / € y^{-1}
0.700	1.20	14	4	210	1330	180 000
0.800	0.60	12	3	120	830	100 000
0.900	0.40	8	2	68	480	60 000
0.980	0.20	4	2	34	210	30 000
0.990	0.10	4	2	30	190	26 000
0.999	0.05	2	1	16	90	14 000
1.000	0.00	1	1	12	40	11 000

5.1.5 Conclusion on solvent recovery cascade

The use of a membrane cascade in improving the performance of membranes in solute concentration and solvent recovery of a dilute API solution was demonstrated. The separation was particularly challenging as it was done on a small API (molecular weight under 300Da). The separation capability of this membrane cascade is not limited by the separation performance of the membrane used. Competent engineering, with the aid of easily available equipment, can be used to augment the separation capacity of otherwise loose membranes. The system is controllable through the manipulation of the recycle ratio, and is flexible, robust and reliable in the event of changing feed conditions. On the other hand, the difficulty in energy integration on such a cascade, due to the dominant use of electricity in this operation, and the high cost of the membrane relative to its performance, make such a cascade economically uncompetitive at the moment. However, with the emergence of better membranes, such cascades might become attractive as the lower energy

requirements provide a good hedge against energy price volatility that has characterised the last decade (Kojima, 2009).

5.2 Solute Fractionation and Solvent Exchange

The state-of-the-art single-stage diafiltration processes used for solute fractionation / solvent recovery are not robust due to the sensitivity of their performance to slight deviations in membrane rejection. Furthermore, full solute fractionation on a single membrane stage requires total membrane rejection of the desired compound and such a rejection is not always possible. The requirement for process flexibility in the pharmaceutical industry also demands that any membrane process should function without stringent need for total rejection of any solute.

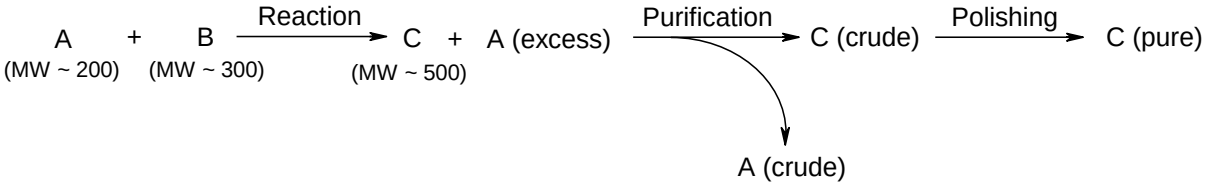

Scheme 5.1: Scheme for the production of a developmental API (Compound C) at UCB Pharma S.A. Compounds A and B were reacted in a coupling reaction, with the less costly Compound A added in excess to increase conversion of the more costly Compound B. A purification step was needed to purify Compound C first before a crystallisation step could be used to obtain a pure Compound C.

5.2.1 Case study and process development

In the synthesis of a developmental API at UCB Pharma S.A., a final coupling process between 2 reagents A and B was used to form the API, Compound C (see Scheme 5.1). Reagent A has a molecular weight of about 200Da; B has a molecular weight of about 300Da; and C has a molecular weight of about 500Da. The addition of excess A, which was less costly than B, was desired because it increased the in-situ yield of Compound C from 70%, when equimolar amounts of A and B was used, to 100%, when a much higher ratio of A to B was used. The corresponding cycle time for the reaction was also reduced from 3 days to 1 day. However, this addition of excess A was constrained by traditional separation techniques at UCB Pharma. These compounds (A, B and C) were all neutral and hence typical acid/base treatment and water wash of the organic phase were unable to remove excess A from C. Furthermore the crystallisation processes developed were unable to purify C when too much A was present. Since conventional purification processes at UCB Pharma were ineffective,

an OSN process was the only possible purification method that could remove most of reagent A from Compound C, after reagent B was completely consumed, before a final crystallisation step could be used to polish Compound C (see Scheme 5.1). At the end of the reaction step in Scheme 5.1, the binary weight purity of C was 0.60 and 0.40 for A. The target for OSN purification was to increase the purity of C to 0.80, while reducing the purity of A to 0.20, to enable the polishing step of the crude mixture.

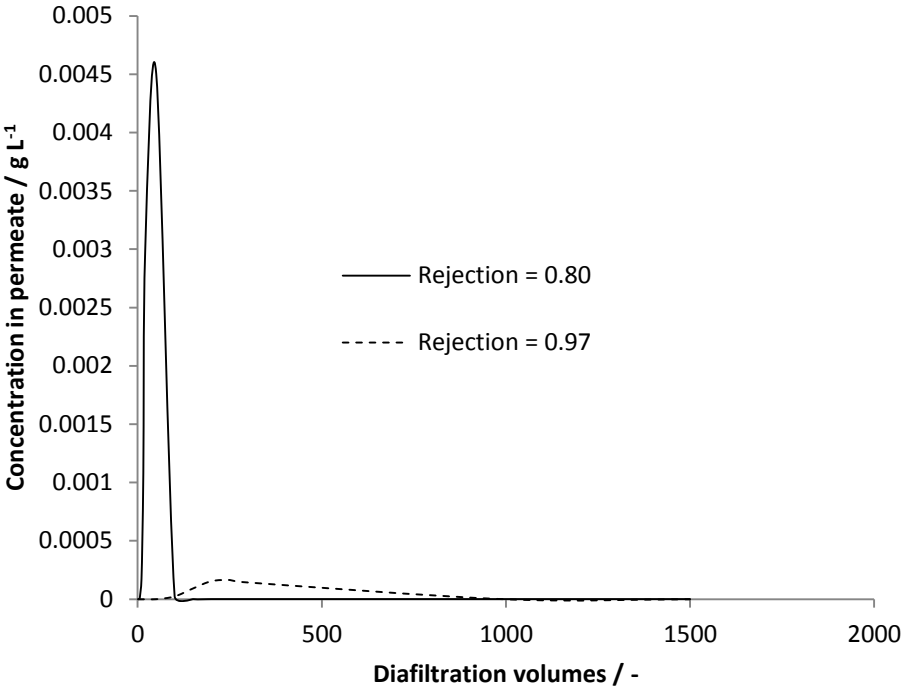

Figure 5.9: Diafiltration of a solution, containing 2 solutes of 10g L^{-1} each, across an 8-stage cascade. The rejection of the more permeable solute was 0.80 and its elution from the cascade was more apparent at first. The rejection of the less permeable solute was 0.97 and it eluted only after further diafiltration volumes were delivered. In contrast to chromatography, the less permeable solute can be collected from the retentate rather than through elution from the cascade.

As the rejection of C by the membrane was not absolute, a new process had to be determined for the successful fractionation of A from C. While in theory, a series of membrane stages be used as the

stationary phase for chromatography (see Figure 5.9), the increase in the number of stages is not as trivial as traditional chromatography and a simpler process had to be developed.

A new membrane process should address 2 challenges faced in constant volume diafiltration to be economically competitive. Firstly, the consumption of diafiltering solvent for solute fractionation needs to be reduced. Secondly, the loss of the less permeable solute needs to be minimised even as increasingly high purities of the separated solutes are achieved, if total rejection of the solute is impossible. The desired outcome might be realised with the appropriate stream recycles. Work on solute fractionation via liquid-liquid extraction has been published (Brian, 1972; Robbins & Cusack, 1998). This was adapted to design 2 types of membrane cascades, with the relative permeability of one solute over the other through a membrane driving the separation. A McCabe-Thiele approach was used to develop the process models for the membrane cascades. To simplify the process models, the partial molar volumes of the solutes were ignored i.e. the volume of the solution was assumed to remain unchanged with solute solvation.

A solute fractionating cascade would take the form illustrated in Figure 5.10. A feed solution containing the solutes to be separated is fed into the feed stage. It is then channelled progressively through the retentate chambers of a series of membrane units below the feed, termed the stripping section of the cascade, where it is stripped of the more permeable solute with a countercurrent flow of solvent media (stripping fluid). The staged process in the stripping section encourages maximal depletion of the stripping solvent stream as it is reused over a number of stages. Eventually, a stream enriched with the less permeable solute exits as the retentate of the 1st stage. Simultaneously, the increasingly depleted stripping solvent is sent upwards of the stripping section into the feed stage, where it strips the feed solution for one final stage. This depleted solvent stream exiting as the permeate of the feed stage is then sent up through a purifying section which attempts to further retain the less permeable species relative to the more permeable solute. This is achieved through a series of membrane stages and appropriate recycling of the permeate stream from the final stage back into the purifying section.

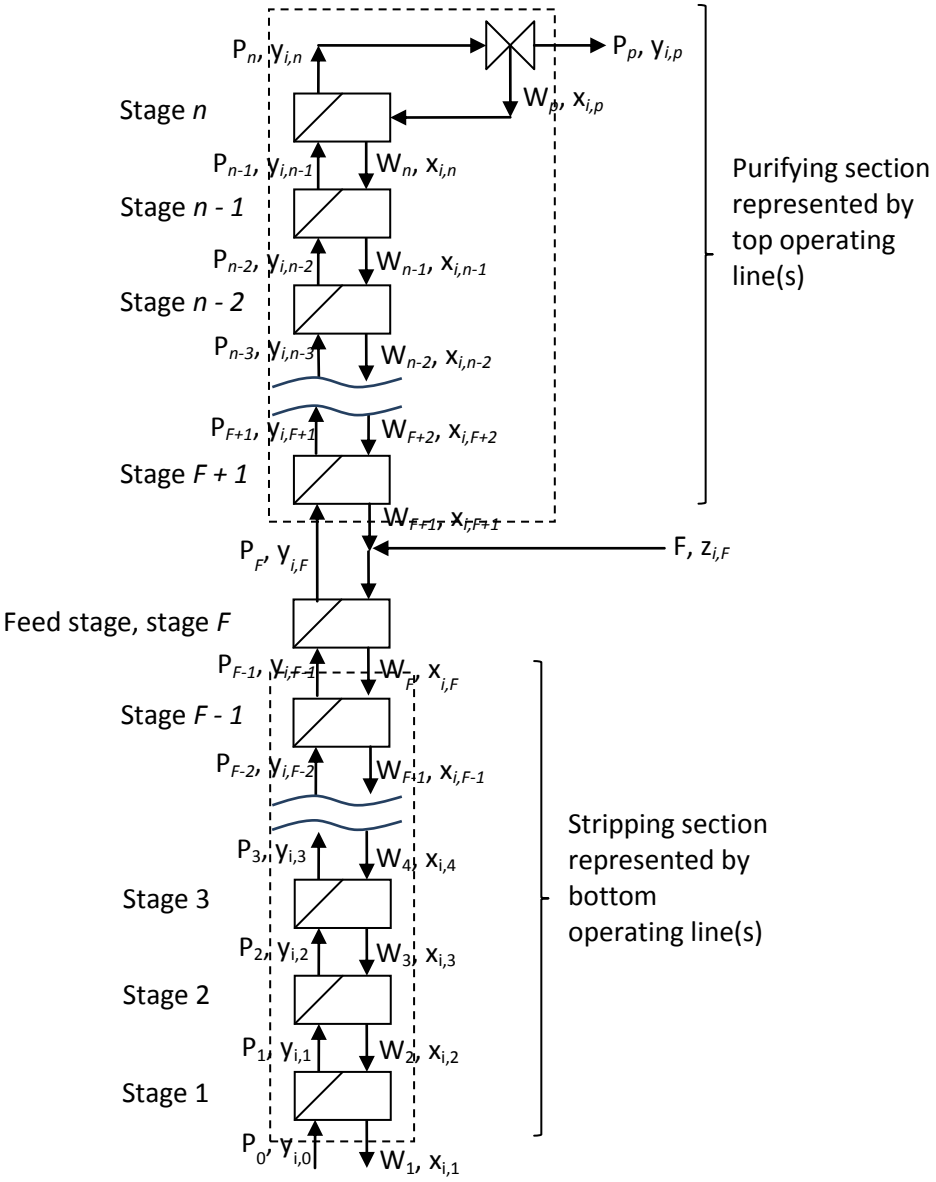

Figure 5.10. Schematic of a continuous solute-fractionating membrane cascade. The solution to be fractionated is fed into the feed stage *F*. A countercurrent flow of stripping (diafiltering) fluid is channelled into the retentate chamber of stage 1 via P_0. The permeate stream from stage *n* is partially recycled back into the purifying section to recover the less permeable solute. The retentate from stage 1 is the stripped product stream enriched in the less permeable solute. The net permeate from the cascade in stream P_p is the purified product stream enriched in the more permeable solute.

To develop a process model, the material balance over the stripping section was analysed first $(i = A, B, C, \ldots;\ j = 0,1, \ldots, n\ )$.

$$P_j y_{i,j} + W_1 x_{i,1} = W_{j+1} x_{i,j+1} + P_0 y_{i,0} \qquad \textbf{Equation 5.17}$$

By rearranging the material balance, the stripping section can be described by the operating line equation

$$y_{i,j} = \frac{W_{j+1}}{P_j} x_{i,j+1} - \frac{W_1}{P_j} x_{i,1} + \frac{P_0}{P_j} y_{i,0} \qquad \textbf{Equation 5.18}$$

If the feed stage is included in the material balance analysis with the stripping section, Equation 5.19 will adequately describe the material balance of the streams around the feed stage

$$W_{F+1} x_{i,F+1} + F z_{i,F} + P_0 y_{i,0} = W_1 x_{i,1} + P_F y_{i,F} \qquad \textbf{Equation 5.19}$$

This can be rearranged to

$$y_{i,F} = \frac{W_{F+1}}{P_F} x_{i,F+1} + \frac{F}{P_F} z_{i,F} - \frac{W_1}{P_F} x_{i,1} + \frac{P_0}{P_F} y_{i,0} \qquad \textbf{Equation 5.20}$$

On the other hand, the general material balance equation of the purifying section can be expressed as

$$P_j y_{i,j} = W_{j+1} x_{i,j+1} + P_p y_{i,p} \qquad \textbf{Equation 5.21}$$

Hence, the operating line for the purifying section on a McCabe-Thiele plot is

$$y_{i,j} = \frac{W_{j+1}}{P_j} x_{i,j+1} + \frac{P_p}{P_j} y_{i,p} \qquad \textbf{Equation 5.22}$$

If the permeate flux in all stages were assumed to be constant for initial design, Equation 5.22 can be expressed as

$$y_{i,j} = \frac{R}{1+R} x_{i,j+1} + \frac{1}{1+R} y_{i,p}$$ **Equation 5.23**

Where

$$R = \frac{W_p}{P_p}$$ **Equation 5.24**

In each stage the partitioning lines, which dictate how the solutes partition across the membrane, can be expressed as

$$y_{i,j} = \left(1 - R_{i,j}\right) x_{i,j}$$ **Equation 5.25**

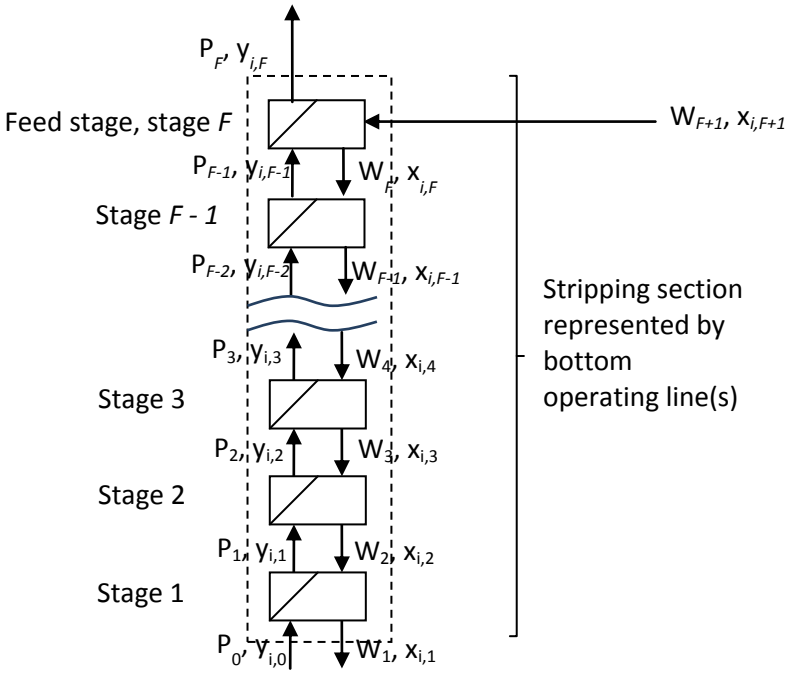

Figure 5.11. Schematic of a staged membrane cascade for permeable stripping. The solution to be purified is fed into the feed stage *F*. A countercurrent flow of stripping (diafiltering) fluid is fed into the retentate chamber of stage 1 via P_0. The retentate from stage 1 is the stripped product stream enriched in the less permeable solute. The permeate from the feed stage, enriched in the more permeable solute, is the waste stream from the cascade.

This fractionating cascade can be simplified when the rejection of one species approaches unity. In such a scenario, the use of a purifying section becomes redundant as very little of the less permeable species will be lost from of the stripping section. On the other hand, the stripping section will still be utilised to maximise depletion of the stripping solvent. Such a cascade was first proposed by Lin and Livingston (2007) for solvent exchange and is shown in Figure 5.11. This is termed a permeable stripping cascade in this work.

In this case, the material balance over the whole cascade $(i = A, B, C, \dots;\ j = 0,1, \dots, n\ )$. is

$$P_j y_{i,j} + W_1 x_{i,1} = W_{j+1} x_{i,j+1} + P_0 y_{i,0} \qquad \textbf{Equation 5.26}$$

The operating line for the whole cascade is thus simply

$$y_{i,j} = \frac{W_{j+1}}{P_j} x_{i,j+1} - \frac{W_1}{P_j} x_{i,1} + \frac{P_0}{P_j} y_{i,0} \qquad \textbf{Equation 5.27}$$

If the solvent used for stripping is pure, the final term can be removed for increased simplicity.

The partitioning line in this cascade can be expressed with Equation 5.25.

5.2.1.1 Degree of freedom analysis

Solute fractionating cascade (Figure 5.10)

Assuming that a pure solvent is used for the stripping process, the parameters of the cascade will be the flows and recycle ratio (F, P_p, W_1, P_0, R) and the solute concentrations for each solute *i* ($z_{i,F}$, $x_{i,1}$, $y_{i,p}$).

Efficient use of the cascade requires a constant stripping flow throughout the whole cascade. This aims to avoid dilution or concentration of the less permeable solute in the retentate of the first stage.

$$P_0 = P_1 = P_2 = \cdots = P_{n-1} = P_n \qquad \textbf{Equation 5.28}$$

The flow balance around the cascade is

$$P_p + W_1 = F + P_0 \qquad \textbf{Equation 5.29}$$

For every solute species *i* in the cascade, there is a solute balance equation over the whole cascade

$$P_p y_{i,p} + W_1 x_{i,1} = F z_{i,F} \qquad \textbf{Equation 5.30}$$

Note that Equation 5.24 is still valid. Hence for each solute, there are 8 variables in the whole cascade and 4 independent equations giving 4 degrees of freedom. For initial process design, the flow and composition of the stream to be treated will be known (F, $z_{i,F}$). Therefore 2 more parameters have to be set for the equation set to be solved.

Permeable stripping cascade (Figure 5.11)

It was assumed that a pure solvent is used for the stripping process. The parameters of the cascade will be the flows and recycle ratio (W_{F+1}, P_F, W_1, P_0) and the solute concentrations for each solute *i* ($z_{i,F}$, $x_{i,1}$, $y_{i,p}$).

Efficient use of the cascade also requires a constant stripping fluid flow throughout the whole cascade, hence Equation 5.31 should be obeyed.

$$P_0 = P_1 = P_2 = \cdots = P_{F-1} = P_F \qquad \textbf{Equation 5.31}$$

The flow balance about the cascade is

$$P_F + W_1 = W_{F+1} + P_0 \qquad \textbf{Equation 5.32}$$

For every solute species *i* in the cascade, there is a solute balance equation over the whole cascade

$$P_p y_{i,p} + W_1 x_{i,1} = F z_{i,F} \qquad \textbf{Equation 5.33}$$

For each solute, there are 7 variables for in the whole cascade and 3 independent equations giving 4 degrees of freedom. For initial process design, the flow and composition of the stream to be treated will be known (W_{F+1}, $x_{i,F+1}$). Therefore 2 more parameters have to be set for the equation set to be

solved. P_0 and $x_{i,1}$ were specified for the target solute and P_0 and $W_1$for the other solutes in this thesis.

5.2.2 Factors affecting permeable stripping cascade

The simplicity of the permeable stripping cascade made it an attractive process to evaluate further. Simulations were performed for the sensitivity analysis of the performance of the permeable stripping cascade in stripping Compound A from Compound C. The separation problem involved purification of a binary solute solution containing Compound C, with purity of 0.60, and Compound A to a target Compound C purity of 0.80 in the retentate stream from stage 1. The cascade was assumed to operate such that Equation 5.31 was fulfilled and that the solutes' rejections were constant in all stages.

In this section, it was assumed that A had a single pass rejection of 0.90 while C had a single pass rejection of 0.99, unless otherwise stated. Simulations were performed for different cascades, each with a different number of stages. The descriptors for the permeable stripping cascade process were defined using equations from Equation 5.34 to Equation 5.37.

The purity of Compound C produced by the cascade was expressed by

$$X_{C,1} = \frac{x_{C,1}}{x_{C,1} + x_{A,1}} \qquad \textbf{Equation 5.34}$$

The yield of C by

$$Yield_C = \frac{W_1 x_{C,1}}{W_{F+1} x_{C,F+1}} \qquad \textbf{Equation 5.35}$$

The purity of A in the eluent was represented by

$$Y_{A,F} = \frac{y_{A,F}}{y_{A,F} + y_{C,F}} \qquad \textbf{Equation 5.36}$$

While the yield of A in the cascade by

$$Yield_A = \frac{P_F y_{A,F}}{W_{F+1} x_{A,F+1}}$$ **Equation 5.37**

5.2.2.1 Effect of the number of membrane stages

The simulations showed that an increase in the number of stages decreased the amount of stripping solvent required for the purification. For example, with a single stage the ratio of $\frac{P_0}{W_{F+1}}$ required was 23.0. The addition of a 2nd stage decreased the ratio to 9.90. If the permeate flux through the membrane was directly proportional to membrane area, the change in configuration would result in a 57% reduction of solvent consumption while requiring 90% of the area of membrane used. Further increases in the number of stages reduced the consumption of stripping solvent further. However, the improvement became marginal beyond 4 stages (see Figure 5.12). The decrease in solvent consumption due to the additional number of stages was also more pronounced when a more stringent purification target was required. When using a single stage to purify the solution from a C purity of 0.60 to 0.80 and 0.90, the ratio of $\frac{P_0}{W_{F+1}}$ required was 23.0 and 125.0, respectively, while purification to 0.95 was impossible. Using 2 stages, the purification to 0.80, 0.90 and 0.95 required a $\frac{P_0}{W_{F+1}}$ ratio of 9.9, 21.1 and 38.2, respectively.

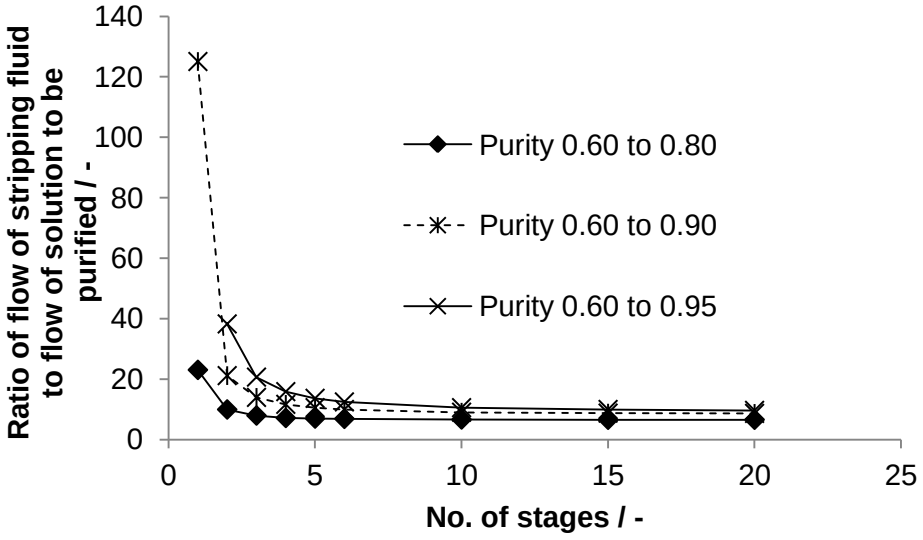

Figure 5.12. Effect of increasing the number of stages on the stripping solvent flow to solution feed flow ratio. An increase in the number of stages decreased the stripping solvent consumption but the rate of decrease became marginal beyond 4 stages.

The decrease in solvent consumption was a result of the cascade design, which enabled the reuse of permeate from stage *j* to strip the solute in stage *j + 1.* There were 2 consequences to this feature; firstly, an enrichment of the more permeable species into higher stage numbers occurred; secondly, the spare stripping capacity of the permeate stream from the $(j-1)^{th}$ stage could be used in the j^{th} stage.

An increase in the number of stages also resulted in an increase in C yield and A purity along with a decrease in A yield. Similarly, the increase in C yield and A purity became marginal beyond 4 membrane stages and plateaued at around 0.93 and 0.87, respectively. There was also no further fall in the yield of A when more than 4 stages were used (see Figure 5.13).

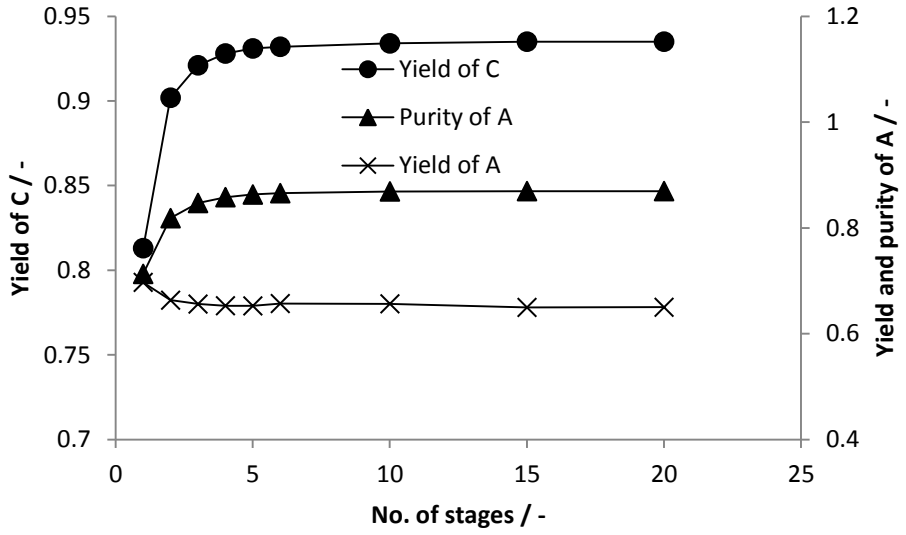

Figure 5.13. Effect of increasing the number of stages on the yield of C in the retentate from stage 1 and the yield and purity of A obtained in the permeate stream from stage *F*.

Evidently, there was a limit to the use of only the stripper section in augmenting the separation performance of a membrane. However, it was encouraging because the use of minimal number of stages was predicted to produce a significant productivity boost for the cascade.

5.2.2.2 Relative permeation factor

The relative permeation factor (Equation 4.31) determined separation performance in solute fractionation. Simulations were performed for a 3-stage permeable stripping cascade, but with variations to the rejection values of A and C. The separation performance of this cascade is summarised in Table 5.8.

The relative permeation factor for A over C was shown to determine the yields of both A and C from the cascade and purity of A in the permeate. Total rejection of the less permeable compound (which will translate to a separation factor of infinity), C, was desirable. However, it was not necessarily essential for an adequate separation, as a sufficiently high separation factor between the target solutes would suffice. This can be inferred from the identical separation quality for No. 1 – 4 in Table 5.8.

Table 5.8. Summary of the effect of varying solute rejections on the separation performance of a 3-stage membrane cascade in purifying a binary feed solution containing Compounds A and C from C purity of 0.60 to 0.80. No. 1 – 4 had increasing difference in rejections between C and A but had the same relative permeation factor of A over C; these entries had the same separation performance but increasing separation productivity, as determined by the flow ratio of stripping fluid to feed solution to be treated. No. 5 – 8 had the same difference in rejections between C and A but had decreasing relative permeation factor of A over C; these entries had worsening separation performances but very similar separation productivity.

No.	$R_{C,S}$ / -	$R_{A,S}$ / -	$(R_{C,S} - R_{A,S})$/ -	$\frac{1}{R_{C,S}-R_{A,S}}$ / -	$\alpha_{A/C,S}$ / -	$\frac{P_0}{W_4}$ / -	$Yield_C$ / -	$Yield_A$ / -	$Y_{A,F}$ / -
1	0.9999	0.9990	0.0009	1 110	10.00	787	0.921	0.654	0.847
2	0.9990	0.9900	0.0090	111	10.00	78.7	0.921	0.654	0.847
3	0.9900	0.9000	0.0900	11.1	10.00	7.87	0.921	0.654	0.847
4	0.9000	0.0000	0.9000	1.11	10.00	0.787	0.921	0.654	0.847
5	0.9000	0.3000	0.6000	1.67	7.000	1.17	0.883	0.671	0.793
6	0.8000	0.2000	0.6000	1.67	4.000	1.13	0.776	0.711	0.679
7	0.7000	0.1000	0.6000	1.67	3.000	1.10	0.678	0.746	0.607
8	0.6000	0.0000	0.6000	1.67	2.500	1.09	0.585	0.781	0.557

The relative difference between solute rejections did not correlate well with the performance of the cascade. This was evident from the differing separation performances in No. 5 – 8 in Table 5.8. Therefore the use of rejection values, which is commonly used in membrane characterisation, to predict the success of solute fractionating is not effective.

5.2.2.3 Rejection effects

While the individual rejection values of the solutes and their relative differences did not seem to have any correlation with the overall separation performance of the cascade, it was a good gauge of the productivity of the cascade. A large difference in the rejections of A and C led to a smaller $\frac{P_0}{W_4}$ ratio required. In fact, the inverse of the relative difference in rejection was in the same order of magnitude as the ratio of the flow of stripping solvent to the flow of solution to be treated in almost all the entries in Table 5.8.

A high rejection for the less permeable solute had the tendency to lead to good fractionation performance because the cascade will more likely operate close to a pinch point for the solute. Operation close to the pinch point will result in little change in solute concentration per cascade stage (See Figure 5.14). A pinch occurs when the operating line and the partitioning line intersect in the x > 0 region. Since the partitioning lines always intersect at the origin and the operating lines always intersect y = 0 in the x > 0 region, the condition in Equation 5.38 must be fulfilled for the partitioning line and the operating line to intersect.

$$\frac{P_j}{W_{j+1}} < \frac{1}{1 - R_{i,j}} \qquad \textbf{Equation 5.38}$$

One can see that with a higher rejection, the boundary space to fulfil the inequality becomes larger. Furthermore, a higher rejection allows for the use of a much higher stripping solvent to feed solution ratio (See Table 5.9).

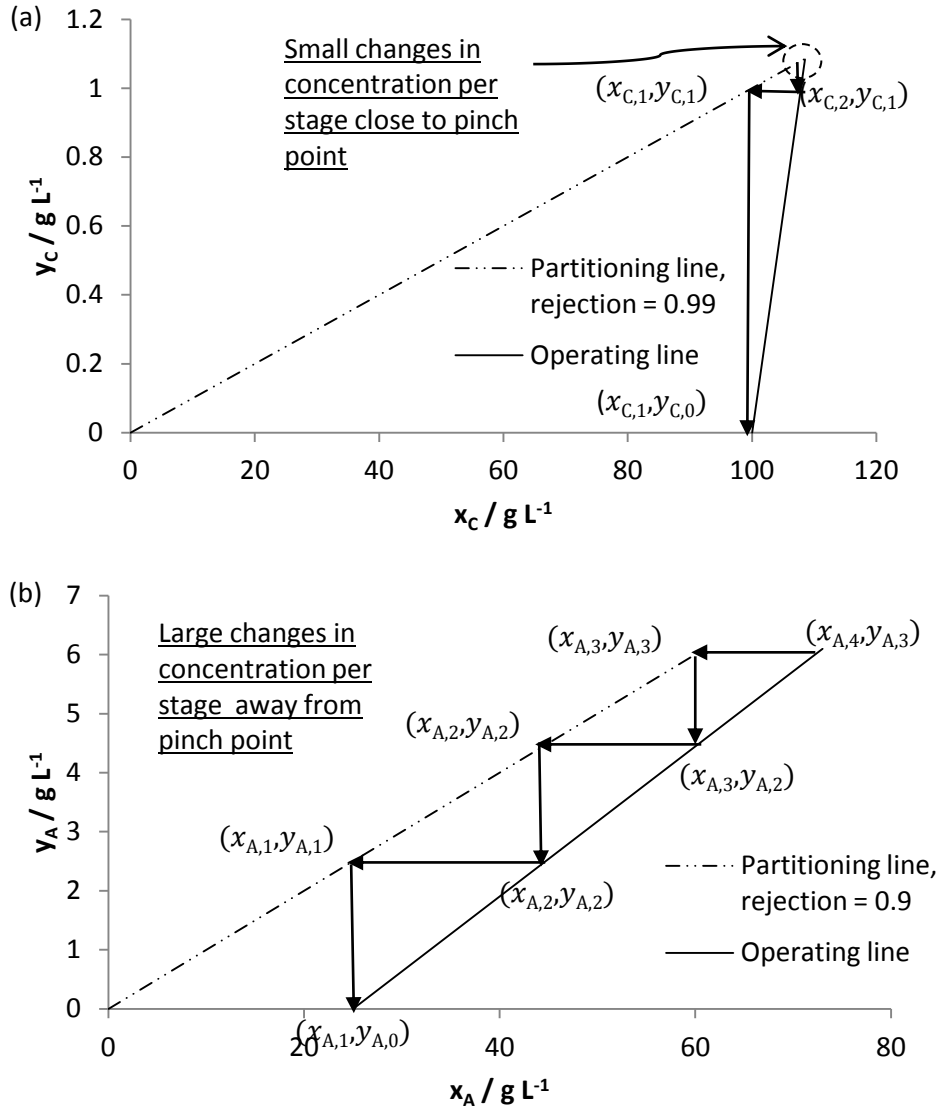

Figure 5.14. McCabe-Thiele type representation of a 3-stage permeable stripping cascade operating at $\frac{P_0}{W_4} = 7.87$ used to purify a binary solution containing Compounds A and C, with C purity of 0.60, to C purity of 0.80 with C concentration of 100g L^{-1} in the product stream. The conditions here correspond to $R_{C,j} = 0.99$ and $R_{A,j} = 0.9$. (a) shows the stripping of the less permeable C while (b) shows the stripping of the more permeable A. In (a), operation close to the pinch point ensures a smaller change in concentration per stage than in (b), where the cascade operates away from the pinch point. Consequently, there is little stripping of C relative to A, giving rise to a purification of C in the retentate stream of the cascade.

Table 5.9. Dependence of ease of operating cascade close to pinch point on the rejection of solute across the membrane. A high rejection allows a much higher stripping solvent to feed solution flow ratio and still allows the intersection of the operating and partitioning lines which is a prerequisite for pinch condition

No.	$R_{C,S}$ / -	$\frac{1}{1-R_{C,S}}$ / -
1	0.9999	10 000
2	0.9990	1 000
3	0.9900	100
4	0.9000	10
5	0.8000	5.0
6	0.7000	3.3
7	0.6000	2.5

5.2.3 Comparison with constant volume diafiltration

The most apparent effect of using the cascade instead of diafiltration was the considerable decrease (about 30% decrease in solvent use comparing all entries in Table 5.8 with Table 4.1) in the amount of solvent required for the purification. Take for example the purification of 1L day^{-1} of a solution with Compound C purity of 0.60 to a purity of 0.80. A comparison of No. 1 in both Table 5.8 and Table 4.1 revealed that for every 1L day^{-1} of solution treated using constant volume diafiltration, 1090L of stripping solvent was needed per day; this was much higher than the 787L day^{-1} required for the 3-stage cascade process under the same conditions. If the diafiltration process was assumed to require 2 trains of equipment to keep up with the cascade's capacity (See Figure 5.15 for schematic representation), and if the membrane flux was identical in both processes, the diafiltration setup would use only 8% less membrane area than the 3-stage cascade and yet incur a 30% increase in solvent consumption.

Less obvious is the increase in yield of the less permeable solute. Simulations showed a modest increase in C yield (2 – 7 percentage point increase) when using the cascade process as an alternative to constant volume diafiltration. This along with the decrease in solvent use will certainly contribute to a lower operating cost compared to diafiltration.

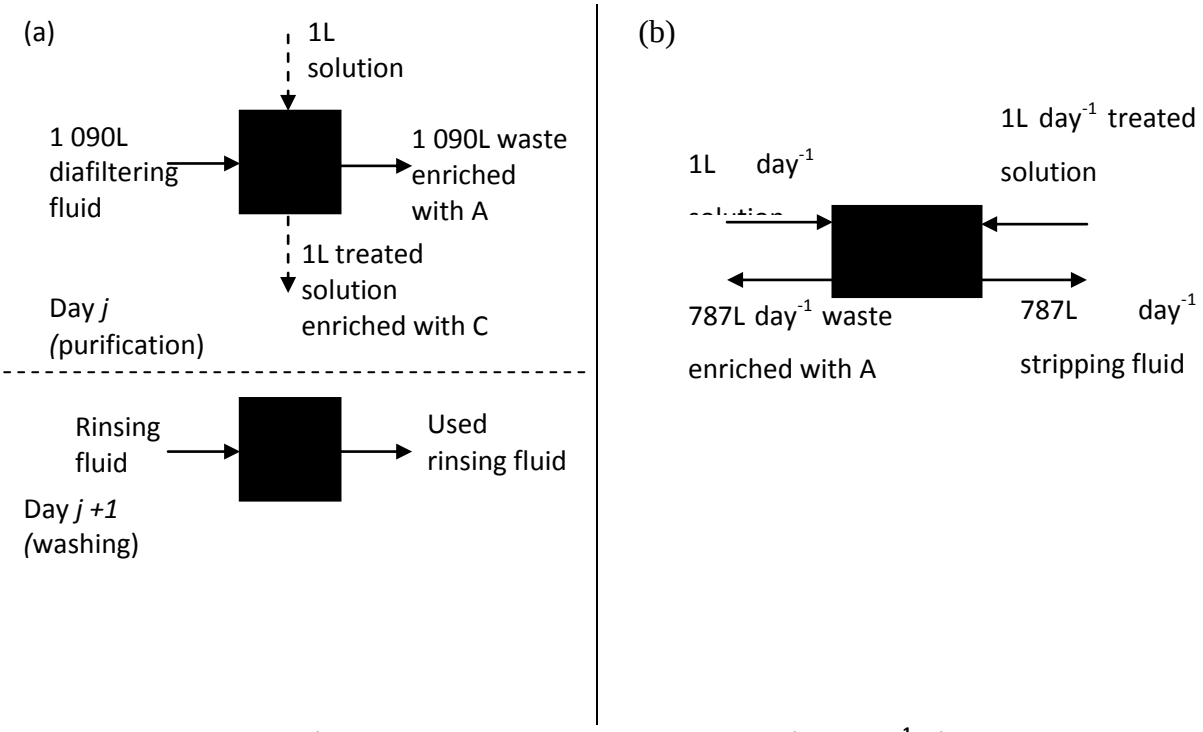

Figure 5.15. Schematics of the membrane processes used to purify 1L day^{-1} of a solution containing Compound C with purity of 0.60 to purity of 0.80. The membranes used in both processes reject 0.9990 of Compound A and 0.9999 of Compound C. (a) shows a single train of the diafiltration process where the 1L solution was diafiltered over a single day and equipment rinsed over the next day. (b) represents the 3-stage cascade process where 1L day^{-1} of solution was continuously purified.

The cascade's advantage over constant volume diafiltration was more apparent when higher levels of purification were needed. Comparisons between simulations of constant volume diafiltration and a 3-stage cascade were made for the purification of increasing C purity (see Table 5.10). The amount of solvent savings a 3-stage cascade could realise, over constant volume diafiltration, was higher when purifying from 0.60 to 0.95 (saving of 7.7L diafiltering solvent per L solution) than to 0.80 (saving of 3.0L diafiltering solvent per L solution). The yield improvement of C when using the cascade, which was critical to the economic feasibility of the process, was also more apparent when purifying to 0.95 (4.1 percentage points) than to 0.80 (2.4 percentage points).

While the simulations have shown the potential of this membrane cascade, it was more interesting to provide an operating example of it to demonstrate its feasibility. Therefore this cascade was constructed to demonstrate its capability to separating Compound C from Reagent A.

Table 5.10: Comparison of single stage constant volume diafiltration and a 3-stage permeable stripping cascade in the purification of a solution with a Compound C purity of 0.60 to various purity levels. Entries 1a – 1c were simulations for a single stage constant volume diafiltration. Entries 2a – 2c were simulations for a 3-stage permeable stripping cascade. A purification to higher purities accentuated the advantages in solvent requirements of the cascade. Furthermore, there was a much better Compound C yield.

No.	$R_{C,S}$ / -	$R_{A,S}$ / -	C Purity[a] / -	Ratio[b] / -	$Yield_C$[c] / -	$Yield_A$[d] / -	A Purity[e] / -
1a	0.9900	0.9000	0.80	10.9	0.897	0.664	0.811
1b	0.9900	0.9000	0.90	19.9	0.819	0.863	0.761
1c	0.9900	0.9000	0.95	28.3	0.754	0.940	0.718
2a	0.9900	0.9000	0.80	7.9	0.921	0.656	0.847
2b	0.9900	0.9000	0.90	13.9	0.861	0.857	0.805
2c	0.9900	0.9000	0.95	20.6	0.795	0.938	0.753

[a] Target purity of Compound C in the retentate, of the single stage diafiltration or from stage 1 of the 3-stage cascade, at the end of the purification.
[b] Volume of stripping solvent required to purify per unit volume of a binary solution containing A and C, with a C purity of 0.60.
[c] Yield of Compound C in the retentate, of the single stage diafiltration or from stage 1 of the 3-stage cascade, at the end of the purification.
[d] Yield of Compound A in the permeate, of the single stage diafiltration or from stage 3 of the 3-stage cascade, at the end of the purification.
[e] Purity of Compound A in the permeate, of the single stage diafiltration or from stage 3 of the 3-stage cascade, at the end of the purification.

5.2.4 Results and discussion

Initial recirculation experiments were first performed to determine a suitable membrane-solvent combination and operating pressure. After which, a 3-stage permeable stripping cascade was constructed as shown in Figure 5.16 and operated over 56h to purify a stream of reagent A and Compound C.

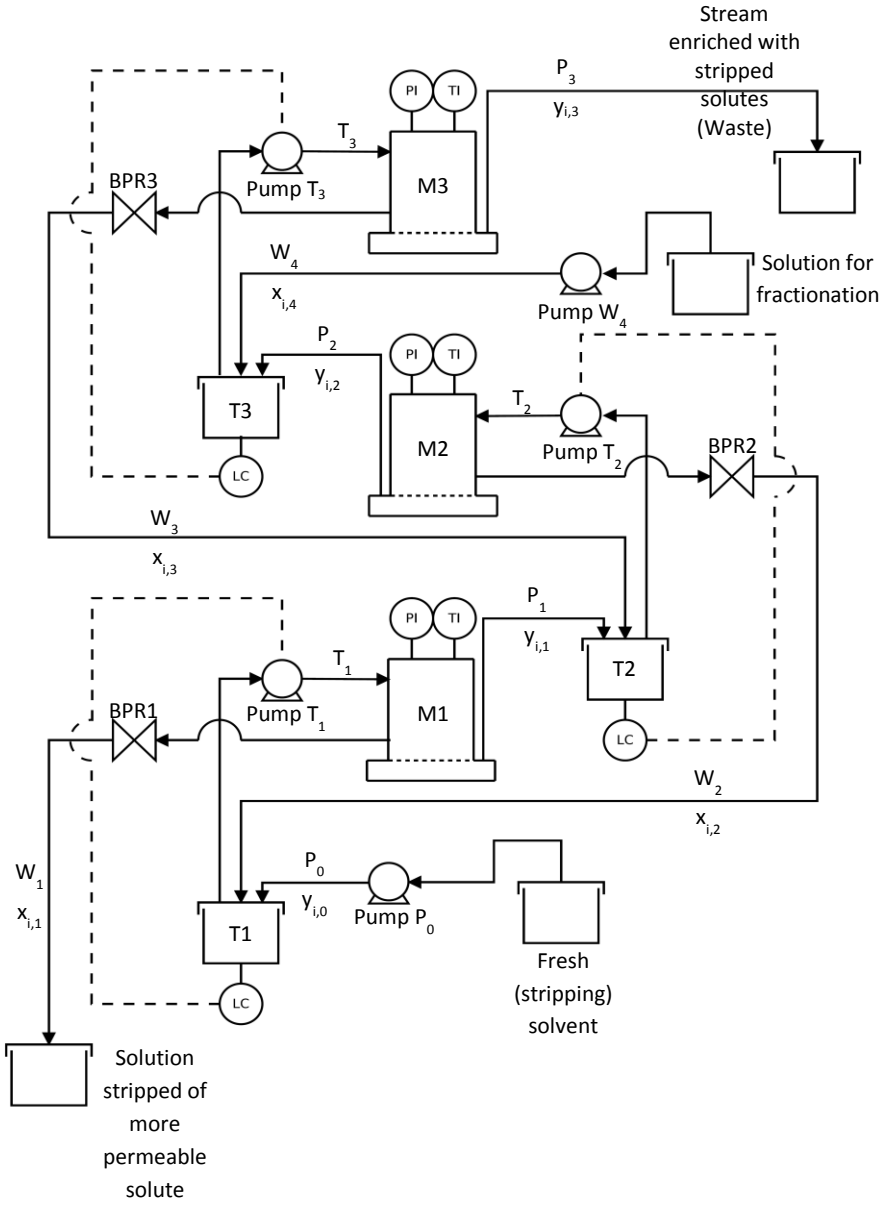

Figure 5.16. Schematic of the 3-stage solute fractionating membrane cascade. M1, M2 and M3 are membrane units holding flatsheet membrane coupons. T1, T2 and T3 are buffer tanks on weighing scales connected to a computer running a LabView code for the implementation of a level controller. The numbers correspond to the membrane stage they feed into. The dotted lines denote the control loop used for control to maintain steady state operation of the cascade. LC = level controller, PI = pressure indicator, BPR = back pressure regulator, TI = temperature indicator.

5.2.4.1 Recirculation experiments

In the original process, the post-reaction mixture containing Reagent A and Compound C was in a methyl tertiary butyl ether (MTBE) solution. Initial screening of the PuraMem® series membranes was performed to determine the partitioning of the solutes in an MTBE solution. However, none of the membranes tested were able to partition either A or C close to unity, although the membranes were able to reject C more readily. This resulted in a very low relative permeation factor of A compared to C.

A decision was made to perform a solvent switch to methanol (MeOH) so that hydrophilic DuraMem® series membranes could be screened for solute partitioning. MeOH had the advantages of being unreactive and cost-effective while being compatible with the downstream crystallisation process. As it turned out, C was almost totally rejected by the DuraMem® series membranes when the methanolic solution was filtered across it, resulting in a much higher relative permeation factor of A compared to C.

Solutions of A and C in MTBE were initially filtered across PuraMem® 280 and PuraMem® S membranes. Despite the high fluxes (see Figure 5.17) and significant differences in the rejection of A and C (see Figure 5.18 and Figure 5.19) on PuraMem® S and PuraMem® 280, the relative permeation factor of A over C was low (see Figure 5.20). With such selectivities, the predicted yields of C from either constant volume diafiltration or the 3-stage permeable stripping cascade were low. Do note that pressure was the independent variable in these tests; the rejections and relative permeation factors were plotted against flux to facilitate the choice of membranes because a high flux and high relative permeation factor were needed for a suitable membrane. The pressure used was not critical as long it was within the design range of the equipment.

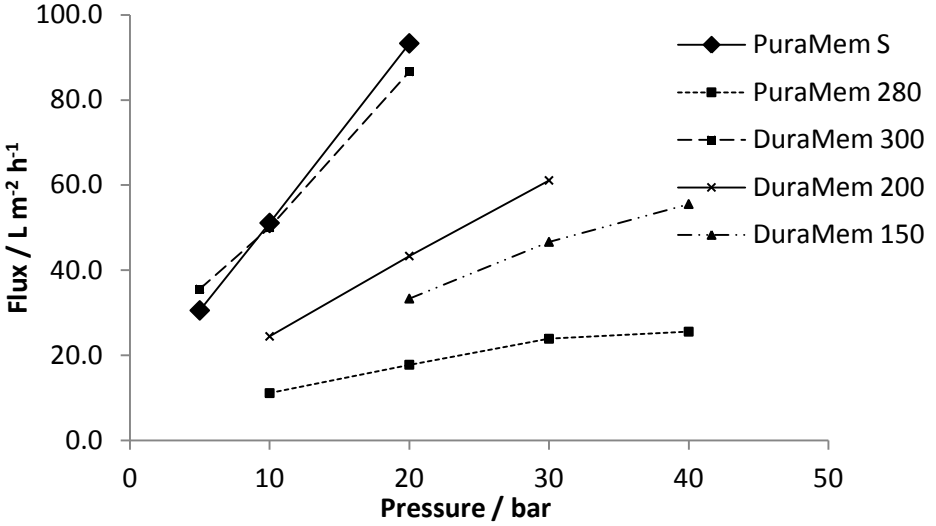

Figure 5.17. Relationship between fluxes across the 5 membranes tested and the pressure in the retentate tank. Recirculation experiments for the PuraMem® S and PuraMem® 280 membranes were performed using a solution of A and C in MTBE. The filtration experiments for the DuraMem® series membranes were performed using a solution in MeOH. The solutions were maintained at 30˚C.

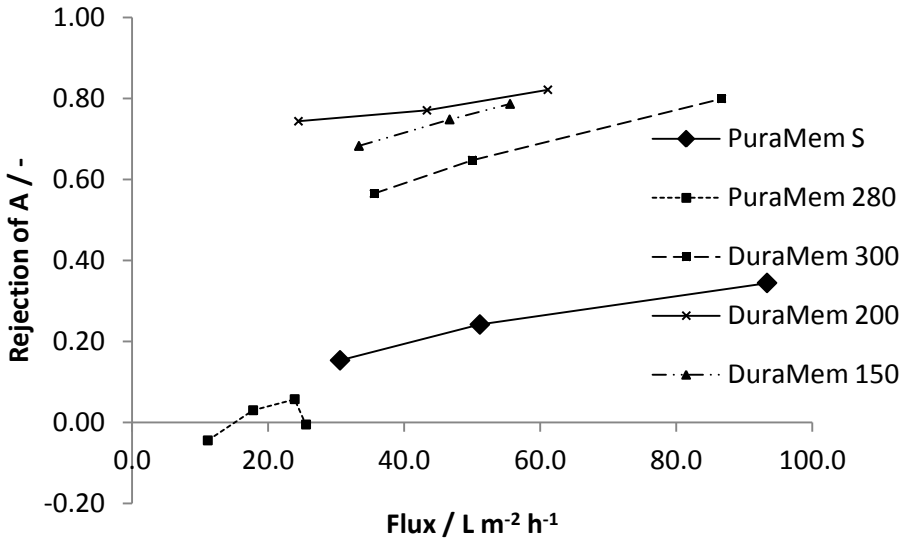

Figure 5.18. Relationship between the rejection of A across the 5 membranes tested and the flux across the membrane. Recirculation experiments for the PuraMem® S and PuraMem® 280 membranes were performed using a solution of A and C in MTBE. The filtration experiments for the DuraMem® series membranes were performed using a solution in MeOH. The solutions were maintained at 30˚C.

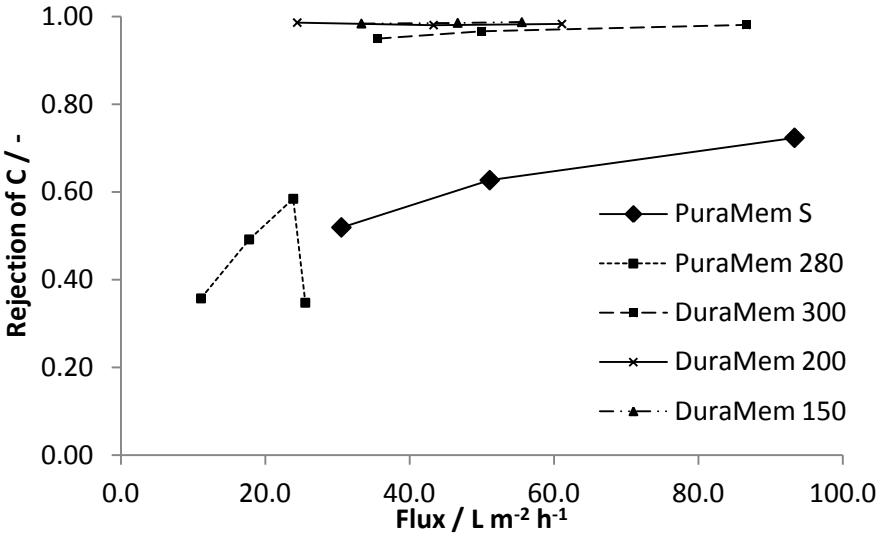

Figure 5.19. Relationship between the rejection of C across the 5 membranes tested and the flux across the membrane. Recirculation experiments for the PuraMem® S and PuraMem® 280 membranes were performed using a solution of A and C in MTBE. The filtration experiments for the DuraMem® series membranes were performed using a solution in MeOH. The solutions were maintained at 30˚C.

The concurrent solvent switch to MeOH and use of DuraMem® series membranes gave significantly higher selectivities (see Figure 5.20) despite somewhat lower rejection differences. In a sense this is very similar to the process of changing the mobile phase and stationary phase in chromatography. Different solvent (mobile phase) and membrane (stationary phase) combinations can produce a variety of results. DuraMem® 300 gave a combination of high flux and moderately high relative permeation of A over C (see Figure 5.20) at 10bar and 30°C. Hence it was used, at this pressure and temperature, in the cascade demonstration. The pressure was not increased further as there was no discernible improvement to membrane selectivity and also because further increases in permeate flux would make control of the cascade difficult due to the low capacity of the HPLC pumps.

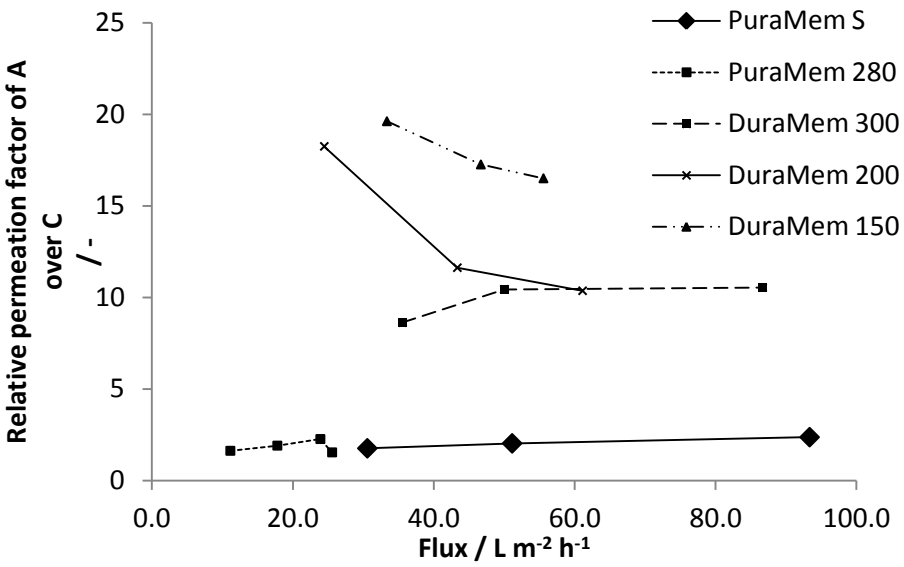

Figure 5.20. Relationship between the relative permeation factor of A over C across the 5 membranes tested and the flux across the membrane. Recirculation experiments for the PuraMem® S and PuraMem® 280 membranes were performed using a solution of A and C in MTBE. The filtration experiments for the DuraMem® series membranes were performed using a solution in MeOH. The solutions were maintained at 30˚C. Note the much higher permeation factors for the DuraMem® series membranes, which are essential for a successful fractionation. The combination of high flux values and relative permeation factor for DuraMem® 300 made it a desirable membrane for the separation.

5.2.4.2 Cascade operation

The cascade was first operated with a countercurrent flow of pure MeOH with a pressure of 10bar and 30°C in each cascade stage. Setting $W_4 = 1.000ml\ min^{-1}$ and adjusting the countercurrent flow, we realised that the condition $P_0 > 3.500ml\ min^{-1}$ must be fulfilled for the steady flow to be achieved. Lowering the countercurrent flow any further caused a depressurising of the final stage.

The cascade was used for solute fractionation continuously for 56h. However, the cascade was stopped for 1h to replace the pump seal in P3 at 27h. The flow rate ratio was also changed at 32h.

A solution containing 0.57-0.60 C was eventually purified to 0.78-0.79 C with a $\frac{P_0}{W_4}$ ratio of 3.5. A solution containing 0.57 C was purified to 0.83 with a $\frac{P_0}{W_4}$ ratio of 5.0.

5.2.4.3 Long stabililisation time

Due to the large cascade dead volume (c.a. 2.5L) relative to the flow rates into the cascade (0.80-4.00ml min^{-1}), the time for steady state to be reached was substantial. The first appearance of detectable amounts of C occurred 3h after the start of the separation, while the cascade approached steady state between 7 – 27h from the start of the stripping process; sampling 23h after the start of the stripping process revealed that the solute balances were at or below 5% (see Figure 5.21) though it increased again at 27h possibly due to difficulties for the cascade to approach steady state. Disturbance of the cascade by stopping the cascade or changing the flow ratio were disruptive as seen from solute balances from operating times 27h to 36h in Figure 5.21. Stopping the cascade for 1h to replace the pump seal at 73h increased the net balance of C in the cascade to 27.3% from 13.5%. The change of the flow ratio at 32h similarly caused an increase in C balance to 54.3% (sample at 36h) from 27.3% (sample at 30h). Further operation of the cascade for more than 20h stabilised operation of the cascade once again, as seen in solutes balances at operating time 56h when the balances for C and A were brought to -5.6% and 4.6% respectively.

The balance of the solute in Figure 5.21 was defined as

$$Balance_i = \frac{Flow\ solute\ i\ in - Flow\ solute\ i\ out}{Flow\ solute\ i\ in} \times 100\% \qquad \textbf{Equation 5.39}$$

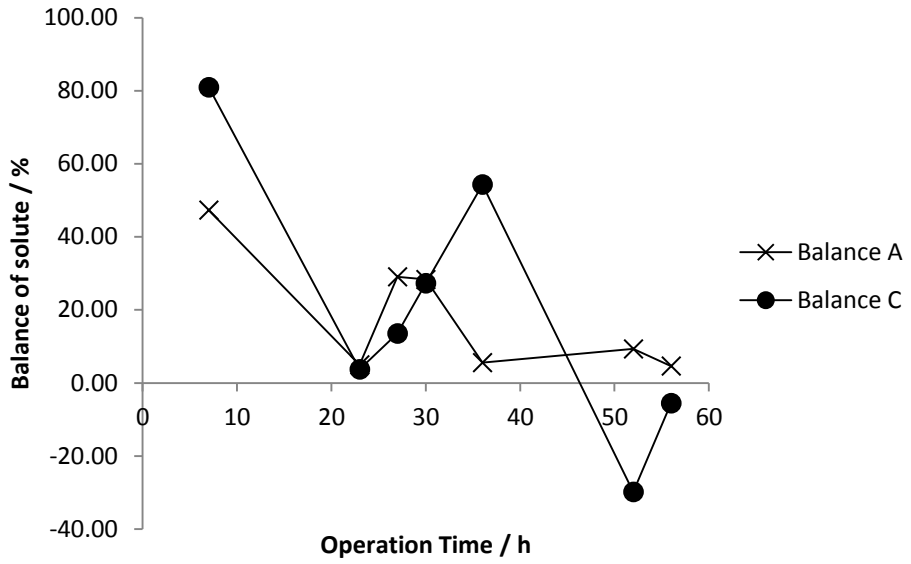

Figure 5.21. Solute balance of A and C over the cascade during cascade operation. Note that the cascade was disturbed first at 27h to replace the pump seal in pump T_3 and at 32h when the flow rate ratio of stripping solvent to solution to be treated was changed

5.2.4.4 Effect of stripping solvent to solution flow ratio

An increase in the flow ratio from 3.5 to 5.0 caused the purity of C produced to increase (see Samples 4 and 7 in Table 5.11) from 0.78 to 0.83. This was in line with expectations as an increased ratio increased the stripping of A from the solution due to the higher availability of stripping solvent. The yield of A also increased from 0.47 to 0.69 as more of A was flushed out with the countercurrent stripping flow. The increase in the yield of C from 0.68 to 1.01 and purity of A from 0.88 to 0.93 were due to factors other than the change in flow ratio and cannot be explain by the simplified model described in Section 5.2.1. A more rigorous use of the model, which is shown in Section 5.2.4.5, was needed for the explanation.

Table 5.11: Table summarising the performance of the cascade during operation, with comparison with the model-predicted performance shown on the right side of the table. The cascade was operated continuously for 56h, only stopping at Time = 27h to replace the pump seal in one of the pumps. The flow ratio of the stripping solvent and the solution to be treated was changed at Time = 32h. The model was in agreement with what was observed, as long as sufficient time was provided for the cascade to approach steady state.

Sample	Time / h	$\frac{P_0}{W_4}$ / -	Determined from experiment				Determined from model			
			$X_{C,1}$ / -	$Yield_C$ / -	$Y_{A,3}$ / -	$Yield_A$ / -	$X_{C,1}$ / -	$Yield_C$ / -	$Y_{A,3}$ / -	$Yield_A$ / -
1	7	3.5	0.71	0.17	0.93	0.42	0.60	0.96	0.59	0.05
2	23	3.5	0.79	0.84	0.76	0.61	0.66	0.88	0.63	0.31
3	27	3.5	0.79	0.73	0.72	0.45	0.66	0.80	0.64	0.39
4	30	3.5	0.78	0.68	0.88	0.47	0.68	0.96	0.88	0.32
5	36	5.0	0.81	0.39	0.91	0.82	0.96	0.88	0.86	0.95
6	52	5.0	0.83	1.26	0.92	0.57	0.79	0.96	0.93	0.66
7	56	5.0	0.83	1.01	0.93	0.69	0.73	0.96	0.90	0.54

Table 5.12: Flow table showing recorded flow rates of flows sampled during cascade operation.

Sample	Time / h	Measured flows / ml min^{-1}		Pumps' flows / ml min^{-1}					Inferred flows / ml min^{-1}			
		W_1	P_3	P_0	T_1	T_2	T_3	W_4	P_1	W_2	P_2	W_3
1	7	2.00	2.30	3.50	6.12	6.05	4.04	1.00	4.12	2.62	3.04	1.74
2	23	1.95	2.30	3.50	5.20	4.55	3.80	1.00	3.25	1.70	2.80	1.50
3	27	1.70	2.70	3.50	5.20	4.50	4.00	1.00	3.50	1.70	3.00	1.30
4	30	1.55	2.90	3.50	5.20	5.36	4.70	1.00	3.65	1.70	3.70	1.80
5	36	0.70	4.00	4.00	4.10	4.50	4.79	0.80	3.40	0.10	3.99	0.79
6	52	1.50	3.00	4.00	4.70	5.09	4.87	0.80	3.20	0.70	4.07	1.87
7	56	1.35	3.50	4.00	5.38	5.93	5.37	0.80	4.03	1.38	4.57	1.87

Table 5.13: Concentration table showing sampled concentrations of A and C during operation of cascade.

Sample	Time / h	Concentration of solutes in various streams / g l^{-1}													
		Stripped solution		Stage 1		Stage 2				Stage 3		Stripped waste		Feed Solution	
		$x_{C,1}$	$x_{A,1}$	$y_{C,1}$	$y_{A,1}$	$x_{C,2}$	$x_{A,2}$	$y_{C,2}$	$y_{A,2}$	$x_{C,3}$	$x_{A,3}$	$y_{C,3}$	$y_{A,3}$	$x_{C,4}$	$x_{A,4}$
1	7	1.75	0.73	0.04	0.19	3.77	1.68	0.12	0.58	10.46	5.21	0.17	2.47	20.49	13.58
2	23	8.77	2.38	0.03	0.62	8.17	3.15	0.17	1.31	13.42	6.34	1.14	3.59	20.49	13.58
3	27	10.00	2.68	0.04	0.70	10.31	3.94	0.19	1.52	9.70	5.24	1.15	2.98	23.24	17.76
4	30	10.19	2.85	0.03	0.74	11.81	4.95	0.12	1.64	13.38	7.71	0.38	2.86	23.24	17.76
5	36	10.44	2.49	0.03	0.65	15.15	5.67	0.10	1.89	13.89	8.17	0.30	2.92	23.24	17.76
6	52	15.65	3.19	0.04	0.74	13.95	4.94	0.05	1.61	8.94	5.50	0.22	2.70	23.24	17.76
7	56	13.97	2.82	0.03	0.70	13.21	4.76	0.05	1.44	9.03	5.57	0.22	2.78	23.24	17.76

Table 5.14: Relationship between the flux from each membrane stage and the solute rejection in the corresponding stage. Note the lower single pass solute rejections correspond to the lower fluxes in that stage. Direct control of permeate flux in each stage might be a better strategy for flow control compared to pressure control in each stage.

Sample	Time / h	Stage 1			Stage 2			Stage 3		
		f_1 / $Lm^{-2}h^{-1}$	$R_{C,1}$/ -	$R_{A,1}$/ -	f_2 / $Lm^{-2}h^{-1}$	$R_{C,2}$/ -	$R_{A,2}$/ -	f_3 / $Lm^{-2}h^{-1}$	$R_{C,3}$ / -	$R_{A,3}$/ -
1	7	46	1.00	0.75	34	0.97	0.65	26	0.98	0.53
2	23	36	1.00	0.74	31	0.98	0.58	26	0.92	0.43
3	27	39	1.00	0.74	33	0.98	0.61	30	0.88	0.43
4	30	41	1.00	0.74	41	0.99	0.67	32	0.97	0.63
5	36	38	1.00	0.74	44	0.99	0.67	44	0.98	0.64
6	52	36	1.00	0.77	45	1.00	0.67	33	0.98	0.51
7	56	45	1.00	0.75	51	1.00	0.70	39	0.98	0.50

5.2.4.5 Process model validation

The derived process model was put to the test. Experimentally determined flows (see Table 5.12), feed solution composition (see Table 5.13) and rejections (see Table 5.14) were used in the process model to determine the performance of the cascade relative to the actual performance of the cascade (see Table 5.11). More details on the use of the model are located in Appendix 8.5.

There was a convergence in the predicted cascade performance and actual cascade performance, especially for samples 3, 6 and 7 (see shaded cells in Table 5.11), where steady state behaviour was approached. In these samples, the magnitudes of difference were all below 25%.

Do note that the divergence between the experimental results and model values in sample 1 – 2 and 4 – 5 was due to the long stabilisation time, as a result of the high residence time in the cascade, required for the cascade to reach steady state. The large difference between experimental performance in samples 1 and 2 and the performance predicted by the model was because the cascade did not reach steady state. Steady state was approached only at 27h (sample 3). Since the cascade was stopped at 27h to replace a pump seal, the cascade once again required approximately another 27h to reach steady state. Hence samples 4 and 5, taken 3h and 9h after replacement of the pump seal respectively, showed cascade performances that diverged from the performance predicted by the model. It took another 25h for the cascade to equilibrate back to steady state, when experimental cascade performance started to converge with the model predicted performance.

5.2.4.6 Comparison with constant volume diafiltration

A constant volume diafiltration using DuraMem® 300 membranes was performed at 10bar and 30°C. The same purification produced a Compound C yield of 0.88 due to the non unity rejection of C across the membrane. 2.58L of diafiltering fluid was required per 1.00L of solution purified, making diafiltration more productive than the cascade (5.00L diafiltering fluid per L solution) in terms of solvent consumption. However the decrease in process yield, from quantitative recovery in the cascade process after 52h, meant that the diafiltration process was not economically feasible due to the high cost of the lost API (Compound C). There was also no scope for process enhancement, making diafiltration a more rigid process.

The successful use of diafiltration required the use of the tightest DuraMem® 150 membrane at 40bar and 30°C to decrease Compound C loss into the permeate stream. In doing so the same separation increased the yield of Compound C to 0.95 while requiring 5.60L of diafiltering volume per 1L of solution treated. This translated to an increase in solvent consumption (0.60L increase per L solution purified) over the cascade for a comparable separation performance. Importantly, constant volume diafiltration required a specific membrane while the cascade was able to utilise a looser membrane. This is a testament to the flexibility of the cascade process.

While the long residence time with the current set of equipment and flow rates means that the cascade process will only be more productive than the constant volume diafiltration process if more than 13.5L of solution was treated, the time to reach steady state can be reduced by decreasing the size of the stage relative to the flow rate of the pump.

5.2.4.7 Economic feasibility

Due to confidentiality reasons, costing information cannot be revealed in this work. However, evaluation of the use of this cascade revealed that the raw material cost savings from the increased in-situ yield of the API (Compound C), enabled by the purification using a 3-stage permeable stripping cascade, was 2 orders of magnitude higher than the annualised cost of the cascade. Therefore an implementation of the cascade process was expected to decrease the cost for the production of the API.

5.2.4.8 Challenges

The process is currently compromised by insufficient control over the flow rates in the cascade. This led to each membrane stages having varying degrees of $\frac{P_j}{W_{j+1}}$ ratios (see Table 5.12). This resulted in cascade inefficiencies as some stages did not perform to the designed stripping capacity. A better implementation of the process would involve control of permeate flux from each membrane stage directly with a flow controller. Such a controller would regulate the retentate flow from each stage with feedback response from the permeate flow rate from the same stage. Additionally this control might potentially regulate the solute rejection in each stage as the solute rejection seems to be correlated with the flux from the membrane in each stage (see Table 5.14). Furthermore such a control strategy would be able to regulate the cascade independently of the differing osmotic

pressures in each stage. This is advantageous over regulation of pressure in each stage where pressure offset might be necessary to compensate for the higher osmotic pressures in some stages.

The process, in its current form, is relatively inflexible. In an idealised process, the flow of the stripping solvent will be a function of membrane area at constant temperature, constant effective transmembrane pressure and constant rejection. Therefore this flow will be fixed at the design phase of the process. Hence it is likely the only way to change the stripping solvent to solution flow ratio will be through the manipulation of the flow rate of the feed solution to be purified. On the other hand, the maximum solute purification capacity of the cascade will be proportional to the maximum concentration of solution which it can treat. The higher the solution concentration this cascade can take, the higher the capacity of the cascade. In view of these limitations, the strategy for designing such a cascade will involve determining the maximum solution concentration which the cascade can handle and oversizing the cascade stages to ensure leeway in varying operational parameters.

5.2.5 Conclusion on permeable stripping cascade

As a result of the constraints in manufacturing and process development in the pharmaceutical industry, a solute fractionating cascade that can be modified rapidly has been proposed. This cascade was able to reduce solvent usage significantly and increase separation yield with minimal added stages. Furthermore the cascade was predicted to be more productive and effective in solute fractionation than constant volume diafiltration, which is the state of the art in membrane-driven solute fractionation.

The purification of a developmental API from an excess reagent was demonstrated using this cascade. Firstly suitable solvent and membrane switches improved the single stage membrane separation. With this improved combination of solvent and membrane, the API purification was demonstrated using the 3-stage permeable stripping cascade. The feasibility of the cascade was confirmed experimentally, in line with predictions by the developed process model. The cascade was able to purify a solution with API (Compound C) purity of 0.6 to 0.8 to enable further polishing with a crystallisation step. While a higher degree of purification beyond a Compound C purity of 0.8 was theoretically possible, constraints in flow control made necessary increases in the stripping fluid to solution feed flow ratio difficult. Additional equipment is required for a better implementation of the process.

5.3 Materials and methods

5.3.1 Membrane cascade

The cascade was a staged membrane process. Each stage was composed of a membrane cell, a pump and a weight (level) controller. The solution to be concentrated was fed in the centre of the cascade to demonstrate how both the stripping and rectifying sections of the cascade worked.

5.3.2 Membrane cell

The membrane cells were designed based on Evonik-MET (UK) deadend filtration cells. Each cell could hold an estimated 500ml of fluid to be filtered across a membrane coupon with an active filtration area of 54cm^2 at the bottom of the cell. A magnetic stirrer above the membrane provided the turbulence to mitigate concentration polarization. The cell had 3 ports at the bottom, one port on top and 2 ports on the cap of the cell. A pressure gauge was connected at the bottom for pressure monitoring close to the membrane coupon. A proportional relief valve was also connected at the bottom and used to regulate the pressure above the membrane coupon. A resistive thermometer was inserted into a port at the cap and connected to a stirrer hotplate on which the cell was placed. This provided real time temperature regulation in the cell and magnetic stirring at the same time. The inlet flow from the pump was connected to the top port of the cell. The other port on the cap was left opened until the cell was fully filled with liquid, and then plugged with a swage cap to ensure no gas remained in the membrane unit.

5.3.3 Membranes

PuraMem® 280, PuraMem® S, DuraMem® 150, DuraMem® 200 and DuraMem®300 flatsheet membranes purchased from Evonik-MET (UK) were used in the experiments. PuraMem® 280 and PuraMem® S were used for solutions in methyl tertiary butyl ether (MTBE). The more hydrophilic DuraMem® 150, DuraMem® 200 and DuraMem® 300 membranes were used for the solution in methanol (MeOH). Flatsheet DuraMem® 300 membranes were used in the cascade.

5.3.4 Chemicals

In Section 5.1, the API was available at UCB Pharma S.A. The solvent mixture recovery was a mixture of 90% ethyl acetate and 10% methanol by volume. HPLC grade solvents purchase from Merck were used.

In Section 5.2, Reagent A and Compound C were available at UCB Pharma. The HPLC grade solvents (acetonitrile, MeOH and MTBE) were purchased from Merck KGaA and used without further processing. The rest of the reagents were purchased from Sigma Aldrich.

5.3.5 Analytical methods

In Section 5.1, the composition of the solvent mixture was determined using gas chromatography and flame ionisation detection (GC-FID). An Agilent 6890 series GC system was used.

In both Sections 5.1 and 5.2, the concentrations of the API, reagent A and Compound C were determined using HPLC with a Xbridge C18 50 x 4.6mm column from Waters, maintained at 35°C, employing a gradient method. The HPLC system used was a Waters 2695 series HPLC system. Three solvents lines were used: Deionised water (solvent A); acetonitrile (solvent B); and 7.9g L^{-1} ammonium hydrogen carbonate solution with 1vol% ammonia solution (28%) added (solvent C). The eluent flow was kept constant at 3ml min^{-1} for the 5min required for complete elution. For the first 0.33min, the eluent was, by volume, 80% solvent A, 10% solvent B and 10% solvent C. The composition was changed to 90% solvent B and 10% solvent C for the rest of the elution.

5.3.6 Solvent recovery cascade operation (Section 5.1)

The cascade was constructed as shown in Figure 5.5. The cascade employed 3 membrane units (M1, M2 and M3) connected in series, such that the permeate stream from the j^{th} unit was fed into the $(j-1)^{th}$ unit while the retentate from the $(j+1)^{th}$ unit was fed into the j^{th} unit. A pair of metering valves, MV-W_p and MV-P_p were used to split the permeate stream from the final unit such that some of the permeate was recycled back into the cascade. This acted as a means to control permeate flow out of the cascade without changing the sizing of the final unit or the operating pressure in that stage. During operation, the membrane units were pressurised with fluid fed in using Merck-Hitachi syringe pumps (model L-6200A). Between each unit, a buffer tank (T1, T2 and T3) collected the permeate from the $(j+1)^{th}$ unit and the retentate from the $(j-1)^{th}$ unit (with the exception of the first stage) to be fed into the j^{th} unit.

During startup, the buffer tanks (T1, T2, and T3) were first filled up to the setpoint level through the addition of solvent or solution. Next the membrane units (M1, M2, and M3) were pressurized by feeding fluids into the units. The pressure in each unit was regulated around the set pressure using a pressure control valve. During startup, feed flow was prescribed at a fixed rate into T2. Pump T_2 was then set to maximal flow to pressurize M2. As fluid flow started in P_2 and W_2, pumps T_3 and T_1 were started respectively at maximal flow. When each membrane unit was pressurized to the prescribed pressure, the controllers of the corresponding feed pumps were switched on to regulate the level of the buffer tanks from which the membrane units gained their feed.

During operation, the cascade was run continuously by recirculating about 5L of a 5g L^{-1} API solution in the methanol/ethyl acetate solvent mixture. The extents of opening of the pair metering valves, which controlled the recycle ratio back into the cascade, were the main parameters that were changed. At certain periods of time, where pump flows and scale readings were constant for at least 15min, samples were taken to determine flows P_p and W_1, and concentration of API in all the streams labelled.

When shutting down the cascade, all pumps were switched off and fluids were allowed to exit from the membrane units over an hour so that they could depressurise.

5.3.7 Permeable stripping cascade operation (Section 5.2)

The cascade was deployed as illustrated in Figure 5.16. The cascade employed 3 membrane units (M1, M2 and M3) connected in series. The permeate stream from the j^{th} unit was fed into the $(j+1)^{th}$ unit (with the exception of the 1st unit) while the retentate stream from the $(j+1)^{th}$ unit was fed into the j^{th} unit (with the exception of the final unit). HPLC grade solvent used for stripping the more permeable solute was fed into the 1st unit while the solution containing the solutes to be fractionated was fed into the last (3rd) unit. The permeate stream from the final (3rd) unit, which was essentially a dilute solution enriched in the more permeable solute, was collected and analysed over time. The retentate stream from the 1st unit, being enriched in the less permeable solute, was also collected and analysed over time.

During operation, the membrane units were pressurised with fluid fed in using HPLC pumps (Merck-Hitachi L-6200). The pressure in each membrane unit was regulated with a back pressure regulator. The temperature of the fluid in each unit was regulated with a hotplate receiving feedback from a

resistance thermometer inserted into the unit. Before each membrane unit, a buffer tank (T1, T2 and T3) collected the fluids to be fed into the unit.

Before start-up, the buffer tanks (T1, T2 and T3) were filled above the setpoint level by adding fresh stripping solvent. The tanks which provide the feed for Pump P_0 and Pump W_4 were filled with large volumes of HPLC grade MeOH. The membrane units were then pressurised by feeding the fluid into the units. Once the set pressures were reached in all the units, countercurrent feed flows were prescribed by Pump P_0 and Pump W_4 into T1 and T3, respectively. Simultaneously, the controllers for Pumps T_1, T_2 and T_3 were switched on to regulate the liquid levels in the buffer tanks. The feed rates for Pump P_0 and Pump W_4 were varied to determine the lowest $\frac{P_0}{W_4}$ ratio achievable on this cascade.

Two batches of solution were made up by mixing a weighted amount of A and C in HPLC grade MeOH. The concentrations of these batches were verified with HPLC analysis after solution preparation. The feed tube for Pump W_4 was inserted into one of these batches after determination of the limits of the cascade. When the first batch was exhausted, the tube was inserted into the next batch. The cascade was then left to run continuously over 56h with the controllers adjusting the pump flow rates until steady state was reached. The flow rates of the controlled pumps and weight of each buffer tank were monitored during operation and samples were taken from the cascade at time intervals where pump flows and scale reading were constant for at least 15 minutes. Flow samples for W_1 and P_3 were taken over a measured time interval to determine their flow rates. The rest of the flow rates were determined from the reading on the pumps or inferred using the flow balance around each membrane unit. For the other labelled streams, only sufficient volumes for HPLC analysis were taken over short periods of time to avoid excessive perturbations in the system.

When shutting down the cascade, all pumps were switched off and fluids allowed to exit from the membrane units over an hour to ensure full depressurisation.

5.3.8 Control

Regulation of the levels in the buffer tanks between each membrane unit was done through the control of pumps that drew their feed from the tanks. The pumps were controlled with the aid of a LabView procedure. The permeate from unit *(j – 1)* and retentate from unit *(j + 1)* flowed into the buffer tank (denoted by T*j*) between units *j* and *(j – 1)*, while the pump (Pump T_j) drew from the buffer tank to feed into unit *j*. The level in each buffer tank was monitored through its weight. This

weight was kept constant by a PI controller algorithm that changed the pump flow based on feedback from the weighing scale, sampling every 100ms.

Each controller was first tuned employing the Ziegler-Nichols closed-loop tuning method (Ziegler & Nichols, 1993) (refer to Figure 5.5 and Figure 5.16 for control loop denoted by dotted lines). The controllers were then further fine-tuned to obtain minimal drift from the average feed flow while making sure controller gain was sufficient to keep the weight reading of each tank within ±1g of the setpoint.

5.4 Conclusion

The use of process engineering to develop new membrane process configurations have been shown to increase the range of scope for commercial membranes. Through various process modifications such as solvent changes and stage configurations, membranes can be made versatile for a variety of processes.

6. Conclusions and Further Work

6.1 Conclusions

The achievement of the key scientific deliverables listed in Chapter 1 is a testament to the success of this work. The following were covered in various Chapters of this thesis.

1. Review of various membrane transport models (Chapter 2).
2. Case study on the use of process modifications on solutes to improve OSN separation, including their relevance in improving solute rejection and their use for membrane performance predictions (Chapter 3).
3. Review of common OSN processes and their inherent limitations (Chapter 4).
4. Case study for the use of process engineering to address the limitation of the state of the art OSN processes (Chapter 5).

The development of tools and methods to enable the use of organic solvent nanofiltration in the chemical synthesis of APIs, from the perspective of a pharmaceutical company, is the central theme of this work. Identification of membrane screening as one of the most time-consuming steps in membrane process development led to evaluation of membrane transport models for the prediction of membrane performance in lieu of membrane screening. In the hope of circumventing the need for the use of a 'perfect' membrane, further attempts were made to develop a structured approach to process modification to enable the use of commercial membranes without the requirement for total rejection of the target compound.

The Donnan Steric Pore Model can be used to predict membrane performance from independently determined membrane physical properties. Its ability to correlate membrane performance with membrane physical characteristics was the reason for the evaluation of DSPM as a predictive tool for membrane transport. However, the Hagen-Poiseuille equation in the DSPM was unable to accurately predict solvent permeation through nanofiltration membranes. This led to attempts to improve the prediction of the DSPM by replacing the Hagen-Poiseuille equation with a predictive molecular dynamics tool. Unfortunately, molecular dynamics simulations were computationally tedious. Coupled with the inability of current methods to independently determine membrane properties

such as pore size and membrane tortuosity accurately and quickly, the DSPM is unable to provide a competitive advantage over conventional experimentation.

Process chemistry can selectively manipulate solute rejection and in turn can be used to increase the applicability of the limited range of membranes on the market. Both the selective addition of charge to solutes and increase in molecular size of solutes were able to enhance the membrane rejection of the targeted solutes. The use of pH control for targeted manipulation of the membrane permeation selectivity of various solutes was presented. After which, the polyalkylation approach was used to augment the size of an organocatalyst, enabling the successful recycling of an organocatalyst on a single membrane stage. These 2 case studies demonstrated the role process chemistry plays in improving the versatility of OSN processes.

However, process chemistry was not always able to address the issues facing conventional membrane processes. The processes were reviewed and the common problems they face are non-robustness and inflexibility, often due to the sensitivity of the processes to single pass rejection. Thus, cascade processes were designed, with the aim to provide an alternative process for use in the pharmaceutical industry, by addressing these problems.

A membrane cascade was first designed to enable the use of membranes with incomplete solute retention in pure solvent recovery. The consistency of the cascade performance despite discrepancies in the single pass rejection proved the improved reliability of the cascade over a single stage process. Following which, another cascade was designed and demonstrated for the separation of 2 solutes, despite being unable to reject the target solute completely. These cascade designs provided the means for more extensive and flexible use of commercial membranes than conventional membrane processes. Furthermore, the modular designs of the cascades meant that the processes could be repurposed for other separation problem through simple reconfiguration of the stages, facilitating their deployment in the typical multipurpose API production plant. The flexibility of these cascades is the main advantage cascades developed in this work have over other cascades mentioned in literature.

All together, the work in this thesis presents ways to improve the ease of membrane process development in the pharmaceutical industry and provides a reference for common separation problems in the industry which can be resolved with OSN.

6.2 Recommendations for Further Work

While this work has opened up greater possibilities for application of membrane processes in the pharmaceutical industry, a few things still need to be resolved and improved upon. The following should be done, in the listed order, to improve upon the work in this thesis.

The design of the membrane stages for the cascades in this work was not perfect. On hindsight, undue consideration for high residence times in each membrane unit resulted in retentate volumes that were excessively large relative to the pump' flow capacities. The rejection across each membrane unit should stay constant when the whole cascade reaches steady state, hence having a large residence time in each unit is not paramount to operation of the cascade. In fact, it unnecessarily prolonged the duration required for experimentation. Further work on the membrane cascades should utilise smaller membrane units, which cost less to build, to facilitate experimentation.

While membrane cascades have been demonstrated, the process control over them has not been perfect leading to inconsistent stage performance. The performance of the cascades can be further improved, and made more robust, by controlling the pressure control valve in each stage with deviation of permeate flow in each stage from the setpoint providing feedback to the control valve. This can be done easily, albeit with significant investment, using flow controllers that are already on the market.

It will be a challenge for multistage membrane processes to compete with thermal processes due to the use of costlier electricity for pump operation. Furthermore while heat can be integrated in thermal processes, it is much harder to integrate electrical power used for the pumps in the multistage membrane processes. Energy recovery solutions on the market can recover energy from the pressurised retentate stream to pressurise the feed stream to each cascade stage (Flowserve, 2012), however these need to be evaluate in the context of OSN.

In the case when cascade flexibility is not paramount, various established optimisation techniques (Gassner & Marechal, 2010; Voros et al. 1997) can be used to optimise cascade design, bringing down capital and operating cost. This can be further explored when processes are run continuously for large production volumes, especially in the realms of fine and bulk chemicals.

Though an elevation in the molecular weight of a solute is known to increase its membrane rejection, certain side groups have been shown to provoke a higher membrane rejection. This relationship needs to be elucidated and perhaps quantified meaningfully, perhaps not unlike a group contribution method, before a structured method of polyalkylation can be used. Further experimentation on various solutes would be needed to do this.

On a similar note, polyalkylation was used to anchor catalytic sites to a relatively small 1,3,5-tris(bromomethyl)benzene anchor molecule in this work. A much larger anchor molecule can be synthesised by attaching ethylene glycol subunits to 1,3,5-tris(bromomethyl)benzene. The synthesis process, however, is tedious and expensive, hence it was not pursued in this work. It would be good to synthesise this to elucidate the effect of size on the solute rejection across the membrane. Furthermore, it would help to understand if there is a hard limit on the number of subunits that can be added before the increased solution viscosity would impede solvent permeation. The hypothesis of whether such spacer molecules can increase catalytic activity by reducing steric hindrance to the entrance of substrate, while still retaining the selectivity of the catalyst also should be tested.

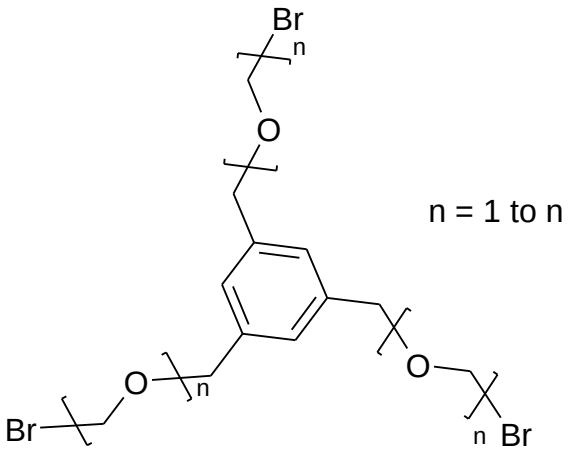

Figure 6.1: Structure of enlarged anchor molecule with ethylene glycol subunits added as spacer molecules.

Finally, the use of the DSPM is hindered by the uncertainty in the structures and characterisation of OSN membranes. Further refinement of methods currently in development is needed so that precise and direct determination of an OSN membrane's structural characteristics such as membrane pore size, tortuosity and separation layer thickness can be performed to facilitate the use of the DSPM.

This is the hardest amongst the suggestions listed, in no small part due to the difficulty in characterising the structure of OSN membranes (Stawikowska & Livingston, 2012).

7. References

Abejón, R., Garea, A., & Irabien, A. (2012). Integrated countercurrent reverse osmosis cascades for hydrogen peroxide ultrapurification. *Computers & Chemical Engineering*, *41*, 67–76.

am Ende, D. J. (2011). *Chemical Engineering in the Pharmaceutical Industry: An Introduction*, (pp. 3–20). Hoboken, New Jersey: John Wiley & Sons, Inc.

Anderson, J. L., & Quinn, J. A. (1974). Restricted transport in small pores. *Biophysical Journal*, *14*(2), 130–150.

Antonucci, V., Yen, D., Kelly, J., Crocker, L., Dienemann, E., Miller, R., & Almarrsson, O. (2002). Development of a nanofiltration process to improve the stability of a novel anti-MRSA carbapenem drug candidate. *Journal of pharmaceutical sciences*, *91*(4), 923–932.

Anyanwu, U. K., & Venkataraman, D. (2005). Soxhlet-dialysis: a method to recover soluble polymer supported catalysts. *Green Chemistry*, *7*(6), 424–425.

Avendano-Jimenez, C., & Frentrup, H. (2010). *NEMD Program.*

Barker, P. E., & Till, A. (1992). Using multistage techniques to improve diafiltration fractionation efficiency. *Journal of Membrane Science*, *72*(1), 1–11.

Berger, L. I., Covington, A. K., Fox, R. B., Frederikse, H. P. R., Fuhr, J. R., Gschneidner, K. A., Hammond, C. R., Hampson, R. F., Holden, N. E., Jenkins, H. D. B., Kehiaian, H. V., Kerr, J. A., Lias, S. G., Lovas, F. J., Martin, W. C., Miller, J. S., Miller, T. M., Reader, J., Roobottom, H. K., Sharma, B. L., Snyder, L. E., Stocker, D. W., Taylor, B. N., Trippe, T. G., Vanysek, P., Wiese, W. L., Wilks, E. S., & Wohlfarth, C. (2001). *Fluid Properties*, chap. 6, (pp. 6–1–6–195). Florida: Chemical Rubber Publishing Company, 82nd ed.

Berkessel, A., & Gröger, H. (2005). *Large-Scale Applications of Organocatalysis*, (pp. 393–408). Weinheim, FRG: Wiley-VCH Verlag GmbH & Co. KGaA.

Bowen, W. R., & Mohammad, A. W. (1998). Diafiltration by Nanofiltration: Prediction and Optimization. *AIChE Journal*, *44(8)*, 1799–1812.

Bowen, W. R., Mohammad, A. W., & Hilal, N. (1997). Characterisation of nanofiltration membranes for predictive purposes – use of salts, uncharged solutes and atomic force microscopy. *Journal of Membrane Science*, *126*, 91–105.

Bowen, W. R., & Welfoot, J. S. (2002). Modelling the performance of membrane nanofiltration – critical assessment and model development. *Chemical Engineering Science*, *57*, 1121–1137.

Brian, P. L. T. (1972). *Staged Cascades In Chemical Processing*. Prentice-Hall.

Caus, A., Braeken, L., Boussu, K., & Van der Bruggen, B. (2009). The use of integrated countercurrent nanofiltration cascades for advanced separations. *Journal of Chemical Technology & Biotechnology*, *84*(3), 391–398.

Cheang, B., & Zydney, A. L. (2003). Separation of α -lactalbumin and β -lactoglobulin using membrane ultrafiltration. *Biotechnology and Bioengineering*, *83*(2), 201–209.

Chen, F.-X., Shao, C., Wang, Q., Gong, P., Zhang, D.-Y., Zhang, B.-Z., & Wang, R. (2007). An enantioselective michael addition of malonate to nitroalkenes catalyzed by low loading demethylquinine salts in water. *Tetrahedron Letters*, *48*(48), 8456–8459.

Chen, H., Jin, Y., Jiang, R., Sun, X.-L., Li, X.-Y., & Zhang, S.-Y. (2008). New cinchona alkaloid ester derivatives as catalysts in asymmetric â interruptedâ Feistâ“Bénary reaction. *Catalysis Communications*, *9*(9), 1858–1862.

Chen, H., Wang, Q. F., Sun, X. L., Luo, J., & Jiang, R. (2010). Cinchona alkaloid ester derivatives as ligands in the asymmetric dihydroxylation and aminohydroxylation of alkenes. *Mendeleev Communications*, *20*(2), 104–105.

Childress, A.E., Elimelech, M. (1996). Effect of solution chemistry on the surface charge of polymeric reverse osmosis and nanofiltration membranes. *Journal of Membrane Science*, 253-268.

Childress, A.E., Elimelech, M. (2000). Relating nanofiltration membrane performance to membrane charge (electrokinetic) characteristics.*Environmental Science & Technology*, 3710-3716.

Constable, D. J. C., Jimenez-Gonzalez, C., & Henderson, R. K. (2006). Perspective on solvent use in the pharmaceutical industry. *Organic Process Research & Development*, *11*(1), 133–137.

Cuartas-Uribe, B., Alcaina-Miranda, M. I., Soriano-Costa, E., & Bes-Piá, A. (2007). Comparison of the behavior of two nanofiltration membranes for sweet whey demineralization. *Journal of dairy science*, *90*(3), 1094–1101.

Da Silva, J.R., Macado W.M., Pereira, J.A.B., Damil, J.C.R., Caixado, C.A.C., Filipe, A.E.P. (2008). *2,3,4,5-Tetrahydoxy6-sulfooxy hexanoic acid, pharmaceutically acceptable salts and equilibrium forms thereof, processes for their preparation, pharmaceutical compositions and comprising such compounds and their medical use*. US Patent Application 2008/0279808.

Danelli, T., Annunziata, R., Benaglia, M., Cinquini, M., Cozzi, F., Tocco, G. (2003). Immobilization of catalysts derived from *Cinchona* alkaloids on modified poly(ethylene glycol). *Tetrahedron: Asymmetry, 14*, 461–467

Darvishmanesh, S., Firoozpour, L., Vanneste, J., Luis, P., Degreve, J., & Bruggen, B. V. (2011). Performance of solvent resistant nanofiltration membranes for purification of residual solvent in the pharmaceutical industry: experiments and simulation. *Green Chemistry.*, *13*(12), 3476–3483.

Deen, W. M. (1987). Hindered transport of large molecules in liquid-filled pores. *AIChE Journal*, *33*(9), 1409–1425.

Deng, L., Li, H., Wang, Y., Wu, F. (2009). *Asymmetric carbon-carbon-bond-forming reactions catalyzed by bifunctional cinchona alkaloids*. US Patent 7582764

Déon, S., Dutournié, P., & Bourseau, P. (2007). Modeling nanofiltration with Nernst-Planck approach and polarization layer. *AIChE Journal*, *53*(8), 1952–1969.

Dickerson, T. J., Reed, N. N., & Janda, K. D. (2002). Soluble polymers as scaffolds for recoverable catalysts and reagents. *Chemical Reiews*, *102*(10), 3325–3344.

Dijkstra, H. P., Kruithof, C. A., Ronde, N., Van De Coevering, R., Ramón, D. J., Vogt, D., Van Klink, G. P., & Van Koten, G. (2003). Shape-persistent nanosize organometallic complexes: synthesis and application in a nanofiltration membrane reactor. *The Journal of organic chemistry*, *68*(3), 675–685.

Dijkstra, H. P., Meijer, M. D., Patel, J., Kreiter, R., van Klink, G. P. M., Lutz, M., Spek, A. L., Canty, A. J., & van Koten, G. (2001). Design and performance of rigid nanosize multimetallic cartwheel pincer compounds as Lewis-Acid catalysts. *Organometallics*, *20*(14), 3159–3168.

Dijkstra, H. P., Steenwinkel, P., Grove, D. M., Lutz, M., Spek, A. L., & van Koten G (1999). Design of novel hexametallic cartwheel molecules from persubstituted benzene compounds. *Angewandte Chemie (International ed. in English)*, *38*(15), 2185–2188.

Dijkstra, H. P., van Klink, G. P. M., & van Koten, G. (2002). The use of ultra- and nanofiltration techniques in homogeneous catalyst recycling. *Accounts of Chemical Research*, *35*(9), 798–810.

Dixon, D. J., & Hynes, P. S. (2005). Enantioselective organocatalytic michael addition of malonate esters to nitro olefins using bifunctional cinchonine derivatives. *Chemical Communications*, (35), 4481–4483.

Eldrige, R. B. (1993). Olefin/paraffin separation technology: a review. *Industrial & Engineering Chemistry Research*, *32*(10), 2208–2212.

FDA (2011). Frequently asked questions on patents and exclusivity. Available online http://www.fda.gov/Drugs/DevelopmentApprovalProcess/ucm079031.htm

Federsel, H.-J. (2006). In search of sustainability: process R&D in light of current pharmaceutical industry challenges. *Drug Discovery Today*, *11*(21-22), 966–974.

Ferreira, F. C., Branco, L. C., Verma, K. K., Crespo, J. a. G., & Afonso, C. A. M. (2007). Application of nanofiltration to re-use the sharpless asymmetric dihydroxylation catalytic system. *Tetrahedron: Asymmetry*, *18*(14), 1637–1641.

Filtration+Separation. (2006). Pharma: Cash cow? *Filtration+Separation*, *43*(7), 26–27.

Flowserve. (2012). Available online www.flowserve.com

Fritzmann, C., Lowenberg, J., Wintgens, T., & Melin T. (2007). State-of-the-art of reverse osmosis desalination. *Desalination, 216,* 1–76

Gassner, M., & Maréchal, F. (2010). Combined mass and energy integration in process design at the example of membrane-based gas separation systems. *Computers & Chemical Engineering*, *34*(12), 2033–2042.

Geens, J., De Witte, B., & Van der Bruggen, B. (2007). Removal of API's (active pharmaceutical ingredients) from organic solvents by nanofiltration. *Separation Science and Technology*, *42*(11), 2435–2449.

Ghazali, N. F., Ferreira, F. C., White, A. J. P., & Livingston, A. G. (2006). Enantiomer separation by enantioselective inclusion complexation-organic solvent nanofiltration. *Tetrahedron: Asymmetry*, *17*(12), 1846–1852.

Ghosh, R. (2003). Novel cascade ultrafiltration configuration for continuous, high-resolution proteinâ"protein fractionation: a simulation study. *Journal of Membrane Science*, *226*(1-2), 85–99.

Ghoshal, M., Schwenzer, K. S., & Wu, R. S. (1998). *QUINIDINE IMMUNOASSAY AND REAGENTS*. US Patent 5741715

Giffels, G., Beliczey, J., Felder, M., & Kragl, U. (1998). Polymer enlarged oxazaborolidines in a membrane reactor: enhancing effectivity by retention of the homogeneous catalyst. *Tetrahedron: Asymmetry*, *9*(4), 691–696.

Gröger, H. (2008). Asymmetric organocatalysis on aÂ technical scale: Current status and future challenges. vol. 2007/2 of *Ernst Schering Foundation Symposium Proceedings*, chap. 82, (pp. 227–258). Berlin, Heidelberg: Springer Berlin Heidelberg.

Gunderson, S. S., Brower, W. S., O'Dell, J. L., & Lightfoot, E. N. (2007). Design of membrane cascades. *Separation Science and Technology*, *42*(10), 2121–2142.

Hagmeyer, G., & Gimbel, R. (1998). Modelling the salt rejection of nanofiltration membranes for ternary ion mixtures and for single salts at different pH values. *Desalination*, 247-256.

Hajamis, U. D., Gadre, J. N., & Pednekar, S. (1999). Asymmetric dihydroxylation of olefins by osmium tetroxide coordinated with chiral cinchona alkaloid. *ChemInform*.

Han, H., & Janda, K. D. (1997a). Multipolymer-Supported substrate and ligand approach to the sharpless asymmetric dihydroxylation. *Angewandte Chemie International Edition in English*, *36*(16), 1731–1733.

Han, H., & Janda, K. D. (1997b). A soluble polymer-bound approach to the sharpless catalytic asymmetric dihydroxylation (AD) reaction: Preparation and application of a [(DHQD)2PHAL-PEG-OMe] ligand. *Tetrahedron Letters*, *38*(9), 1527–1530.

Hellweg, S., Fischer, U., Scheringer, M., & Hungerbuhler, K. (2004). Environmental assessment of chemicals: methods and application to a case study of organic solvents. *Green Chemistry*, *6*(8), 418–427.

ICH (2000). Good manufacturing practice guide for active pharmaceutical ingredients q7. Tech. rep.

Jew, S-s. & Park, H-g. (2009). Cinchona-based phase-transfer catalysts for asymmetric synthesis. *Chemical Communication*, 7090–7103

Jonsson, G., & Boesen, C.E. (1975). Water and solute transport through cellulose acetate reverse osmosis membranes. *Desalination*, 145-165.

Katraro, R., Letzion, R., Linder, C., Rehovot, Nemas, M., & Gedera (1997). Multi-stage membrane system and process. US Patent 5676832

Kleij, A. W., Gossage, R. A., Jastrzebski, J. T., Boersma, J., & van Koten G (2000). The "dendritic effect" in homogeneous catalysis with Carbosilane-Supported Arylnickel(II) catalysts: Observation of Active-Site proximity effects in Atom-Transfer radical addition. *Angewandte Chemie (International ed. in English)*, *39*(1), 176–178.

Kojima, M. (2009). Government response to oil price volatility. Tech. rep., The World Bank.

LaPorte, T. L., Wang, C., & Jones, G. S. (2011). *Process Development and Case Studies of Continuous Reactor Systems for Production of API and Pharmaceutical Intermediates*, chap. 23, (pp. 437–456). Hoboken, New Jersey: John Wiley & Sons, Inc.

Lee, J.-H., Yoo, M.-S., Jung, J.-H., Jew, S.-s., Park, H.-g., & Jeong, B.-S. (2007). Polymeric chiral phase-transfer catalysts derived from cinchona alkaloids for enantioselective synthesis of Î±-amino acids. *Tetrahedron*, *63*(33), 7906–7915.

Li, H., Wang, Y., Tang, L., & Deng, L. (2004). Highly enantioselective conjugate addition of malonate and β-Ketoester to nitroalkenes: asymmetric C-C bond formation with new bifunctional organic catalysts based on cinchona alkaloids. *Journal of American Chemical Society*, *126*(32), 9906–9907.

Li, H., Wang, Y., Tang, L., Wu, F., Liu, X., Guo, C., Foxman, B. M., & Deng, L. (2005). Stereocontrolled creation of adjacent quaternary and tertiary stereocenters by a catalytic conjugate addition. *Angewandte Chemie International Edition*, *44*(1), 105–108.

Lightfoot, E.N. (2006). *MEMBRANE CASCADE-BASED SEPARATION.* US Patent 7141171

Lightfoot, E. N., Root, T. W., & O'Dell, J. L. (2008). Emergence of ideal membrane cascades for downstream processing. *Biotechnology Progress*, *24*(3), 599–605.

Lin, J. C., & Livingston, A. G. (2007). Nanofiltration membrane cascade for continuous solvent exchange. *Chemical Engineering Science*, *62*(10), 2728–2736.

Loh, X. X., Sairam, M., Bismarck, A., Steinke, J. H. G., Livingston, A. G., & Li, K. (2009). Crosslinked integrally skinned asymmetric polyaniline membranes for use in organic solvents. *Journal of Membrane Science*, *326*(2), 635–642.

Matsuura, T., & Sourirajan, S.. (1981). Reverse osmosis transport through capillary pores under the influence of surface forces. *Industrial Engineering & Chemical Process Design & Development*, 273-282.

Mayani, M., Filipe, C. D. M., & Ghosh, R. (2010). Cascade ultrafiltration systems-integrated processes for purification and concentration of lysozyme. *Journal of Membrane Science*, *347*(1-2), 150–158.

McCandless, F. P. (1994). A comparison of membrane cascades, some one-compressor recycle permeators, and distillation. *Journal of Membrane Science*, *89*(1-2), 51–72.

McCandless, F. P. (1999). Stage extent of separation in ideal countercurrent recycle membrane cascades. *Journal of Membrane Science*, *154*(1), 15–23.

Morvan, J. (2012). Rising interest of big pharma creates immense growth potential for contract manufacturing organisations, says Frost & Sullivan. Available online http://www.frost.com/prod/servlet/press-release.pag?ctxixpLink=FcmCtx1&searchQuery=Aiswariya+Chidambaram&bdata=aHR0cDovL3d3dy5mcm9zdC5jb20vc3JjaC9jYXRhbG9nLXNlYXJjaC5kbz9xdWVyeVRleHQ9QWlzd2FyaXlhK0NoaWRhbWJhcmFtQH5AU2VhcmNoIFJlc3VsdHNAfkAxMzI4MTI0Mjg2OTg4&docid=252003643&ctxixpLabel=FcmCtx2.

Mulder, M. (1996). *Basic Principles of Membrane Technology*. Dordrecht, The Netherlands: Kluwer Academic Publishers.

Muller, C., & Vogt, D. (2011). Recent advances in the recycling of homogeneous catalysts using membrane separation. *Green Chem.*, *13*(9), 2247–2257.

Nair, D., Luthra, S. S., Scarpello, J. T., White, L. S., Freitas dos Santos, L. M., & Livingston, A. G. (2002). Homogeneous catalyst separation and re-use through nanofiltration of organic solvents. *Desalination*, *147*(1-3), 301–306.

Nghiem, L. D., Schäfer, A. I., & Elimelech, M. (2005). Pharmaceutical retention mechanisms by nanofiltration membranes. *Environ. Sci. Technol.*, *39*(19), 7698–7705.

Niemi, H., & Palosaari, S. (1993). Calculation of permeate flux and rejection in simulation of ultrafiltration and reverse osmosis processes. *Journal of Membrane Science,* 123-137.

Pariya, C., Jayaprakash, K. N., Sarkar, A. (1998). Alkene metathesis: new developments in catalyst design and application. *Coordination Chemistry Reviews, 168*, 1–48

Park, H.-g., Jeong, B.-s., Yoo, M.-s., Park, M.-k., Huh, H., & Jew, S.-s. (2001). Trimeric cinchona alkaloid phase-transfer catalyst: α,α',α''-tris[O(9)-allylcinchonidinium]mesitylene tribromide. *Tetrahedron Letters*, *42*(28), 4645–4648.

Park, H.-g., & Jew, S.-s. (2009). Cinchona-based phase-transfer catalysts for asymmetric synthesis. *Chemical Communications.*, (46), 7090–7103.

Peeva , L.G., Gibbins, E., Luthra, S.S., White, L.S., Stateva, R.P, & Livingston, A.G. (2004). Effect of concentration polarisation and osmotic pressure on flux in organic solvent nanofiltration. *Journal of Membrane Science*, 121-136.

Pink, C. J., Wong, H.-t., Ferreira, F. C., & Livingston, A. G. (2008). Organic solvent nanofiltration and adsorbents; a hybrid approach to achieve ultra low palladium contamination of post coupling reaction products. *Organic Process Research and Development*, *12*(4), 589–595.

Robbins, L. A., & Cusack, R. W. (1998). *Liquid-Liquid Extraction Operations and Equipment*. Chemical Engineering Series. McGraw-Hill, seventh ed.

Roberge, D. M., Ducry, L., Bieler, N., Cretton, P., & Zimmermann, B. (2005). Microreactor technology: A revolution for the fine chemical and pharmaceutical industries? *Chemical Engineering & Technology*, *28*(3), 318–323.

Rundquist, E. (2010) Email sent to Weiming Eugene Siew, 10th May.

Rundquist, E., Pink, C., Vilminot, E., & Livingston, A. (2012a). Facilitating the use of counter-current chromatography in pharmaceutical purification through use of organic solvent nanofiltration. *Journal of Chromatography A*, *1229*, 156–163.

Rundquist, E. M., Pink, C. J., & Livingston, A. G. (2012b). Organic solvent nanofiltration: a potential alternative to distillation for solvent recovery from crystallisation mother liquors. *Green Chem.*, *14*(8), 2197–2205.

Salih, A. (2010). Molecular Simulation of the Adsorption and Transport Properties of Carbon Dioxide, Methane, Water and Their Mixtures in Coal-like Structures. PhD thesis, Imperial College London.

Schlenk, C., Kleij, A. W., Frey, H., & van Koten, G. (2000). Macromolecular-Multisite catalysts obtained by grafting diaminoaryl palladium(II) complexes onto a Hyperbranched-Polytriallylsilane support. *Angewandte Chemie*, *39*(19), 3445–3447.

See Toh, Y. H., Lim, F. W., & Livingston, A. G. (2007a). Polymeric membranes for nanofiltration in polar aprotic solvents. *Journal of Membrane Science*, *301*(1-2), 3–10.

See Toh, Y. H., Loh, X. X., Li, K., Bismarck, A., & Livingston, A. G. (2007b). In search of a standard method for the characterisation of organic solvent nanofiltration membranes. *Journal of Membrane Science*, *291*(1-2), 120–125.

See Toh, Y. H., Silva, M., & Livingston, A. (2008). Controlling molecular weight cut-off curves for highly solvent stable organic solvent nanofiltration (OSN) membranes. *Journal of Membrane Science*, *324*(1-2), 220–232.

Sereewatthanawut, I., Lim, F. W., Bhole, Y. S., Ormerod, D., Horvath, A., Boam, A. T., & Livingston, A. G. (2010). Demonstration of molecular purification in polar aprotic solvents by organic solvent nanofiltration. *Org. Process Res. Dev.*, *14*(3), 600–611.

Sherwood, T. K., & Pigford, R. L. (1952). *Solvent Extraction*. Chemical Engineering Series. McGraw-Hill.

Sheth, J. P., Qin, Y., Sirkar, K. K., & Baltzis, B. C. (2003). Nanofiltration-based diafiltration process for solvent exchange in pharmaceutical manufacturing. *Journal of Membrane Science*, *211*(2), 251–261.

Silva, P., Han, S., & Livingston, A.G. (2005). Solvent transport in organic solvent nanofiltration membranes *Journal of Membrane Science*, 49-59.

So, S., Peeva, L. G., Tate, E. W., Leatherbarrow, R. J., & Livingston, A. G. (2010). Organic solvent nanofiltration: A new paradigm in peptide synthesis. *Org. Process Res. Dev.*, *14*(6), 1313–1325.

Spear, M. (2006). Separations in flux. Available online http://www.chemicalprocessing.com/articles/2006/025/

Stawikowska, J., & Livingston, A. G. (2012). Nanoprobe imaging molecular scale pores in polymeric membranes. *Journal of Membrane Science*, *413-414*, 1–16.

Székely, G., Bandarra, J., Heggie, W., Sellergren, B., & Ferreira, F. C. (2011). Organic solvent nanofiltration: A platform for removal of genotoxins from active pharmaceutical ingredients. *Journal of Membrane Science*, *381*(1-2), 21–33.

Székely, G., Bandarra, J., Heggie, W., Sellergren, B., & Ferreira, F. C. (2012). A hybrid approach to reach stringent low genotoxic impurity contents in active pharmaceutical ingredients: Combining molecularly imprinted polymers and organic solvent nanofiltration for removal of 1,3-diisopropylurea. *Separation and Purification Technology*, *86*, 79-87

Toy, P. H., & Janda, K. D. (2000). Soluble Polymer-Supported organic synthesis. *Accounts of Chemical Research*, *33*(8), 546–554.

Tsoukala, A., Peeva, L., Livingston, A. G., & Bjørsvik, H.-R. (2012). Separation of reaction product and palladium catalyst after a heck coupling reaction by means of organic solvent nanofiltration. *ChemSusChem*, *5*(1), 188–193.

Tung, K., Jean, Y.C., Nanda, D., Lee, K.R., Hung, W.S., Lo, C.H., & Lai, J.Y. (2009). Characterization of multilayer nanofiltration membranes using positron annihilation spectroscopy. *Journal of Membrane Science*, 147-156.

Van der Bruggen, B., Schaep, J., Wilms, D., & Vandecasteele, C. (1999).Influence of molecular size, polarity and charge on the retention of organic molecules by nanofiltration. *Journal of Membrane Science*, 29-41.

Vandezande, P., Gevers, L. E. M., & Vankelecom, I. F. J. (2008). Solvent resistant nanofiltration: separating on a molecular level. *Chemical Society Reviews*, *37*(2), 365–405.

Vanneste, J., Ormerod, D., Theys, G., Van Gool, D., Van Camp, B., Darvishmanesh, S., & Van der Bruggen, B. (2012). Towards high resolution membrane-based pharmaceutical separations. *Journal of Chemical Technology & Biotechnology*, (p. n/a).

Voros, N. G., Maroulis, Z. B., & Marinos-Kouris, D. (1997). Short-cut structural design of reverse osmosis desalination plants. *Journal of Membrane Science*, *127*(1), 47–68.

White, L. S., & Nitsch, A. R. (2000). Solvent recovery from lube oil filtrates with a polyimide membrane. *Journal of Membrane Science*, *179*(1-2), 267–274.

Wijmans, J. G., & Baker, R. W. (1995). The solution-diffusion model: a review. *Journal of Membrane Science*, *107*(1-2), 1–21.

Wöltinger, J., Bommarius, A. S., Drauz, K., & Wandrey, C. (2001). The chemzyme membrane reactor in the fine chemicals industry. *Org. Process Res. Dev.*, *5*(3), 241–248.

Yan, L. J., Liu, Q. Z., & Wang, X. L. (2009). Novel chiral thioureas for highly enantioselective michael reactions of malonates to nitroalkenes. *Chinese Chemical Letters*, *20*(3), 310–313.

Ye, J., Dixon, D.J., Hynes, P.S. (2005). Enantioselective organocatalytic Michael addition of malonate esters to nitro olefins using bifunctional cinchonine derivatives. *Chemical Communications,* 4481–4483.

Zarkadas, D., & Sirkar, K. K. (2011). *Membrane Systems for Pharmaceutical Applications*, chap. 16, (pp. 299–314). Hoboken, New Jersey: John Wiley & Sons, Inc.

Zhang, K.-S., Sun, J.-T., & He, B.-L. (1999). Synthesis of 1,3-Bis(9-O-quinyl)isophthalate and its preliminary study in the asymmetric dihydroxylation of olefins. *Chemical Journal of Chinese Universities*, *20*, 900–902.

Ziegler, J.G., Nichols, N.B. (1993). Optimum Settings for Automatic Controllers. *Journal of Dynamic Systems, Measurements, and Control, 115*(2B), 220–222

Zydney, A. L. (1998). Protein separations using membrane filtration: New opportunities for whey fractionation. *International Dairy Journal*, *8*(3), 243–250.

8. Appendices

8.1 Derivation for Solvent Transport Equation in the DSPM

Membrane pores are assumed to be circular and straight in the DSPM. No slip condition is assumed between the fluid in the pore and the pore walls. Furthermore, the fluid is assumed to be Newtonian in behavious i.e. $\tau = \eta \frac{\partial u}{\partial y}$.

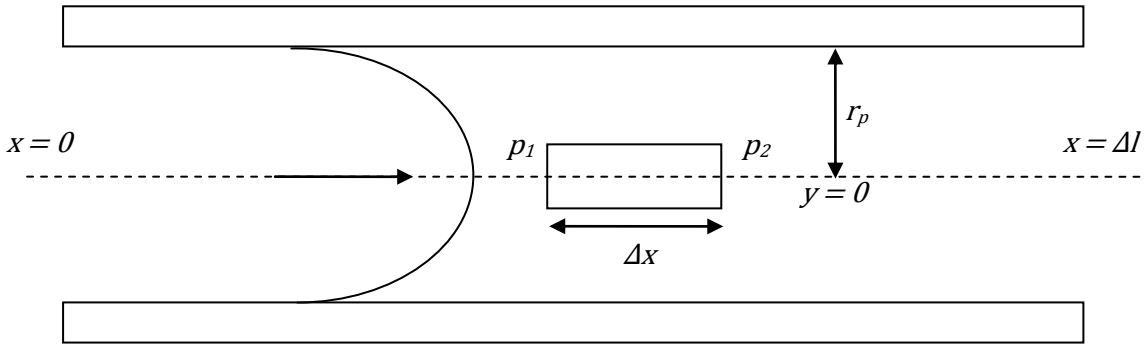

Figure 8.1. Schematic representing solvent flow in a straight and circular membrane pore. Note the control volume with length of *Δx* used for momentum balance analysis.

The y-coordinates are defined by $y = r_p - r$. Hence

$$\partial y = -\partial r \rightarrow \frac{\partial u}{\partial y} = -\frac{\partial u}{\partial r} \qquad \textbf{Equation 8.1}$$

As a Newtonian fluid, the dynamic viscosity of it can be expressed with

$$\tau = \eta \frac{\partial u}{\partial y} = -\eta \frac{\partial u}{\partial r} \qquad \textbf{Equation 8.2}$$

The shear stress on the fluid due to the wall is

$$F_s = \tau(2\pi r\Delta x) = -2\eta\frac{\partial u}{\partial r}(\pi r\Delta x) \quad \textbf{Equation 8.3}$$

Taking a momentum balance across the control volume yields

$$\pi r^2(p_1 - p_2) = -2\eta\frac{\partial u}{\partial r}(\pi r\Delta x) \quad \textbf{Equation 8.4}$$

By rearranging and integrating on both sides, taking into account the no slip conditions at the pore wall, the following equation can be obtained

$$(p_{e1} - p_{e2})\int_{r_p}^{r} r\,\partial r = -2\eta(\Delta x)\int_0^u \partial u \quad \textbf{Equation 8.5}$$

Rearranging, a general solution for fluid velocity in the x-direction can be obtained

$$u = \frac{-(p_{e1} - p_{e2})}{4\eta\Delta x}\left(r^2 - r_p^2\right) \quad \textbf{Equation 8.6}$$

Since the linear velocity follows a parabolic profile, the maximum velocity occurs in the centreline of the pore where $r = 0$

$$u_{max} = \frac{(p_{e1} - p_{e2})}{4\eta\Delta x}r_p^2 \quad \textbf{Equation 8.7}$$

Therefore the average fluid velocity in the pore, which is equivalent to the superficial velocity across the membrane, can be expressed in terms of the pressure drop across the control volume by

$$v_p = \frac{-(p_{e1} - p_{e2})}{8\eta\Delta x}r_p^2 \quad \textbf{Equation 8.8}$$

If the pores in the membrane represent a membrane porosity of ε, conservation of fluid volume across the pore will yield

$$A\varepsilon v_p = J_p A \quad \textbf{Equation 8.9}$$

Hence, by expressing Equation 8.8 in terms of the pressure drop across the membrane pore and rearranging the resulting equation after substituting Equation 8.9, solvent transport across the membrane pore can be related to membrane flux with

$$J_p = \frac{-r_p^2 \Delta p_e}{8\eta\left(\frac{\Delta l}{\varepsilon}\right)} \qquad \textbf{Equation 8.10}$$

8.2 Synthesis Steps for Compounds in Chapter 3

Preparation of 5

To a solution of quinidine (4.0g) in dried DMF (30ml) under nitrogen pressure, NaH (1.36g, 60wt% suspension in mineral oil) was added in small portions. The mixture was stirred at room temperature for 2h. A solution of 1,3,5-tris(bromomethyl)benzene (1.1g, 97wt%) in dried DMF (10ml) was then slowly added to the mixture using a syringe under stirring. The reaction was quenched with deionized water after 5h.

The pH of the mixture was adjusted to 1 by adding HCl (0.1M) and washed with n-hexane (300ml). The pH of the aqueous phase was then adjusted to 14 by adding solid NaOH. Ethyl acetate (1L) was added to dissolve all particulates in the mixture and the aqueous phase removed. The organic phase was washed with 2.5L deionized water and then concentrated to dryness.

Normal phase preparative chromatography then used to purify the residue on a Kromasil column using a mobile phase containing dichloromethane:methanol (89:11 v/v 1.1% ammonium hydroxide). Isolated yield 42%.

^{1}H NMR (400MHz, $(CD_3)_2SO$) δ 8.69 (d, J = 4.1Hz, 1H), 7.96 (d, J = 7.9, 1H), 7.50 (br, 1H), 7.44 (d, J = 2.6Hz, 6.9Hz, 1H), 7.40 (dd, J = 2.6Hz, 6.9Hz, 1H), 7.15 (s, 1H), 5.88-6.00 (m, 1H), 5.17 (br, 1H), 4.95 (d, J = 17.4Hz, 1H), 4.86 (d, J = 10.4Hz, 1H), 4.32 (dd, J = 12.7Hz, 23.2Hz, 2H), 3.79-3.85 (m, 3H), 3.03-3.14 (m, 1H), 2.83-2.93 (m, 1H), 2.60-2.70 (m, 1H), 2.41-2.50 (m, 1H), 2.10-2.20 (m, 1H), 2.08(br, 1H), 1.79-1.89 (m, 1H), 1.64 (br, 1H), 1.35-1.59 (m, 3H); HRMS m/z for (M + H+) = 1087.6

Preparation of 6

To a solution of quinidine (10g) in dried DMF (70ml) under nitrogen pressure, NaH (3.4g, 60wt% suspension in mineral oil) was added in small portions. The resulting mixture was stirred at room temperature for 2h. A solution of 1,3,5-tris(bromomethyl)benzene (2.75g, 97wt%) in dried DMF (10ml) was slowly added to the mixture using a syringe under stirring. The reaction was quenched with deionized water (200ml) after 19h. Dichloromethane (400ml) was added to the mixture and then washed with deionized water (2 x 200ml). The organic phase was then removed and dried in vacuo yielding 16.6g of a brown oil.

Sodium ethanethiolate (18g, 90wt%) was added to this oil along with dried DMF (180ml) and the mixture was stirred under nitrogen pressure and under reflux (110°C). The reaction was left to cool to room temperature after 24h and then quenched with deionized water (180ml). The pH of the mixture was adjusted to 1 using HCl (1M) and washed with ethyl acetate (2 x 250ml + 100ml). The aqueous layer pH was then adjusted to 8 using ammonium hydroxide and washed with dichloromethane (3 x 250ml). The organic layers were collected and washed with deionized water (2 x 500ml) before drying in vacuo. 4.1g of a dry brown solid was obtained. Isolated yield = 53%.

^{1}H NMR (400MHz, $(CD_3)_2SO$) δ 10.20 (br, 1H), 8.62 (d, J = 4.3Hz, 1H), 7.92 (dd, J = 3.4Hz, 8.9Hz, 1H), 7.50 (br, 1H), 7.39 (s, 1H), 7.32 (d, J = 9.0Hz, 1H), 7.20 (d, J = 14.5Hz, 1H), 5.79-6.00 (m, 1H), 5.12 (br, 1H), 4.95 (d, J = 17.0Hz, 1H), 4.85 (d, J = 10.3Hz, 1H), 4.33 (dd, J = 6.4Hz, 11.8Hz, 2H), 3.16 (br, 1H), 2.99 (br, 1H), 2.73 (br, 2H), 2.60 (br, 1H), 2.11-2.27 (m, 1H), 1.78-2.00 (m, 1H), 1.67 (br, 1H), 1.40-1.56 (m, 2H), 1.03-1.38 (m, 1H); HRMS m/z for (M+3H+) = 349.2, (M + 2H+) = 523.8, (M + H+) = 1045.7.

Preparation of 7

To a mixture of quinidine (3.3g) and 1,3,5-tris(bromomethyl)benzene (1.2g, 97wt%), a solvent mixture of ethanol/DMF/chloroform (30ml 5:6:2 by volume) was added. The mixture was stirred under reflux (100°C) for 18h. The mixture was then cooled to room temperature and ether added to it until the solution turned colourless. A precipitate was filtered off and washed with a solvent mixture of ether/acetone (750ml 1:2 vol/vol). The precipitate was then dried in vacuo to afford a dry brown powder (2.8g). Isolated yield = 63%

^{1}H NMR (MHz, $(CD_3)_2SO$) δ 8.85 (d, J = 4.6Hz, 1H), 8.26 (br, 1H), 8.06 (d, J = 9.7Hz, 1H), 7.80-7.84 (m, 1H), 7.55 (dd, J = 2.1Hz, 9.7Hz, 1H), 7.45-7.50 (m, 1H), 6.75-6.87 (m, 1H), 6.62 (s, 1H), 5.97-6.10 (m, 1H), 5.10-5.19 (m, 2H), 4.81-4.95 (m,, 1H), 3.69-3.81 (m, 2H), 3.44 (s, 3H), 3.15-3.26 (m, 1H), 2.89 (s, 2H), 2.31-2.47 (m, 1H), 2.08 (br, 2H), 1.93 (br, 1H), 1.65-1.80 (m, 2H), 1.10-1.24 (m, 1H); HRMS m/z for (M^{3+}) = 363.

Preparation of 8

O-desmethylquinidine (2g) was mixed with deionized water (40g). Solid NaOH (0.24g) was added to this mixture and stirred at room temperature until a clear yellow solution was formed. The aqueous solution was washed with dichloromethane (2 x 12ml). The aqueous phase was mixed with isopropanol (50ml) and dried in vacuo. A dry yellow solid was produced (1.9g) and mixed with dried DMF (10ml). A solution of 1,3,5-tris(bromomethyl)benzene (0.63g) in dried DMF (10ml) was slowly added to this mixture using a syringe. The whole reaction mixture was stirred at room temperature for 4 days. Ethyl acetate (20ml) was then added into the mixture over 5min using a dropping funnel followed by aqueous ammonium chloride (70ml, 14wt%) also using a dropping funnel. The mixture was left to stir for 19h, after which the crystals were filtered off and washed with NaOH (2 x 25ml, 0.1M) and deionized water (3 x 25ml). The residue was then dried in vacuo. 1.2g of a brown solid produced. Isolated yield = 68%

Procedure for Michael addition reaction in Table 3.2

Trans-β-nitrostyrene (60mg, 0.4mmol), dimethyl malonate (158mg, 1.2mmol), naphthalene (30mg) and the catalysts were placed in cylindrical tubes. THF (0.4ml) was then added to each tube and the resulting mixture stirred at -20°C using a Teflon-coated stir bar. The mixtures were sampled every 24h for HPLC analysis at 230nm. The reaction solutions were purified using preparative thin layer chromatography to produce a purified product for chiral analysis.

(-)-Methyl 2-carbomethoxy-4-nitro-3-phenyl-butyrate, Entries in Table 3.2. This product was obtained as a light yellow oil after flash chromatography (elution gradient: Ethyl acetate/isohexane = ¼ by volume). %ee determined by HPLC analysis [Daicel Chiralcel OD-H, isohexane:IPA, 70:30, 0.9ml/min, column temperature = 24°C, λ = 220nm, t (minor) = 11.7min, t (major) = 13.1min]

Entry 1. This product was obtained with 52% yield and 19% ee from a reaction catalysed with catalyst **3** (10mol%) at -20°C for 12 days.

Entry 2. This product was obtained with 82% yield and 86% ee from a reaction catalysed with catalyst **4** (10mol%) at -20°C for 1 days.

Entry 3. This product was obtained with 44% yield and 7% ee from a reaction catalysed with catalyst **5** (3.3mol%) at -20°C for 18 days.

Entry 4. This product was obtained with 62% yield and 94% ee from a reaction catalysed with catalyst **6** (10mol%) at -20°C for 3 days.

Procedure for Michael addition reaction in Table 3.3

Trans-β-nitrostyrene (60mg, 0.4mmol), dimethyl malonate (158mg, 1.2mmol except for Entry 3 where 53mg, 0.4mmol was used), naphthalene (30mg) and the catalysts were placed in cylindrical tubes (see Table 3.3). THF (0.4ml) was then added to each tube and the resulting mixture stirred at -20°C using a Teflon-coated stir bar. The mixtures were sampled every 24h for HPLC analysis at 230nm. The reaction solutions were purified using preparative thin layer chromatography to produce a purified product for chiral analysis.

(-)-Methyl 2-carbomethoxy-4-nitro-3-phenyl-butyrate, Entries in Table 3.3. This product was obtained as a light yellow oil after flash chromatography (elution gradient: Ethyl acetate/isohexane = ¼ by volume). %ee determined by HPLC analysis [Daicel Chiralcel OD-H, isohexane:IPA, 70:30, 0.9ml/min, column temperature = 24°C, λ = 220nm, t (minor) = 11.7min, t (major) = 13.1min]

Entry 1. This product was obtained with 62% yield and 94% ee from a reaction catalysed with **6** (3.3mol%) at -20°C for 3 days.

Entry 2. This product was obtained with 89% yield and 94% ee from a reaction catalysed with **6** (10mol%) at -20°C for 1 days

Entry 3. This product was obtained with 89% yield and 94% ee from a reaction catalysed with **6** (10mol%) at -20°C for 4 days

Procedure for Michael addition reaction in Table 3.4

The nitrostyrene (0.4mmol), dimethyl malonate (158mg, 1.2mmol), naphthalene (30mg) and catalyst **6** were placed in cylindrical tubes. THF (0.4ml) was then added to each tube and the resulting mixture stirred at -20°C using a Teflon-coated stir bar. The mixtures were sampled every 24h for HPLC analysis at 230nm. The reaction solutions were purified using preparative thin layer chromatography to produce a purified product for chiral analysis.

(-)-Methyl 2-carbomethoxy-4-nitro-3-phenyl-butyrate, Entry 1. This product was obtained as a light yellow oil with 62% yield after flash chromatography (elution gradient: Ethyl acetate / isohexane = ¼ by volume) and 94% ee determined by HPLC analysis [Daicel Chiralcel OD-H, isohexane:IPA, 70:30, 0.9ml/min, column temperature = 24°C, λ = 220nm, t (minor) = 11.7min, t (major) = 13.1min]

(-)-Methyl 2-carbomethoxy-4-nitro-3-(4-methylphenyl)-butyrate, Entry 2. This product was obtained as an off-white solid in 62% yield after preparative thin layer chromatography (elution gradient: Ethyl acetate / iso-hexane = ¼ by volume, R_f = 0.14) and 93% ee determined by HPLC analysis [Daicel chiralcel OD-H, isohexane:IPA, 85:15, 1.0ml/min, column temperature = 18°C, λ = 220nm, t (minor) = 20.0min, t (major) = 22.4min] from a reaction catalysed with catalyst **6** (3.3mol%) at -20°C for 5 days.

(-)-Methyl 2-carbomethoxy-4-nitro-3-(4-fluoro-phenyl)-butyrate, Entry 3. This product was obtained as a colourless oil in 81% yield after flash chromatography (elution gradient: Ethyl acetate/isohexane = ¼ by volume) and 94% ee determined by HPLC analysis [Daicel Chiralcel AD-H, isohexane:IPA, 70:30, 1.0ml/min, column temperature = 22°C, λ = 220nm, t (minor) = 12.2min, t (major) = 7.4min] from a reaction catalysed with catalyst **6** (3.3mol%) at -20°C for 3 days.

(-)-Methyl 2-carbomethoxy-4-nitro-3-(4-nitro-phenyl)-butyrate, Entry 4. This product was obtained as a yellow solid in 88% yield after preparative thin layer chromatography (elution gradient: Ethyl acetate/isohexane = ¼ by volume, R_f = 0.17) and 95% ee determined by HPLC analysis [Daicel Chiralcel OD-H, isohexane:IPA, 50:50, 0.9ml/min, column temperature = 28°C, λ = 220nm, t (minor) = 10.3min, t (major) = 15.6min] from a reaction catalysed with catalyst **6** (3.3mol%) at -20°C for 1 day; ^{1}H NMR (400 MHz, $CDCl_3$) δ 8.23 (dt, J = 2.8Hz, 8.8Hz, 2H), 7.48 (dt, J = 2.7Hz, 8.6Hz, 2H), 4.91-5.02 (m, 2H), 4.35-4.44 (m, 1H), 3.90 (d, J = 8.8Hz, 1H), 3.81 (s, 3H), 3.64 (s, 3H); ^{13}C NMR (400MHz, $CDCl_3$)

δ 167.5, 166.7, 147.8, 143.6, 133.3, 132.5, 129.2, 124.2, 77.0, 54.1, 53.4, 53.1, 42.7; HRMS m/z (M + NH^{4+}) = 344

(-)-Methyl 2-carbomethoxy-4-nitro-3-(2-furyl)-butyrate, Entry 5. This product was obtained as a light yellow in 92% yield after preparative thin layer chromatography (elution gradient: Ethyl acetate/isohexane = ¼ by volume, R_f = 0.20) and 96% ee determined by HPLC analysis [Daicel Chiralcel OD-H, isohexane:IPA, 60:40, 1.0ml/min, column temperature = 22°C, λ = 220nm, t (minor) = 6.4min, t (major) = 15.0min] from a reaction catalysed with catalyst **6** (3.3mol%) at -20°C for 3 days.

Compound 2, Entry 6. This product was obtained as an off-white solid with 67% yield after preparative thin layer chromatography (elution gradient: Ethyl acetate/isohexane = ¼ by volume, R_f = 0.14) and 92% ee determined by HPLC analysis [Daicel Chiralcel OD-H, isohexane:IPA, 85:15, 1.0ml/min, column temperature = 18°C, λ = 220nm, t (minor) = 20.0min, t (major) = 22.4min]

8.3 Derivation For Chromatography Analog

Assume a constant sieving constant, where the sieving constant can be defined as

$$S_i = \frac{y_{i,j}}{x_{i,j}} \qquad \textbf{Equation 8.11}$$

The mass balance over stage *j* can be expressed as

$$d\left(V_j x_{i,j}\right) = (y_{i,j-1} - y_{i,j})dV \qquad \textbf{Equation 8.12}$$

Rearranging and substituting the sieving coefficient, one gets

$$V_j \frac{dx_{i,j}}{dV} = S_i x_{i,j-1} - S_i x_{i,j} \qquad \textbf{Equation 8.13}$$

In stage 1, since the incoming feed is pure solvent, the mass balance changes to

$$V_1 \frac{dx_{i,1}}{dV} = -S_i x_{i,1} \qquad \textbf{Equation 8.14}$$

Rearranging and integrating on both sides

$$\int_{x_{i,1}|_0}^{x_{i,1}} \frac{dx_{i,1}}{x_{i,1}} = \int_0^V -\frac{S_i}{V_1} dV \qquad \textbf{Equation 8.15}$$

Solving and rearranging the integral,

$$x_{i,1} = x_{i,1}|_0 \exp\left(-\frac{S_i V}{V_1}\right) \qquad \textbf{Equation 8.16}$$

In stage 2, mass balance after substituting equation 8.6 and assuming that the retentate volume in all stages are equal to that in stage 1.

$$V_1 \frac{dx_{i,2}}{dV} = S_i x_{i,1}|_0 \exp\left(-\frac{S_i V}{V_1}\right) - S_i x_{i,2} \qquad \textbf{Equation 8.17}$$

Multiply by $\exp\left(\frac{S_i V}{V_1}\right)$ and rearrange,

$$\exp\left(\frac{S_i V}{V_1}\right)\frac{dx_{i,2}}{dV} + \exp\left(\frac{S_i V}{V_1}\right)\frac{S_i}{V_1} x_{i,2} = \frac{S_i}{V_j} x_{i,1}|_0 \qquad \textbf{Equation 8.18}$$

One would notice that the terms on the left hand side can be expressed as the differentiation of a product, hence

$$\frac{d}{dV}\left[\exp\left(\frac{S_i V}{V_1}\right) x_{i,2}\right] = \frac{S_i}{V_j} x_{i,1}|_0 \qquad \textbf{Equation 8.19}$$

Integrating on both sides and rearranging

$$x_{i,2} = x_{i,1}|_0 \frac{S_i V}{V_1} \exp\left(-\frac{S_i V}{V_1}\right) \qquad \textbf{Equation 8.20}$$

In stage 3 and 4, perform the same treatment as shown in equations 8.17-8.20.

$$x_{i,3} = x_{i,1}|_0 \frac{S_i^2 V^2}{1 \times 2V_1^2} \exp\left(-\frac{S_i V}{V_1}\right) \qquad \textbf{Equation 8.21}$$

For stage 4, it is

$$x_{i,4} = x_{i,1}|_0 \frac{S_i^3 V^3}{1 \times 2 \times 3 V_1^3} \exp\left(-\frac{S_i V}{V_1}\right) \qquad \textbf{Equation 8.22}$$

The pattern is apparent that at <u>stage n</u>

$$x_{i,n} = \frac{x_{i,1}|_0}{n!} \left(\frac{S_i V}{V_1}\right)^{n-1} \exp\left(-\frac{S_i V}{V_1}\right) \qquad \textbf{Equation 8.23}$$

The permeate from stage n hence can be expressed as

$$y_{i,j} = S_i x_{i,j} \qquad \textbf{Equation 8.24}$$

8.4 <u>Model Validation Multipass Permeate Cascade</u>

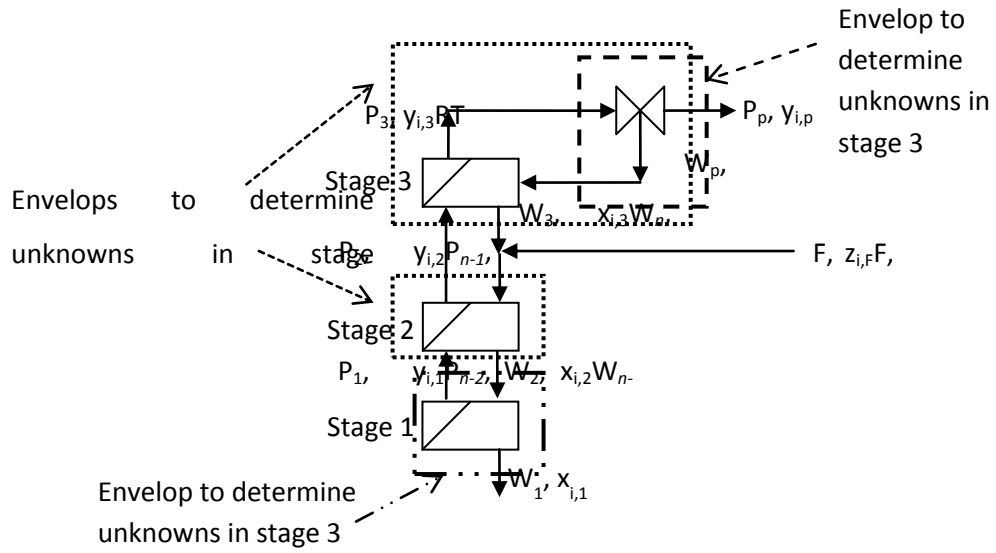

Figure 8.2. Simplified schematic of a 3-stage membrane cascade used in material balance analysis.

In the top most envelop (enclosed in a dotted-line box), 2 unknowns, $x_{i,3}$ and $y_{i,3}$, were identified given that a guess was provided for the value of $x_{i,p} = y_{i,p}$. The top operating line equation,

Equation 8.25 and the partitioning line equation, Equation 8.26 were sufficient to solve for these 2 unknowns.

$$y_{i,3} = \frac{W_p}{P_3} x_{i,p} + \frac{P_p}{P_3} y_{i,p} \qquad \textbf{Equation 8.25}$$

$$x_{i,3} = \frac{y_{i,3}}{(1 - R_{i,3})} \qquad \textbf{Equation 8.26}$$

In the square-dotted envelop above the feed, the remaining unknown was $y_{i,2}$, With a single equation, Equation 8.27, this unknown could be determined

$$y_{i,2} = \frac{W_3}{P_2} x_{i,3} + \frac{P_p}{P_2} y_{i,p} \qquad \textbf{Equation 8.27}$$

An analysis of the square-dotted envelop below the feed revealed that the remaining unknowns was $x_{i,2}$. Equation 8.28 sufficed for solving it.

$$x_{i,2} = \frac{y_{i,2}}{(1 - R_{i,2})} \qquad \textbf{Equation 8.28}$$

The material balance in the bottom operating line equation (Equation 8.29) for the feed stage, stage 2, can be rearranged to obtain Equation 8.30. This can be used to solve for unknown $x_{i,1}$

$$y_{i,2} = \frac{W_3}{P_2} x_{i,3} + \frac{F}{P_2} z_{i,F} - \frac{W_1}{P_2} x_{i,1} \qquad \textbf{Equation 8.29}$$

$$x_{i,1} = \frac{W_3 x_{i,3} + F z_{i,F} - P_2 y_{i,2}}{W_1}$$ **Equation 8.30**

The remaining unknowns in the bottom envelop was $y_{i,1}$. This can be solved by Equation 8.31

$$y_{i,1} = (1 - R_{i,1}) x_{i,1}$$ **Equation 8.31**

Equation 8.32 was not used as this would overspecify the problem.

$$y_{i,1} = \frac{W_2}{P_1} x_{i,2} - \frac{W_1}{P_1} x_{i,1}$$ **Equation 8.32**

The difference between the solute concentration determined experimentally and the expected solute concentration as determined by the model were squared and summed up to determine the sum of squared residuals. $x_{i,1}$ was reiterated until the sum of squared residuals could not be reduced any further.

8.5 Model Validation For Permeable Stripping Cascade

The process model described above was validated by using sampled flow rates and rejections to determine the concentration of A and C in each stream.

Since pure methanol was used as the stripping solvent, Equation 5.27 was simplified to

$$y_{i,j} = \frac{W_{j+1}}{P_j} x_{i,j+1} - \frac{W_1}{P_j} x_{i,1}$$ **Equation 8.33**

We first solved the variables for Compound C. To start off, a guess was provided for $x_{i,1}$. This was used to solve Equation 8.34.

$$y_{i,3} = \frac{W_4}{P_3} x_{i,4} - \frac{W_1}{P_3} x_{i,1}$$ **Equation 8.34**

Next

$$x_{i,3} = \frac{y_{i,3}}{1 - R_{i,3}}$$ **Equation 8.35**

In the next step

$$y_{i,2} = \frac{W_3}{P_2} x_{i,3} - \frac{W_1}{P_2} x_{i,1}$$ **Equation 8.36**

Next

$$x_{i,2} = \frac{y_{i,2}}{1 - R_{i,2}}$$ **Equation 8.37**

Then

$$y_{i,1} = \frac{W_2}{P_1} x_{i,2} - \frac{W_1}{P_1} x_{i,1}$$ **Equation 8.38**

Next

$$x_{i,1} = \frac{y_{i,1}}{1 - R_{i,1}}$$ **Equation 8.39**

Equations from Equation 8.33 to Equation 8.38 were solved simultaneously and $x_{i,1}$ was reiterated until it converged with the value determined by Equation 8.39. This was repeated with Compound A.